

# **DISSERTATION**

submitted to the

Combined Faculties for the Natural Sciences and for Mathematics

of the Ruperto-Carola University of Heidelberg, Germany

for the degree of

Doctor of Natural Sciences

## **Structural and Functional Characterization of the Conserved Nup82 Subcomplex Located on the Cytoplasmic Side of the Yeast Nuclear Pore Complex**

presented by

Diplom-Biotechnologist

Monika Gaik (nee Radwan)

born in:

Sosnowiec, Poland

# DISSERTATION

submitted to the

Combined Faculties for the Natural Sciences and for Mathematics

of the Ruperto-Carola University of Heidelberg, Germany

for the degree of

Doctor of Natural Sciences

presented by

Diplom-Biotechnologist      Monika Gaik (nee Radwan)

born in:                              Sosnowiec, Poland

Oral-examination:                09.07.2014

**Structural and Functional Characterization of the  
Conserved Nup82 Subcomplex Located on the  
Cytoplasmic Side of the Yeast Nuclear Pore Complex**

Referees: Prof. Dr. Ed Hurt

Prof. Dr. Michael Brunner

# Acknowledgements

I would like to thank Prof. Dr. Ed Hurt for giving me the opportunity to work in his group. Thank you for supervising my thesis and the knowledge and experience which you shared with me during my whole PhD work. I thank Prof. Dr. Michael Brunner for being the second referee and the TAC member. My collaboration partners: Elisar Barbar, Alexander von Appen and Martin Beck. I would like to acknowledge: Dr. Martin Koš for being my TAC member and giving me plenty of suggestions and feedbacks, Philip Stelter for laying the groundwork for this project and extremely helpful discussions, Dirk Flemming for his help and experience with electron microscopy. I thank very much Emma Thomson, Philipp Stelter, Jochen Baßler and my husband for proofreading this thesis.

I thank my friends in the lab: Emma for endless guidance, warm atmosphere and a great time after work, Andriana for helping me during my tough days and motivating me to go for sports, Miriam for cheering me up always when I needed it; Lucy, Jessi, Karsten, Johannes, George and Anshuk for amazing integration and many cross-cultural conversations and all lab members and the 4th floor for good vibrations. Special thanks goes to Beate Jannack, Selene Cordeiro and Jutta Müller for their technical assistance and preparation of countless litres of media; Ruth Kunze and Martina Kallas for their kindness, technical advice and a comforting word and Andrea Schliwa for her help with German bureaucracy. I thank my Polish friends which I have met here and thanks to whom I have survived the homesickness. I want to thank my friend Julia Stefanski for

her help, pep-talks and social activities throughout my graduate time.

I would especially like to thank my best friend and beloved husband, Adam, who decided to support my decision of doing a PhD in Germany in 2009 and stayed with it till now. *Kochany, za miłość cierpliwość, wyrozumiałość i codzienne wsparcie nie sposób podziękować. Pomogłeś mi uwierzyć, że dam sobie radę i nigdy we mnie nie wątpiłeś. Kocham Cię.*

My parents and beloved grandmother for everything. *Dziękuję serdecznie Rodzicom i ukochanej Babci Oli za pomoc w osiągnięciu tego celu. Kochani, to wy umożliwiliście mi naukę oraz daliście mi podstawy, na których oparłam swoje dorosłe życie. Wszystko co osiągnęłam było możliwe dzięki Wam i mam nadzieję, że jesteście ze mnie dumni.*

# Contents

<b>Acknowledgements</b>	<b>i</b>
<b>Zusammenfassung</b>	<b>iv</b>
<b>Abstract</b>	<b>vi</b>
<b>1 Introduction</b>	<b>1</b>
1.1 The structure of the Nuclear Pore Complex . . . . .	3
1.2 An overview of the NPC composition . . . . .	5
1.3 The arrangement of the NPC modules . . . . .	9
1.3.1 The Y-shaped Nup84 complex . . . . .	12
1.3.2 The Nsp1 complex . . . . .	14
1.3.3 The Nup82 complex forms a cytoplasmic gate of the NPC . . . . .	15
1.4 Nucleocytoplasmic transport across the NPC . . . . .	18
1.5 The Aim of the PhD . . . . .	23
<b>2 Results</b>	<b>24</b>
2.1 Bioinformatic analysis of the structurally important regions of Nup159, an essential component of the Nup82 complex . . . . .	24
2.2 An essential $\alpha$ -helical sub-region of Nup159-C is required for the Nup82 complex assembly . . . . .	27

2.2.1	Mutant lacking the $\alpha$ -helical (H1) sub-region of Nup159-C loses its association with the NPC . . . . .	29
2.2.2	Recruitment of dynein light chain (Dyn2) is disturbed in <i>nup159-C</i> mutants . . . . .	32
2.3	Structural analysis of the yeast Nup82 complex . . . . .	36
2.3.1	Reconstitution of simplified Nup82 complexes from the yeast <i>Saccharomyces cerevisiae</i> . . . . .	36
2.3.2	The structure of simplified Nup82 complexes revealed by electron microscopy . . . . .	43
2.3.3	Cross-linking mass spectrometry of the Nup82-Nup159C- Nsp1C-Dyn2 complex to map interaction surfaces between the subunits .	50
2.3.4	3D electron tomography of the Nup82 complex . . . . .	53
<b>3</b>	<b>Discussion</b>	<b>55</b>
3.1	The Nup159-C domain is an interaction platform organizing the subunits of the Nup82 complex . . . . .	56
3.2	The conserved Nup82 complex forms an asymmetric assembly . . . . .	58
3.3	The Nup82 complex locates in the cytoplasmic ring and protrudes into the central channel of the NPC . . . . .	61
<b>4</b>	<b>Materials and Methods</b>	<b>64</b>
4.1	Molecular biology and genetic methods . . . . .	64
4.1.1	DNA manipulation and plasmid construction . . . . .	64
4.1.2	Reconstitution of Nup82 complexes in <i>Saccharomyces cerevisiae</i>	65
4.1.3	Construction of yeast strains and basic yeast methods . . . . .	66
4.2	Microbiological methods . . . . .	67
4.2.1	Media for <i>S. cerevisiae</i> and <i>E. coli</i> growth . . . . .	67

---

4.2.2	Analysis of yeast cells growth (dot spots)	68
4.3	Biochemical methods	68
4.3.1	Whole yeast protein extract	68
4.3.2	Reconstitution and affinity purification of Nup82 complexes	69
4.3.3	Western blot analysis	71
4.3.4	Expression and purification of recombinant Nup159 constructs from <i>E. coli</i> for circular dichroism measurements	72
4.4	Microscopic methods	73
4.4.1	Fluorescence microscopy	73
4.4.2	Electron microscopy	73
4.5	Size exclusion chromatography	75
4.6	Multiangle light scattering (MALS)	75
4.7	Cross-linking mass spectrometry	75
4.8	3D EM Data Acquisition	76
4.9	Miscellaneous	77
4.9.1	Protein alignments and secondary structure prediction	77
4.9.2	Structural modelling	77
<b>5</b>	<b>Abbreviations</b>	<b>78</b>
<b>6</b>	<b>Own Publications</b>	<b>81</b>
<b>7</b>	<b>Supplemental Figures</b>	<b>82</b>
	<b>Bibliography</b>	<b>85</b>
	<b>List of Figures</b>	<b>95</b>
	<b>List of Tables</b>	<b>96</b>

# Zusammenfassung

Die Kernporenkomplexe der eukaryotischen Zellen sind riesige Proteinkomplexe, die Doppelmembran des Zellkerns eingebettet sind und den Transport von Molekülen zwischen dem Zytoplasma und dem Kern erlauben. Ein Kernporenkomplex setzt sich aus  $\sim 30$  verschiedenen Nukleoporinen zusammen, die in mehrfacher Anzahl in einer Kernpore vorkommen. Die meisten Nukleoporine sind in stabilen Subcomplexen organisiert. Viele dieser Module wurden bereits charakterisiert, aber die Struktur des tetrameren Nup82-Nup159C-Nsp1C-Dyn2 Komplex, welcher sich auf der zytoplasmatischen Seite des Komplexes befindet und der am Export von mRNA aus dem Kern beteiligt ist, ist bisher unbekannt.

Daher untersuchte ich in meiner Doktorarbeit diesen wichtigen Subkomplex mit dem Fokus auf die konservierte C-terminale Domäne von Nup159. Nup159-C trägt eine essentielle  $\alpha$ -helikale Domäne (H1), welche über sogenannte coiled-coil Interaktionen ein Homo-Dimer ausbilden kann. Mutationen in dieser konservierten Domäne unterdrücken die Homo-Dimer Ausbildung und den Aufbau des tetrameren Nup82-Komplexes. Es konnte gezeigt werden, dass der Bereich zwischen der H1-Untereinheit und der Dynein-interagierenden-Domäne ( $DID_{Nup159}$ ) kritisch für die Bindung von Dyn2 an das  $DID_{Nup159}$  Motiv ist. Es zeigte sich, dass  $DID_{Nup159}$  und H1 einen bestimmten Abstand zur Bindung von Dyn2 brauchen um eine effiziente Assemblierung des Nup82 Komplexes und Einbau in das Kernporengerüst zu gewährleisten. Um den Nup82 Komplex strukturell un-

tersuchen zu können, habe ich diesen Komplex ohne seine flexiblen FG Domänen in Hefezellen rekonstituiert und anschließend isoliert. Biochemische, biophysikalische und elektronen-mikroskopische Untersuchungen zeigten, dass der Nup82 Komplex eine 20 nm längliche Struktur mit einer assymetrischen 'Kopf'-Struktur ausbildet. Die Kopfstruktur ist aus den  $\alpha$ -helikalen C-Domänen von Nup159 und Nsp1, sowie vier Nup82 Moleküle mit unterschiedlichen Eigenschaften aufgebaut. aufgebaut ist aus einem 20 nm langem Stab, bestehend aus dem  $\text{DID}_{\text{Nup159}}$ -Dyn2 Anteil, und einer assymetrischen 'Kopf'- Struktur, welche vier Nup82 Moleküle mit unterschiedlichen Eigenschaften und die  $\alpha$ -helikalen C-Domänen von Nup159 und Nsp1 beinhaltet. Mit dieser Zusammensetzung hat der Komplex insgesamt ein Molekulargewicht im Bereich von einem Megadalton. Desweiteren konnte über quervernetzende Massenspektrometrie eine Interaktionskarte zwischen den vier Untereinheiten des Komplexes erstellt werden.

Die Arbeit gibt somit zum ersten Mal Einblicke in die dreidimensionale (3D) Architektur des Nup82-Nup159C-Nsp1C-Dyn2 Komplexes der Kernpore in welchem die Nup159-C Domäne ein selbst-dimerisierendes Element bildet.

# Abstract

Nuclear pore complexes (NPCs) are huge, proteinaceous assemblies, embedded in the nuclear envelope that act as gateways between the cytoplasm and nucleoplasm. A single NPC is formed from ~30 different nucleoporins, present in multiple copies. The vast majority of nucleoporins is organized in distinct subcomplexes. A number of NPC modules have been described in the past, but the structure of the tetrameric Nup82-Nup159C-Nsp1C-Dyn2 complex, located at the cytoplasmic side of the NPC and involved in nuclear mRNA export, remained elusive.

My PhD study has focused on the conserved C-domain of Nup159, the key sub-unit of the Nup82 complex. Nup159-C harbors an essential  $\alpha$ -helical sub-domain (H1), which is able to homo-dimerize through a coiled-coil interaction. Mutation in this region disturbs homo-dimerization and Nup82 complex assembly. The linker sequence prior to the essential H1 sub-domain turned out to be critical for dynein light chain (Dyn2) recruitment at the DID<sub>Nup159</sub> motif (dynein light chain interacting domain), which binds five Dyn2 dimers. This finding suggests that DID<sub>Nup159</sub> and H1 require a certain distance for Dyn2 binding to ensure the efficient Nup82 complex assembly and incorporation into the NPC scaffold. To gain more insight into the structure of the Nup82 complex, I have applied a method to reconstitute *in vivo* and subsequently isolate the essential structural core of the Nup82 module devoid of flexible FG repeats. Biochemical, biophysical and electron microscopy analysis unravelled that the Nup82 complex consists of a 20 nm stalk formed by the DID<sub>Nup159</sub>-Dyn2 and an asymmetric 'head' structure that contains

four Nup82 molecules with different properties and the  $\alpha$ -helical C-domains of Nup159 and Nsp1, leading to a large assembly with a molecular mass in the megadalton range. Furthermore, cross-linking mass spectrometry allowed to map the interaction regions between four subunits of the complex.

Interestingly, orthologous Nup88-CAN/Nup214 complex of the human NPC is also asymmetrically located at the cytoplasmic side of the pore and allowed to speculate about possible orientation of the yeast Nup82 complex. Based on this data, the first structural model of the conserved Nup82 complex was developed, explaining how this cytoplasmically located module is anchored to the NPC scaffold and at the same time can protrude its FG repeats towards the central transport channel to participate in the nucleocytoplasmic transport. Moreover, both *NUP88* and *CAN/NUP214* in human are linked to cancer, thus the first structural insight in the Nup82 complex could help to better understand the Nup88-/Nup214-associated tumorigenesis mechanism.

In conclusion, the study revealed for the first time the 3D architecture of the Nup82-Nup159C-Nsp1C-Dyn2 complex with Nup159 C-domain forming the key self-dimerizing scaffold.

# 1 Introduction

The evolutionary tree of life consists of three primary branches: bacteria, archaea and eukaryota. The distinctive feature of eukaryotic cells is the presence of organelles separated by lipid membranes (nucleus, nucleolus, mitochondria, Golgi apparatus, endoplasmic reticulum, vacuoles etc.). A remarkable example of cell's compartmentalization is the nucleus, containing the genomic DNA, separated from the cytoplasm by a double membrane called the nuclear envelope (NE), which is continuous with the endoplasmic reticulum (ER). The existence of the nuclear membrane resulted in spatial and temporal separation of transcription and translation. To allow information exchange between the nucleus and the cytoplasm, a transport mechanism had arisen. Bi-directional exchange of molecules occurs via large, proteinaceous structures, known as nuclear pore complexes (NPCs), spanning the inner (INM) and outer nuclear membrane (ONM) (Fig. 1.1). They are composed of proteins called nucleoporins (Nups). The main structural features of the NPC are cytoplasmic filaments and a nuclear basket emanating from the central framework. The central scaffold of the nuclear pore complex is formed by cytoplasmic, nuclear and spoke rings, encircling the transport channel. The inside of the pore is filled with unstructured stretches of phenylalanine-glycine (FG) repeats present in nucleoporins, surrounding the transport channel and directly involved in the nucleocytoplasmic transport [Adams and Wentz, 2013]. The function of the NPC is to allow active transport of large cargo against a concentration gradient as well as passive diffusion of ions and small molecules. The active transit

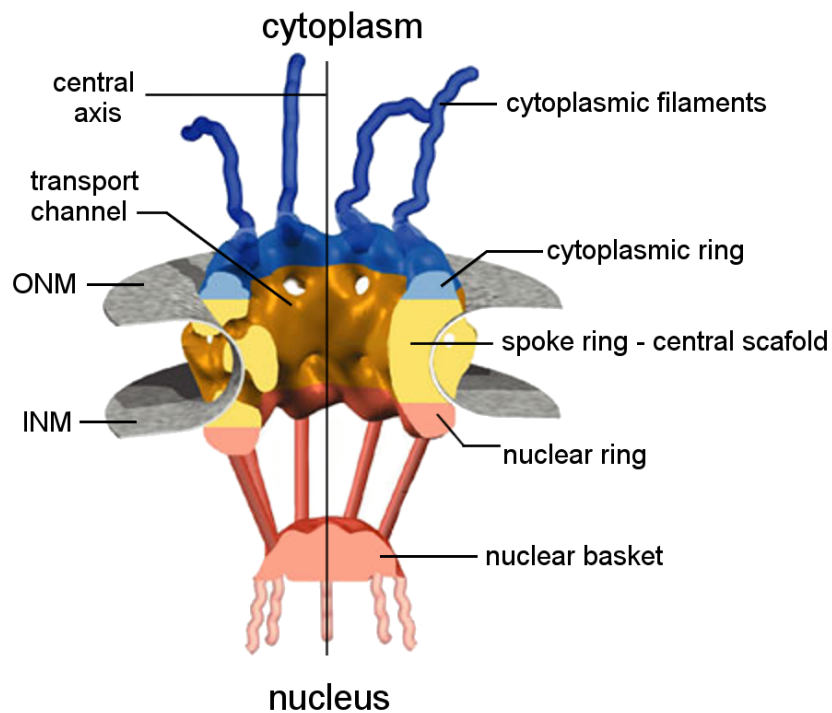


**Figure 1.1:** Model of the nuclear pore complex (NPC).

Schematic representation of the nuclear pore complex (NPC), integrated in the nuclear envelope (NE). The scheme depicts the central spoke-ring (SR), cytoplasmic and nuclear rings, the cytoplasmic filaments protruding into the cytoplasm and the nuclear basket structure facing the nucleus. The eight-fold symmetry of the NPC occur along the central axis. ONM - outer nuclear membrane, INM - inner nuclear membrane, modified from [Fahrenkrog and Aebi, 2003].

of large macromolecules requires energy and nucleocytoplasmic transport receptors, which recognize transport signals and move the cargo through the NPC. Transport signals provide crucial information for the correct transport direction: proteins targeted to the nucleus can harbour a nuclear localization sequence (NLS), while proteins exported from the nucleus carry a nuclear export signal (NES) [Lange et al., 2007]. Apart from the role in nucleocytoplasmic transport a number of nuclear pore proteins are reported to be involved in chromatin organization, gene regulation and DNA repair [Maillet et al., 1996, Casolari et al., 2004, Brickner and Walter, 2004, Zhao and Blobel, 2005, Cabal et al., 2006]. Thus, knowledge of the structural organization of the nuclear pore complex (NPC) is key for understanding the mechanisms of nucleocytoplasmic transport and other nuclear functions mediated by NPCs.

## 1.1 The structure of the Nuclear Pore Complex

The NPC forms a large macromolecular assembly, composed of about 30 different nucleoporins in yeast [Hurt, 1988, Davis and Fink, 1990, Nehrbass et al., 1990, Doye and Hurt, 1997, Fabre and Hurt, 1997, Grandi et al., 1995b, Grandi et al., 1995a, Rout et al., 2000]. The NPC exhibits a characteristic structural appearance with an octagonal symmetry along the central transport channel axis, perpendicular to the nuclear membrane plane and asymmetric substructures located at the cytoplasmic and nucleoplasmic sides of the NPC [Goldberg and Allen, 1993, Kiseleva et al., 2004] (Fig. 1.1). Electron microscopy (EM) studies of amphibian oocytes have shown porous structures perforating the nuclear envelope [Gall, 1967]. Initially, EM analysis of NPCs obtained from the *Xenopus laevis*, revealed the symmetric framework of eight subunits, called spokes, protruding into the central channel. The spoke-ring scaffold surrounds the channel, through which the nucleocytoplasmic transport takes place [Fahrenkrog and Aebi, 2003]. Cryo-EM, electron tomography (ET) and three-dimensional (3D) reconstruction maps of obtained images provided further details of the NPC's structure and allowed to determine an approximate molecular mass (120 MDa) of the vertebrate NPC. In addition to the central transport channel, eight peripheral channels have been observed, which were suggested to provide a path for diffusion of ions and small molecules [Reichelt et al., 1990, Hinshaw et al., 1992, Goldberg and Allen, 1993, Akey and Radermacher, 1993, Stoffler et al., 2003].

Lately, the high-resolution 3D structures of NPCs derived from intact nuclear envelope of *Dictyostelium discoideum*, *Xenopus laevis* and human fibroblast cells have been obtained with cryo-electron tomography technique [Beck et al., 2004, Beck et al., 2007, Frenkiel-Krispin et al., 2010, Maimon et al., 2012, Bui et al., 2013]. These electron microscopic analyses revealed the arrangement of the NPC's central scaffold, which is sandwiched between cytoplasmic and nucleoplasmic rings, from which filamentous

structures project into the nucleoplasm and cytoplasm. On the nucleoplasmic side of the NPC, eight long filaments extend and form a ring-like structure named nuclear basket, whereas on the cytoplasmic side, cytoplasmic filaments protrude from eight knobs (Fig. 1.2 A-B) [Hinshaw et al., 1992, Goldberg and Allen, 1993, Fahrenkrog and Aebi, 2003, Beck et al., 2004, Kiseleva et al., 2004].

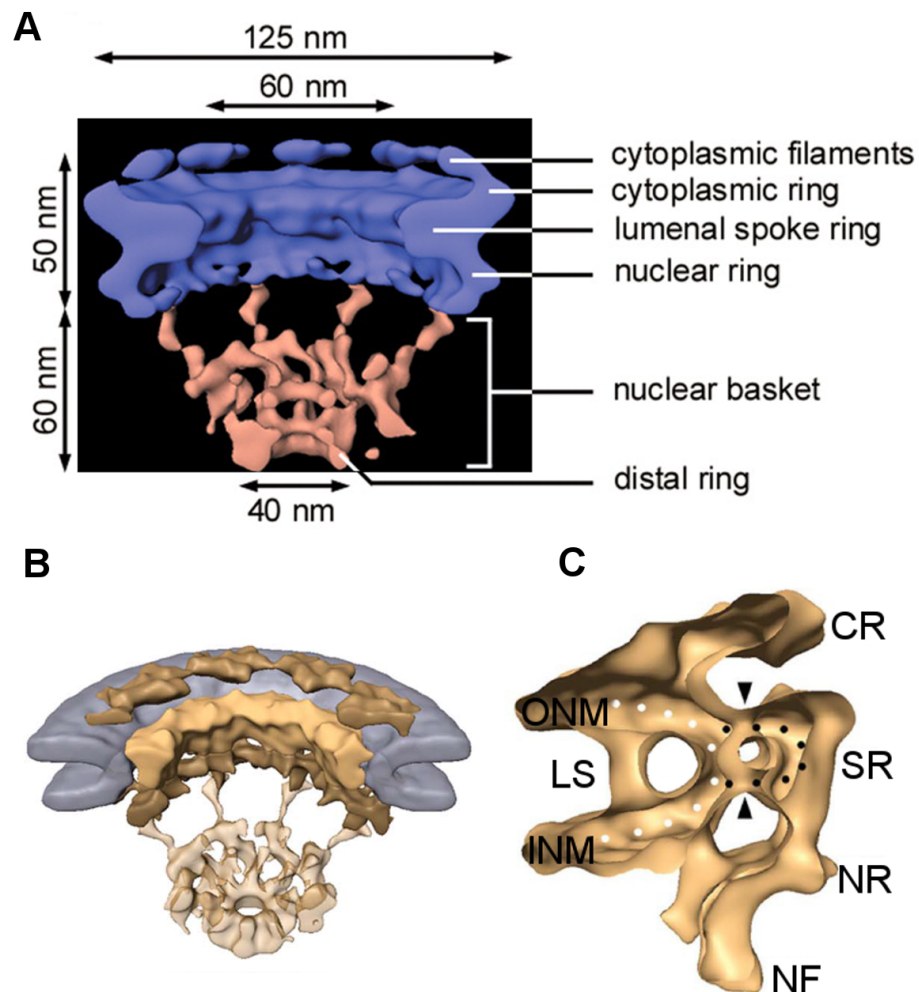


**Figure 1.2:** Scheme of the nuclear pore complex obtained from *Dictyostelium discoideum*

(**A**) An overview of the main features of the NPC with typical dimensions. Cytoplasmic filaments and the nuclear basket with its distal ring are highlighted. Modified from [Beck et al., 2004]. (**B**) Cut-away overview of the NPC with octagonal symmetry along the transport axis. (**C**) Cross-section view of the NPC with the tripartite architecture: cytoplasmic (CR), spoke (SR) and nuclear rings (NR). White dots represent the fused inner and outer nuclear membrane (INM, ONM) and black dots represent the spoke structure. Luminal space (LS) between ONM and INM with supporting luminal connectors. Adapted from [Beck et al., 2007].

The isolation of nuclei from yeast and subsequent enrichment of obtained NPC fraction were performed to describe the structural organization as well as composition of *Saccharomyces cerevisiae* NPCs [Rout and Blobel, 1993, Yang et al., 1998, Kiseleva et al., 1998, Kiseleva et al., 2004]. Observed NPCs are smaller in yeast than in vertebrates ( ~100 nm in diameter and ~40 nm in height in yeast as opposed to ~130 nm x ~80 nm for vertebrates), with molecular mass of ~60 MDa [Rout and Blobel, 1993, Elad et al., 2009]. Although differences between yeast and vertebrate NPCs were observed (e.g. lack of distinct nuclear and cytoplasmic rings), the overall architecture of NPCs is conserved (Fig. 1.2 A). Both yeast and vertebrate NPCs exhibit the inner spoke-ring (SR) structure, surrounding the central transport channel, which is anchored to the nuclear envelope in a similar way [Yang et al., 1998, Beck et al., 2007]. The interaction between the inner spoke-ring and the nuclear membrane was shown on a cut-away view of the *Dictyostelium discoideum* NPC. Each spoke is attached to the fused outer and inner nuclear membrane (Fig. 1.2 C). The cytoplasmic ring (CR) continuously contacts the ONM, while the nuclear ring (NR) is continuous with the spoke-ring (SR) and INM. An intriguing structure is the luminal connector, bridging the outer and inner nuclear membrane in the luminal space (LS), nearby the NPC. It has been proposed that it has a role in stabilization of the fused NE (Fig. 1.2 C) [Beck et al., 2007, Maimon et al., 2012, Bui et al., 2013].

## 1.2 An overview of the NPC composition

Nucleoporins were identified by combination of biochemical approaches, employing antibodies raised against nuclear pore-specific epitopes and genetic screens, which confirmed their physical interaction and function in the NPC [Hurt, 1988, Davis and Fink, 1990, Rout and Blobel, 1993, Doye and Hurt, 1995, Panté and Aebi, 1996, Siniosoglou et al., 1996, Doye and Hurt, 1997, Elad et al., 2009]. Due to the octagonal symmetry of

the NPC, each of  $\sim 30$  nucleoporins occur in eight or multiples of eight copies per pore, resulting in approximately 500-1000 Nups per single NPC [Rout et al., 2000, Hoelz et al., 2011]. The majority of nucleoporins is conserved from yeast to human and arranged in stable sub-complexes (see *Section 1.3*) [Grandi et al., 1995a, Grandi et al., 1995b, Doye and Hurt, 1997, Rout et al., 2000]. Nucleoporins can be classified according to various properties including their localization within the NPC and domain architecture. The localization of particular nucleoporins within the NPC was analyzed by indirect immunofluorescence and immunoelectron microscopy of protein A-tagged strains [Hurt, 1988, Davis and Fink, 1990, Nehrbass et al., 1990, Grandi et al., 1993, Rout et al., 2000]. Based on their location in the NPC nucleoporins are divided into two groups: (1) symmetrically distributed channel nucleoporins and integral membrane proteins of the nuclear envelope, (2) asymmetrically localized nucleoporins at nucleoplasmic or cytoplasmic side of the NPC [Rout et al., 2000, Cronshaw et al., 2002, Brohawn et al., 2009]. Immunogold microscopy showed that most of yeast Nups are symmetrically distributed within the NPC, with a few localized asymmetrically (e.g. Nup1, Mlp1/2, Nup42, Nup159, see Fig. 1.3) [Fahrenkrog et al., 1998, Rout et al., 2000]. Another classification groups nucleoporins according to their main structural domains:  $\alpha$ -solenoids (e.g. Nup192, Nup188), coiled-coils (Mlp1/2),  $\beta$ -propellers (e.g. Seh1, Sec13), FG repeats (e.g. Nup42, Nup1, Nup2, Nsp1), transmembrane helices (Pom34, Pom152, Ndc1), and autoproteolytic domain of Nup98 (Nup145N, Nup100, Nup116) (Fig. 1.3). Many Nups harbour more than one fold type, thus are classified into more than one category. Nevertheless, the principal structural domain feature, used when classifying nucleoporins, is the presence or absence of the unstructured FG repeat domains.

The most frequent domain types, found in nucleoporins, comprise of unstructured FG domains,  $\alpha$ -helical coiled-coil domains, mediating hydrophobic protein-protein interactions,  $\beta$ -propellers and combination of  $\beta$ -propellers with  $\alpha$ -helical solenoids, occurring in the scaffold proteins (Fig. 1.3). Nucleoporins, containing Phe-Gly (FG)-rich repeat



sequences, play an important role in the nucleocytoplasmic transport (see *Section 1.4*). FG domains are natively unfolded and form a non-ordered cohesive meshwork, which is a selective permeability barrier, that lines the inside channel of the NPC. FG domains can interact with transport receptors, facilitating the translocation of larger cargo. Some FG-nucleoporins are found on either cytoplasmic (Nup42, Nup159) or nucleoplasmic (Nup145N, Nup1, Nup2) side of the NPC, while the Nsp1-Nup57-Nup49 complex is symmetrically distributed across the central transport channel (Fig. 1.4) [Fabre and Hurt, 1997, Ho et al., 2000, Rout et al., 2000]. FG domains vary in sequence and length (from 150 to 700 residues), consisting of hydrophobic arrays of FG motifs (FG, FXFG, GLFG, SAFG or PSFG), separated by linkers of hydrophilic residues. Assuming that 11 FG-nucleoporins are present in 8-32 copies in each NPC, it results in  $\sim 10,000$  of FG dipeptides per single NPC, thus FG domains account for approximately 12% of the NPC's mass [Rout et al., 2003, Denning et al., 2003, Strawn et al., 2004, Peters, 2009a, Eisele et al., 2013]. Although FG Nups are required for nucleocytoplasmic transport, most of FG repeat domains are not essential. Deletion analysis of different FG repeat domains in *S. cerevisiae* revealed that up to half of FG domains mass can be deleted without viability loss and only specific combination of FG repeat sequences mutations disturb cell viability, suggesting a substantial redundancy in the FG domain meshwork [Strawn et al., 2004, Terry and Wentz, 2009]. Moreover, FG domains of one asymmetrically located Nup (e.g. Nup1) can be substituted by FG repeat sequences from another asymmetric Nup (e.g. Nup159) [Zeitler and Weis, 2004].

Second domain type occurring in nucleoporins is the coiled-coil motif, containing a characteristic  $\alpha$ -helical fold, where  $\alpha$ -helices are coiled together like strands of rope. Upon folding, the hydrophobic surface is buried inside the  $\alpha$ -helical segments, providing a thermodynamic force for the multiligomerization (two-stranded and three-stranded coiled-coils are the most common). Primary amino-acid structure contains a conserved heptad repeat pattern *hxxhcx*, where *h* is hydrophobic and *c* charged residue [Ma-

son and Arndt, 2004]. The  $\alpha$ -helices may be parallel or anti-parallel and usually adopt a left-handed super-coil [Harbury et al., 1993]. The largest coiled-coil domains were described in yeast Mlp1 and Mlp2 proteins (homologues of vertebrate Tpr), which are the components of long intra-nuclear filaments, attached to the nuclear basket structure of the NPC. Mlp1 and Mlp2 interact with nucleoporins (Nup1, Nup60, Nic96) [Strambio-de Castillia et al., 1999, Kosova et al., 2000] and are involved in the NPC-associated mRNA quality control [Casolari et al., 2004, Galy et al., 2004, Fasken and Corbett, 2009]. In the central channel of the nuclear pore, six nucleoporins harbour predicted coiled-coil domains (Nsp1, Nup159, Nup82, Nup49, Nup57 and Nic96). The Nsp1 is present in two sub-complexes of the NPC (Nsp1-Nup49-Nup57 and Nup82-Nup159-Nsp1) and in both, coiled-coil interactions are crucial for the complex formation (see *Section 1.3.2*) [Bailer et al., 2001, Grandi et al., 1995b, Solmaz et al., 2011].

Another domain type occurring in nucleoporins is a circular arrangement of four to eight anti-parallel  $\beta$ -strands blades of disk-shaped  $\beta$ -propeller. To date six out of nine yeast  $\beta$ -propellers have been structurally characterized (seven-bladed: Nup133, Nup120, Nup159, Nup82, six-bladed: Seh1, Sec13).  $\beta$ -propellers coordinate multi-protein complex assemblies throughout the pore and recruit auxiliary proteins, such as the mRNA export factor Dbp5 to the  $\beta$ -propeller of Nup159 at the cytoplasmic side of the NPC [Debler et al., 2008, Hsia et al., 2007, Weirich et al., 2004].

A big part of the scaffold nucleoporins is folding into non-coiled-coil  $\alpha$ -helical solenoids [Devos et al., 2006]. The classical  $\alpha$ -solenoid structure is characterized by nearly identical two- or three-helix units, repeatedly stacked forming an elongated, super-helical domain observed in nuclear transport receptors. In nucleoporins, three novel  $\alpha$ -helical topologies have been described [Brohawn et al., 2009]. The first, well determined atypical  $\alpha$ -helical arrangement of Nic96 revealed its tripartite J-like topology, composed of 28  $\alpha$ -helices, termed the Ancestral Coatmer Element 1 (ACE1) [Schrader et al., 2008, Brohawn et al., 2008]. ACE1 structure is organized into three joined modules:

a crown, a trunk and a tail with flexible hinges, connecting them, thus allowing slight movement. A distinguishing feature of ACE1 compared to helical repeat structures, is the rigidity of the trunk module and U-turns arrangements within the crown module. The ACE1 fold form an  $\alpha$ -helical scaffold of Nic96, Nup145C, Nup85 and Nup84 proteins [Devos et al., 2006, Brohawn et al., 2008, Onischenko and Weis, 2011]. The second type of  $\alpha$ -helical topology is found in human Nup133 and yeast Nup170, which are characterized by an extended and stretched  $\alpha$ -helical stack at the carboxy-terminus [Whittle and Schwartz, 2009]. Finally, a distinct  $\alpha$ -helical fold was described in the segment of Nup120 from Nup84 complex, which integrates an  $\alpha$ -helical domain with a  $\beta$ -blade insertion, completing its amino-terminal seven-bladed  $\beta$ -propeller structure [Hsia et al., 2007, Brohawn et al., 2009, Seo et al., 2009].

### 1.3 The arrangement of the NPC modules

A hallmark of the NPC is its complexity in organization and composition of diverse modules (sub-complexes) [Grandi et al., 1993, Grandi et al., 1995b, Fabre and Hurt, 1997, Rout et al., 2000, Lutzmann et al., 2002, Devos et al., 2006]. A combination of biochemical, genetic and EM studies has been applied to determine the NPC architecture in atomic detail. The progress in obtaining crystal structures of many nucleoporins has revealed the molecular organization of modules building the NPC [Hoelz et al., 2011]. Nevertheless, the interaction network between neighbouring Nups sub-complexes has not been completely described yet [Alber et al., 2007b, Debler et al., 2008, Onischenko and Weis, 2011]. The nucleoporins arranged into distinct modules are classified into three main layers or zones, according to their function and location across the NPC and function: 'membrane', 'scaffold' and 'barrier' [Schwartz, 2005]. The 'membrane' layer is formed by integral pore membrane proteins (POMs), containing transmembrane domains, which anchor and position the whole NPC in the nuclear envelope. In yeast three

transmembrane nucleoporins (Ndc1, Pom34 and Pom152) exist. The structural link between 'membrane' and neighbouring 'scaffold' layer is formed by two yeast nucleoporins (Nup53 and Nup59), which can directly interact with the nuclear membrane (Nup53), but also with nucleoporins forming the 'scaffold layer' (Nup170, Nup192, Nic96). This layer is formed by large nucleoporins (Nup170, Nup188, Nup192) that constitute a central framework of the inner pore module and links two remaining layers via Nic96 [Flemming et al., 2009, Amlacher et al., 2011]. The 'scaffold' nucleoporins are composed mainly of  $\alpha$ -solenoids and  $\beta$ -propellers domains (Nup170, Nup133, Nup120, Nup84, Nup85, Nup145C etc.). The 'scaffold' layer consist of the most stably associated nucleoporins, forming the core of the NPC, where the inner pore module is sandwiched between two rings of Y-shaped Nup84 complex (Fig. 1.4 and *Section 1.3.1*).

Finally, the 'barrier' layer fills the central channel with nucleoporins containing predominantly FG-rich repeats and coiled-coil domains (Nup49, Nsp1, Nup57, Nup159, Nup100, Nup116, Nup145N, Nup60 etc.) (Fig. 1.4), [Grandi et al., 1995b, Devos et al., 2006, Onischenko and Weis, 2011]. Except for the Nsp1-Nup49-Nup57 complex (see *Section 1.3.2*) located inside the transport channel, the 'barrier' nucleoporins are peripherally associated with either cytoplasmic (Nup82-Nup159-Nsp1-Dyn2 complex see *Section 1.3.3*) or nucleoplasmic (Nup60, Nup2, Nup1, Mlp1/2) side of the NPC (Fig. 1.4) [Grandi et al., 1995a, Hurwitz et al., 1998, Schrader et al., 2008, Amlacher et al., 2011].

A more detailed arrangement of the NPC, based on combined affinity-purified sub-complexes and biocomputational calculation to integrate weak inter-subcomplexes interactions with more stable intra-subcomplexes interactions, was described by Rout and coworkers [Alber et al., 2007a, Alber et al., 2007b]. The sub-complexes were arranged in cylindrical rings, formed by eight connected spokes. The central spoke ring of the NPC is a fundamental symmetry unit, among a membrane ring, two outer rings represented mainly by Y-shaped Nup84 complex and inner rings. Additionally, linker nucleo-

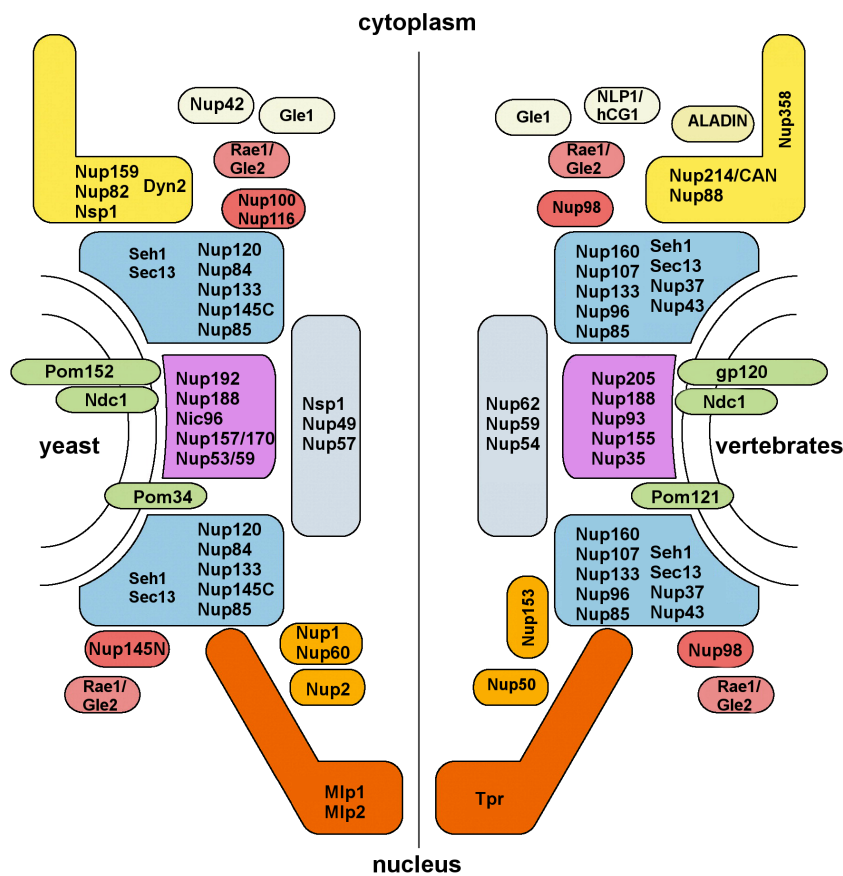


**Figure 1.4:** The arrangement of nucleoporins into NPC modules in yeast and vertebrates

Scheme displays the composition and approximate location of yeast (left) and vertebrate (right) nucleoporin sub-complexes across the NPC. The Nup84 complex (blue), the inner pore ring complex (magenta), the Nsp1-Nup49-Nup57 complex (gray), the Nup82 complex (yellow) and transmembrane nups (green) are shown (details in text). Modified from [Schwartz, 2005, Brohawn et al., 2009].

porins and FG nucleoporins have been defined (Fig. 1.5) [Schwartz, 2005, Alber et al., 2007b]. A detailed immunoprecipitation analysis of nucleoporins showed that most of them are organized in biochemically stable building blocks, leading to a higher order organization of the NPC (Fig. 1.5) [Bailer et al., 2000, Rout et al., 2000, Alber et al., 2007b].

### 1.3.1 The Y-shaped Nup84 complex

The best characterized NPC module is the Nup84 complex, which has been ex-

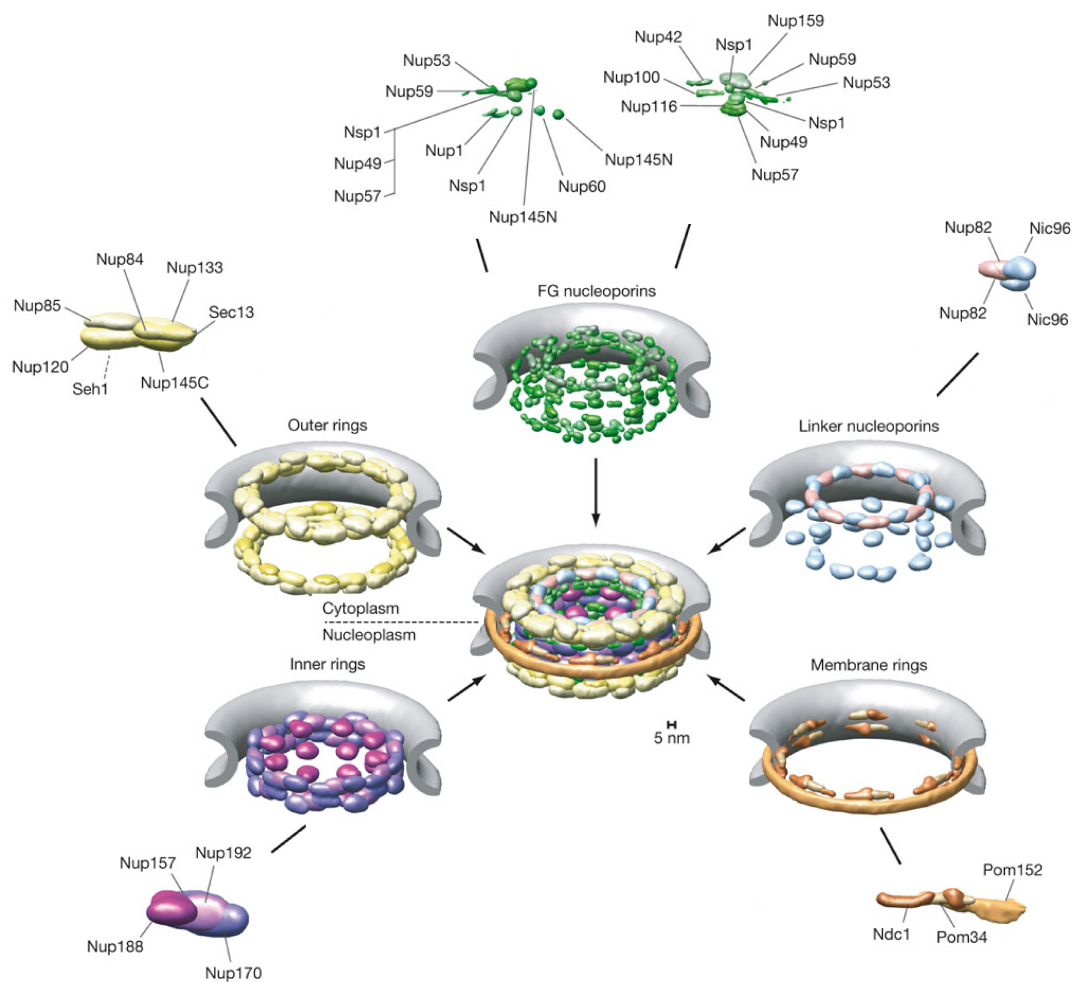


**Figure 1.5:** The overview of NPC's substructures and their nucleoporin composition

Nucleoporins grouped into five distinct rings: outer rings (yellow), the inner ring (dark blue and magenta), membrane rings (orange), the linker nucleoporins (light blue and pink) and the FG nucleoporins (green). The pore membrane is shown in grey. Modified from [Alber et al., 2007a].

tensively studied in yeast (homologous to vertebrate Nup107-Nup160 complex). All members of the hetero-heptameric complex are conserved, but the vertebrate Nup107-Nup160 complex has two additional components (Nup37, Nup43) and associated protein ELYS/Mel-28, required for proper cell division and nuclear pore assembly [Doucet and Hetzer, 2010, Rasala et al., 2006]. Electron microscopy studies revealed an unusual Y-shaped triskelion-like structure of yeast Nup84 complex [Siniosoglou et al., 2000, Lutzmann et al., 2002], composed of seven subunits, which exhibit a certain level of flexibility. In 2002 Lutzmann and coworkers *in vitro* reconstituted the entire com-

plex from recombinantly expressed subunits in *E.coli* (Fig. 1.6 A), which exhibited the characteristic Y-shaped topology in electron microscopy. All components of the Nup84 complex have been crystallized (either full length proteins or domains) and localized in the 3D map of the Y-shaped complex. The core of the complex is composed of Nup84, Seh1-Nup85 hetero-dimer and Nup145C-Sec13 hetero-dimer with peripherally located Nup120 and Nup133 (Fig. 1.6 B) [Kampmann and Blobel, 2009, Nagy et al., 2009].

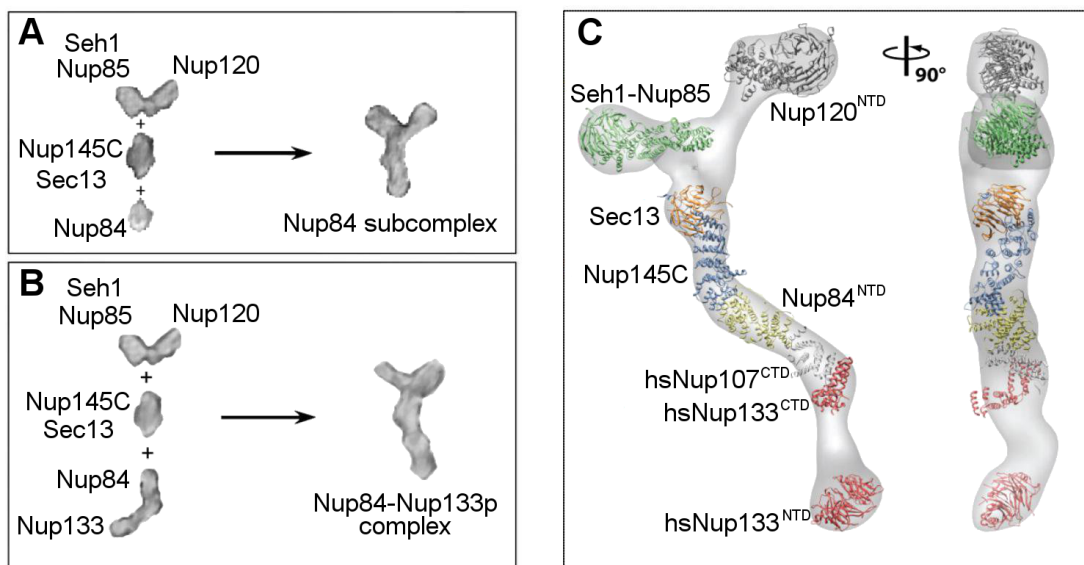


**Figure 1.6:** Topology of the Nup84 complex

(A and B) Protein arrangement within the Y-shaped hexameric Nup84 complex without (A) and with (B) Nup133 protein [Lutzmann et al., 2002]. (C) Docking of crystal structures into the EM 3D volume of the hetero-heptameric Nup84 complex and a 90°-rotated view is shown on the right. Two flexible hinges of the heptamer stem are formed by the contact sites of Nup145C-Nup84 (blue and yellow) and Nup133-Nup84 (yellow and red). Adapted from [Nagy et al., 2009].

The Nup84 complex is localized symmetrically on both sides (outer rings) of the pore - sandwiching the inner pore module (Fig. 1.5) [Alber et al., 2007b, Bui et al., 2013]. Nup84, Nup85 and Nup145C contain the ACE1 domain described above [Brohawn et al., 2008]. Nup120 and Nup133 harbour seven-bladed  $\beta$ -propellers at the N-termini and  $\alpha$ -helices at the C-termini (see Fig. 1.3 and section 1.2). The crystal structure of the Nup133 N-terminal domain revealed a seven-bladed  $\beta$ -propeller with two  $\alpha$ -helical insertions and a disordered loop. The characteristic feature of this loop is a membrane

curvature-sensing motif, named ALPS (ArfGAP1 lipid packing sensor), suggesting that Nup133 is involved in an early stage of NPC biogenesis and shows specificity for curved lipid membranes [Drin et al., 2007, Doucet et al., 2010]. Thus, the Nup84 complex has been proposed to act as a 'membrane-curvature module' similarly to the coat protein complexes (COPI, COPII and clathrin coat) [Devos et al., 2004, Drin et al., 2007]. NPCs and COPII vesicles share a common component - Sec13, which interact in a similar way with Nup145C and the coat protein Sec31. Six-bladed  $\beta$ -propeller of Sec13 interacts with three  $\alpha$ -helices of Nup145C (named Nup145C<sup>DIM</sup> - domain invasion motif), which form additional seventh blade of Sec13, similarly to Seh1 and Nup85 heterodimer [Siniossoglou et al., 1996, Lutzmann et al., 2002, Brohawn et al., 2008, Hsia et al., 2007, Kampmann and Blobel, 2009]. Nup145C is a product of an auto-proteolytic cleavage of precursor protein Nup145. The second product of this post-translational maturation, Nup145N, has the FG repeats domain and contributes to the 'barrier' layer of the NPC (see *Fig. 1.4*). Similarly, the vertebrate homologues of Nup145N (Nup98) and Nup145C (Nup96) are also products of alternative splicing of Nup98-Nup96 precursor mRNA [Teixeira et al., 1999].

### 1.3.2 The Nsp1 complex

The Nsp1-Nup49-Nup57 complex forms a 'barrier' layer inside the transport channel of the NPC. It is attached to the scaffold of the NPC via interaction with amino-terminal coiled-coil domain of Nic96 (*Fig. 1.4*) [Grandi et al., 1995b, Schrader et al., 2008]. All three components of the complex have FG repeat domains in their N-termini and coiled-coil regions in C-termini, which mediate the complex formation (*Fig. 1.3* and *Fig. 1.7 A*). Nsp1 is also a component of the cytoplasmic Nup82-Nup159-Nsp1 complex (see below) [Grandi et al., 1993, Grandi et al., 1995a, Schlaich et al., 1997]. The coiled-coil domain of Nsp1 is organized into four  $\alpha$ -helices (coil 1-4). *In vitro* reconstitution study, revealed that coiled-coil region 2 of Nsp1 binds to Nup57 and Nup82 in a competitive

manner. Moreover, temperature-sensitive mutation in coil 1, leads to a strong mRNA export defect, while mutations in coil 3 and coil 4 cause lack of Nic96 association with the Nsp1-Nup49-Nup57 complex [Bailer et al., 2001]. The orthologous Nup62-Nup58-Nup54 complex in vertebrates has similar organization to yeast Nsp1 module and associates with Nic96 homologue - Nup93 [Grandi et al., 1997]. The crystal structures of coiled-coil domains of Nup58-Nup54 and Nup62-Nup54 hetero-dimers, have shown that Nup58 and Nup62 interact with two distinct regions of Nup54 and weak interaction of Nup58-Nup54 allows the sliding movement between two conformations of formed oligomers. According to this observation it has been proposed that upon rearrangement of Nup58-Nup54 ring the diameter of the central channel can expand from ~20 nm to ~40 nm, allowing the translocation of larger cargo through the NPC [Melcák et al., 2007, Solmaz et al., 2011, Solmaz et al., 2013].

### **1.3.3 The Nup82 complex forms a cytoplasmic gate of the NPC**

Another well-characterized NPC module, the Nup82 complex, is exclusively located at the cytoplasmic side of the NPC and predominantly involved in nuclear mRNA export [Grandi et al., 1995a, Kraemer et al., 1995, Del Priore et al., 1997, Belgareh et al., 1998, Ren et al., 2010, Noble et al., 2011]. Initially, the purified Nup82 complex (Fig. 1.7 A) was suggested to consist of three subunits (Nup82, Nsp1 and Nup159), which bind each other through their carboxy-terminal  $\alpha$ -helical domains via intermolecular coiled-coil interaction [Grandi et al., 1995a, Gorsch et al., 1995, Hurwitz and Blobel, 1995, Belgareh et al., 1998, Rout et al., 2000]. Later on, additional components interacting with the Nup82 complex such as Nup116, Gle2 [Bailer et al., 2000, Ho et al., 2000], Dbp5 and Gle1 [Hodge et al., 1999, Weirich et al., 2004, Noble et al., 2011], as well as Dyn2 [Stelter et al., 2007] were discovered. It has been shown that the largest protein of the Nup82 complex - the Nup159 carries a conserved  $\beta$ -propeller domain at its amino-terminus, recruiting the cytoplasmic DEAD-box RNA helicase Dbp5 and its

cofactor Gle1, thus is involved in termination of the mRNA export at the cytoplasmic pore filaments [Hodge et al., 1999]. The ATPase activity of Dbp5 is triggered by inositol hexakisphosphate (InsP<sub>6</sub>)-bound Gle1 to mediate dismantling of mRNA-protein (mRNP) complexes [Grandi et al., 1995a, Noble et al., 2011, Montpetit et al., 2011].

The Nup159's  $\alpha$ -helically predicted C-terminal domain is essential for its targeting to the Nup82 module and complex assembly [Del Priore et al., 1997, Belgareh et al., 1998]. Between  $\alpha$ -helical C-domain and amino-terminal seven-bladed  $\beta$ -propeller (Fig. 1.7 C) the Nup159 molecule has a long unstructured region, consisting of repeated FG stretches, which are not necessary for the efficient mRNA transport (Fig. 1.7 A) [Del Priore et al., 1997, Weirich et al., 2004, Tran et al., 2007]. Similar to Nup159, Nup82 carries a  $\beta$ -propeller at the N-terminus, which has been crystallized together with an autocatalytic domain of Nup116 and a short tail peptide of Nup159 (Fig. 1.7 B). The extensively decorated seven-bladed  $\beta$ -propeller of Nup82 anchors both an amphipathic  $\alpha$ -helix of Nup159 and the  $\beta$ -stranded arrangement of Nup116's carboxy-terminal part, without direct contact between Nup159 and Nup116 fragments [Yoshida et al., 2011]. Besides the  $\beta$ -propeller, Nup82 possesses a predicted  $\alpha$ -helical segment on the carboxy-terminal, involved in Nup82 complex assembly [Grandi et al., 1995b, Hurwitz and Blobel, 1995]. Nup82 was proposed to act as a docking site for a core complex composed of FG repeat domain-containing nucleoporins Nup159 and Nsp1. Deletion within the carboxy-terminal domain of Nup82 destabilizes its interaction with Nsp1 and Nup159, but does not affect the interaction between Nup159 and Nsp1 [Belgareh et al., 1998]. Nsp1 is the third member of the Nup82 complex, also present in the Nsp1-Nup49-Nup57-Nic96 module (see *Section 1.3.2*) [Hurt, 1988, Grandi et al., 1995a, Solmaz et al., 2011].

In yeast, the small protein dynein light chain (Dyn2), involved in cytoskeleton formation, turned out to be the fourth component of the Nup82 complex [Stelter et al., 2007]. Dyn2 binds to a series of five short linear motifs (DID<sub>Nup159</sub> - Dynein light chain Interacting Domain) inserted between the FG repeats and C-domain of Nup159 (Fig. 1.7

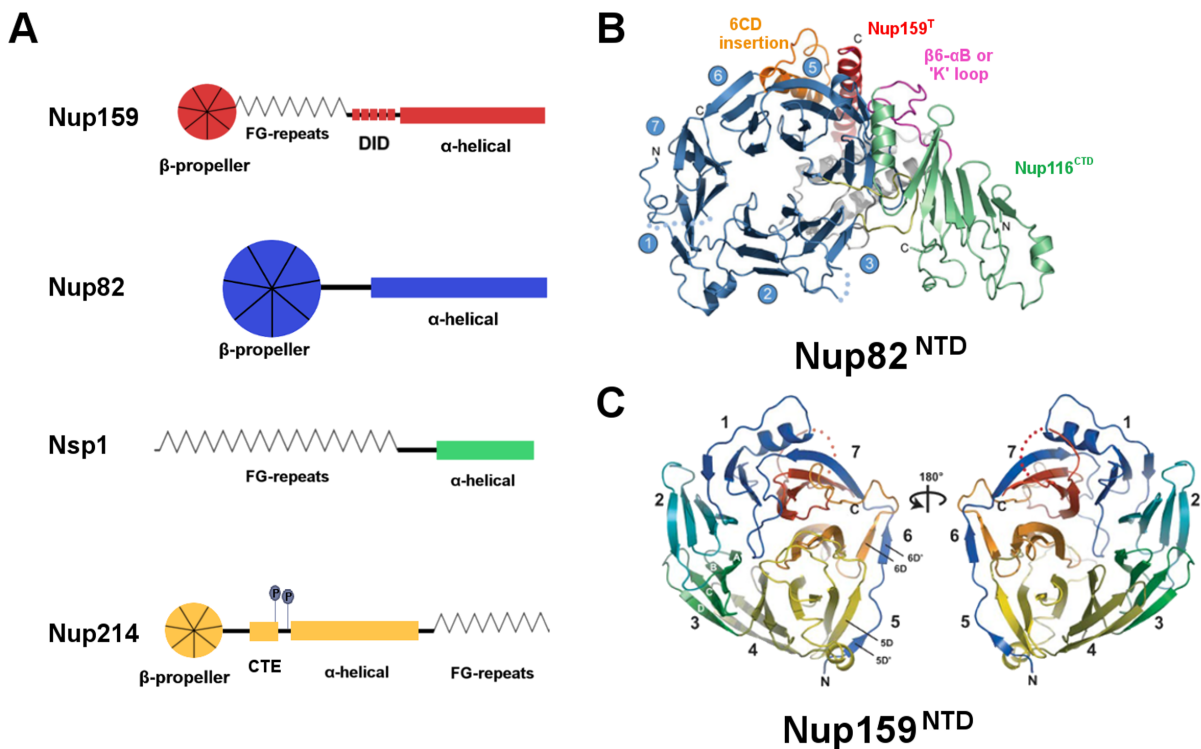


**Figure 1.7:** The architecture of yeast Nup82 complex and human Nup214/CAN

(**A**) Schematic organization of the yeast Nup82 complex and human Nup214/CAN homologue of Nup159. DID, dynein light chain interacting domain of Nup159; CTE domain, C-terminal extended peptide segment. The human Nup214 is longer than yeast Nup159 and its FG repeat domain is at the C-terminus. CTE domain is phosphorylated, marked with P in circles. Prepared according to [Bailer et al., 2001, Weirich et al., 2004, Napetschnig et al., 2007, Yoshida et al., 2011]. (**B**) The crystal structure of the Nup82 amino-terminal  $\beta$ -propeller with Nup116 C-terminal domain and short peptide of Nup159 (tail). The Nup82  $\beta$ -propeller (blue), anchors the carboxy-terminal fragment of Nup116 (green) and the carboxy-terminal tail of Nup159 (red), NTD - N-terminal Domain. Adapted from [Yoshida et al., 2011]. (**C**) The crystal structure of the Nup159  $\beta$ -propeller. Ribbon-represented structure of the amino-terminus seven-bladed  $\beta$ -propeller of Nup159, involved in mRNA export. Adapted from [Weirich et al., 2004].

A). Electron microscopy showed that upon binding of five Dyn2 dimers to recognition motifs of DID<sub>Nup159</sub>, a  $\sim 20$  nm long rigid rod-like structure of two dimerized DID<sub>Nup159</sub> stretches is formed, which could help to protrude Nup159's FG repeats and  $\beta$ -propeller from the NPC into the cytoplasm [Stelter et al., 2007]. Nup159 molecule harbours six linear Dyn2 recognition motifs with characteristic QT (glutamine, threonine) residues, separated by short linkers. Only five out of six motifs bind Dyn2 dimers *in vivo*. Dyn2 is a yeast orthologue of the molecular hub protein DLC8 (dynein light chain), present in dynein motor complex [Vallee et al., 2004] and is abundantly interacting with a wide

spectrum of proteins not related to microtubule-based transport. DLC8 binds preferably to disordered parts of proteins, often in the proximity of coiled-coil domains, increasing their stability [Wang et al., 2004, Rapali et al., 2011, Nyarko et al., 2013]. Upon binding, DLC8 dimers promote self-association of disordered proteins and its structural rearrangement [Barbar, 2008].

A newly developed pulse-chase method, monitoring the time-dependent assembly of the Nup82 complex *in vivo*, revealed that Dyn2 was incorporated into the Nup82 complex with a 5-10 minutes delay. This finding suggests that Dyn2 recruitment occurs after incorporation of the entire module into the NPC [Stelter et al., 2012]. Thus, Dyn2-stabilized dimerization of the Nup82 complex may be an indicator for final assembly into the NPC scaffold. Previously, additional roles of the Nup82 complex has been described, such as inheritance of the NPC from yeast mother to daughter cells [Makio et al., 2013]. Moreover, Nsp1 and Nup159 were reported to be susceptible for oxidative stress-dependent degradation, which allows distinction between undamaged and damaged NPCs during yeast budding [Mason et al., 2005]. This finding implies that yeast Nup82 complex is also involved in NPC quality control during segregation of newly assembled NPCs into the daughter cells.

In higher eukaryotes, the vertebrate homologue proteins of Nup82 (Nup82), Nup159 (Nup214/CAN) and Nsp1 (Nup62) are thought to constitute an orthologous Nup88 complex, but biochemical evidence for such a hetero-trimer does not exist (apart from the association between Nup88 and Nup214/CAN) [Kraemer et al., 1994, Wu et al., 1995, Fornerod et al., 1997, Martínez et al., 1999]. Nup88 and Nup214 have a similar domain organization with amino-terminal  $\beta$ -propellers and C-terminal  $\alpha$ -helical domains when compared to the yeast Nup82 and Nup159, respectively. However, in Nup214 FG repeat sequences are attached to the C-terminus of  $\alpha$ -helical domain (Fig. 1.7 A). The human protein Nup214/CAN has another domain, named CTE (C-terminal extended peptide segment), which undergoes phosphorylation events important for regulation of

Nup214/CAN function [Napetschnig et al., 2007].

Both *NUP214* and *NUP88* in human are often linked to cancer [Köhler and Hurt, 2010], such that Nup88 is overexpressed in a broad spectrum of human malignant tumors [Martínez et al., 1999], and *NUP214* is frequently found in a chromosomal rearrangements related to leukemia [Lindern et al., 1992]. Additionally, Nup358/RanBP2, which only exists in higher eukaryotes and is absent from fungi, interacts with Nup88 and constitutes a 36 nm long and 5 nm thick cytoplasmic filament of the NPC, providing a multi-binding site for the nucleoplasmic transport machinery (see Fig. 1.4) [Delphin et al., 1997, Bernad et al., 2004, Lin et al., 2013]. Nup214 is involved in nuclear mRNA export and recruits the DEAD-box helicase (Ddx19), which is analogous to Dbp5 recruitment to the Nup159 [Napetschnig et al., 2007, Montpetit et al., 2011].

## 1.4 Nucleocytoplasmic transport across the NPC

The permeability barrier of the NPC, formed by nucleoporins harbouring the FG repeat domains (see *Section 1.2*), enables molecules bigger than  $\sim 40$  kDa to be actively transported with the help of nuclear transport receptors ( $\beta$ -karyopherins) and small GTPase Ran. Molecules smaller than 40 kDa (ions, small proteins etc.) passively diffuse across the NPC [Terry and Wentz, 2009]. Nuclear transport receptors bind cargo either directly or via adaptor proteins, shuttle between cytoplasm and nucleoplasm via transient interaction with FG repeat domains, while passing the NPC and release their cargo into the cytoplasm or the nucleus [Bayliss et al., 1999, Chook and Blobel, 1999, Görlich and Kutay, 1999, Lee et al., 2000, Bayliss et al., 2000]. To impose directionality of the transport a gradient of RanGTP/RanGDP must be retained across the nuclear membrane. This state is controlled by the Ran GTPase factors: small G protein - Ran, GTP, GDP, GEF (guanine nucleotide exchange factor) and GAP (GTPase activating protein). Ran can switch between a GDP- and GTP-bound states, with the help of two effectors

GAP (converting RanGTP into RanGDP) and GEF (exchanging GDP for GTP). Ran GTP-hydrolysis is the source of energy for the nuclear transport machinery (Fig. 1.8) [Nachury and Weis, 1999, Fried and Kutay, 2003, Izaurralde et al., 1997].

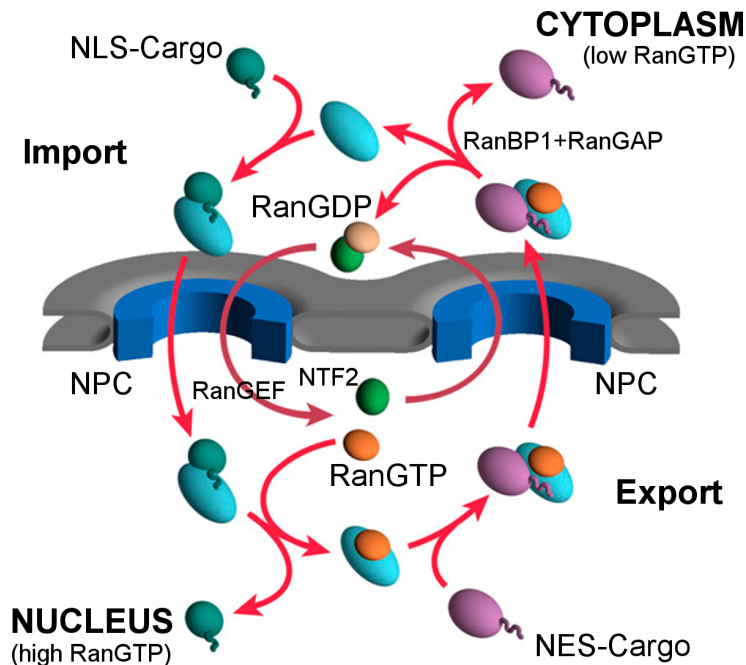


**Figure 1.8:** Simplified model of RanGTP/RanGDP-mediated transport across the NPC

The direction of the karyopherin-mediated transport, through the NPC (blue rings), is determined by the RanGTP/RanGDP gradient. Exportins (light blue) bound to RanGTP (orange) transport cargo (violet) out of the nucleus, while importins transport NLS-cargo (dark green) into the nucleus. Ran GTPase contributes to the transport process by modulating the transport receptor-cargo interaction. Ran has two homologues in yeast, termed Gsp1 and Gsp2 [Görllich and Kutay, 1999]. Modified from [Aitchison and Rout, 2012].

The nucleocytoplasmic transport starts with the formation of the transport receptor-cargo complex, which is translocated through the NPC via FG repeats meshwork. Importins bind their cargo in the cytoplasm, transport and release it in the nucleus, upon RanGTP binding and conformational changes. RanGTP is concentrated in the nucleus due to the Ntf2-mediated nuclear import of RanGDP, which is then converted to RanGTP by RanGEF (Fig. 1.8) [Ribbeck et al., 1998, Bayliss et al., 1999]. In addition, RanGTP can bind to the exportin-cargo complex and facilitate its export outside the nucleus. In the cytoplasm, binding of RanGAP and RanBP1 stimulates the GTP hydrolysis and re-

leases the cargo and RanGDP into the cytoplasm [Izaurralde et al., 1997, Görlich and Kutay, 1999, Güttler and Görlich, 2011].

Karyopherins transport most of the proteins, macromolecules and ribonucleoproteins (RNPs), whereas the mRNA export requires a different transport receptor Mex67-Mtr2 [Segref et al., 1997, Katahira et al., 1999, Strässer et al., 2000], which contains a characteristic NTF2 (nuclear transport factor 2) fold. Mex67-Mtr2 in yeast (TAP-p15 or NXF1-NXT1 in metazoan) is also involved in the export of pre-60S ribosomes during the ribosome biogenesis (together with Arx1 and Xpo1) [Yao et al., 2007, Bradatsch et al., 2007].

The arrangement of the FG repeat domains in the central channel and translocation mechanism through the NPC are still under debate. The unfolded FG domains are characteristic for intrinsically disordered protein domains, observed in proteins undergoing structural rearrangements upon ligands binding. The FG domains adopt different configurations (globular, collapsed coil or dynamic, extended coil) and can inter- and intra-interact with each other [Yamada et al., 2010, Tetenbaum-Novatt and Rout, 2010]. Several transport models have been proposed and each of them postulates the importance of the temporary contacts of nuclear transport receptors-cargo complexes with the FG-rich repeat sequences [Fried and Kutay, 2003, Peters, 2009a].

The 'Brownian affinity gate model' was proposed by Rout and coworkers, suggesting that FG-nucleoporins, located at the cytoplasmic and nucleoplasmic sides of the NPC, serve as initial docking sites for the nuclear transport receptors (NTR). Once NTR-cargo complexes enter the aqueous channel, they become trapped, and the probability of passing the channel by Brownian motion rises. This model depends on the concentration of NTR-cargo complexes at the entrance of the NPC, but does not clearly explain the movement of large cargo through the narrow translocation channel. Moreover, it was demonstrated that docking sites at the cytoplasmic side of the NPC are not required for efficient protein import (Fig. 1.9) [Rout et al., 2000, Walther et al., 2002, Rout et al.,

2003].

The 'selective phase model' of Ribbeck and coworkers suggests the existence of a selective layer inside the channel, formed by FG nucleoporins self-interacting via their disordered FG repeat domains. Transport receptors with cargo can permeate this barrier by interacting with phenylalanine-glycine residues, thus dismantling the Phe-Gly meshwork. It has been shown that recombinant FG domains can form a hydrogen-like phase, which is able to rapidly transverse NTR-cargo complexes [Ribbeck and Görlich, 2001, Frey et al., 2006].

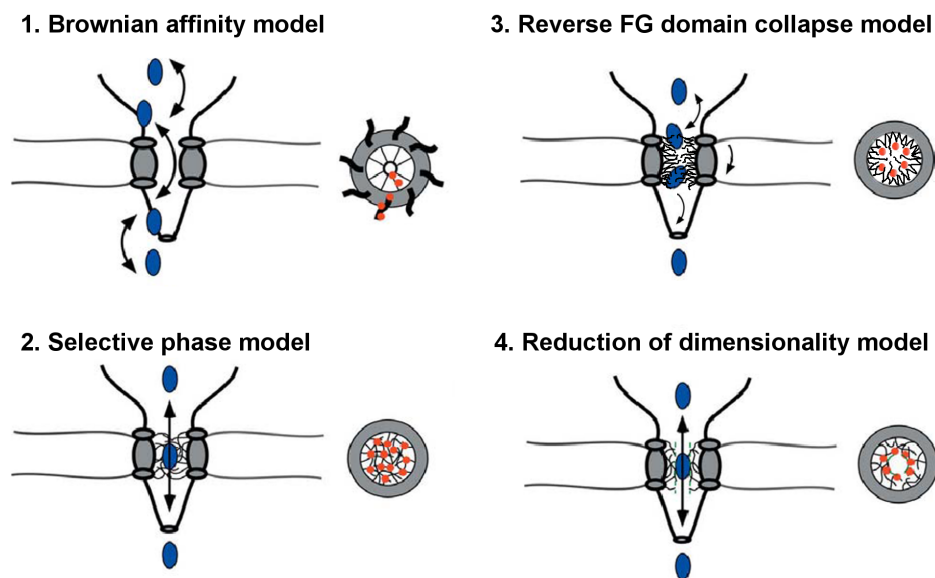


**Figure 1.9:** Models of cargo translocation across the NPC

1. The 'Brownian affinity model' proposes that the nuclear transport receptor-cargo complex (blue and red) initially binds to the cytoplasmic filaments of the NPC, increasing probability of the entrance into the interior.
2. The 'selective phase model' claims the flexible meshwork of 'barrier' nucleoporins, forming a self-interacting FG repeat network, which is dissolved by the NTR-cargo complex passing the channel.
3. In 'reverse FG domain collapse model' FG domains form a 'brush'-like barrier around the NPC's entries, which collapses locally upon NTR-cargo binding.
4. The 'reduction of dimensionality (ROD) model' postulates the co-existence of ~10 nm wide central channel surrounded by flexible layer of FG repeat domains, being pushed aside by the NTR-cargo complex during the translocation process. Modified from [Fried and Kutay, 2003].

The third hypothesis, the 'reverse FG domain collapse model' of Lim and coworkers postulates that the surface-tethered FG repeat domains form 'brush'-like structures, undergoing a reversible, local collapse upon the NTR-cargo complex binding (Fig. 1.9).

Inside the transport channel, the transport complex temporarily binds FG domains until it reaches the transport channel exit and is released by the interaction with RanGTP [Lim et al., 2007].

The 'reduction of dimensionality (ROD) model' proposes that the selective phase of FG domains form one coherent layer on the transport channel wall, leaving an open 10 nm wide tube. This allows free diffusion of small molecules and simultaneous facilitated translocation through the channel of transport complexes, which bind to the FG repeat surface and pass a permeable layer of the FG meshwork. Additionally, this organization assumes certain flexibility of the central channel and allows large assemblies, like ribosomes, to pass the NPC [Peters, 2009b, Terry and Wentz, 2009].

## 1.5 The Aim of the PhD

The 'entrance' question for my doctoral studies had arisen from an earlier discovery in the Hurt lab that dynein light chain (Dyn2) is part of the Nup82 complex in *Saccharomyces cerevisiae*, but the exact function of this interaction remained unknown. However, it had been suggested that dynein light chain, when assembled into the Nup82 complex, could help to position and expose the natively unfolded Phe-Gly domains of Nup159 into the NPC transport channel [Stelter et al., 2007]. During my initial studies in collaboration with Dr. Philipp Stelter in the lab, we noticed that Dyn2 enters the Nup82 complex *in vivo* with certain delay. This finding could be obtained with a novel pulse-chase approach, monitoring *de novo* synthesized Nup82 [Stelter et al., 2012].

Although the Nup82 complex has been genetically and biochemically studied over the past two decades, its structure remained elusive. Only partial structural data were obtained for the  $\beta$ -propeller domains of Nup159 and Nup82 [Weirich et al., 2004, Yoshida et al., 2011]. Therefore, I aimed to perform a structural characterization of the yeast Nup82 complex, which was reconstituted *in vivo* and subsequently isolated by affinity purification. This achievement finally allowed me to analyze the essential carboxy-terminal domain of Nup159, which turned out to be the structural platform for assembly of the Nup82 complex.

## 2 Results

### 2.1 Bioinformatic analysis of the structurally important regions of Nup159, an essential component of the Nup82 complex

All three nucleoporins of the Nup82 complex - Nup159, Nup82 and Nsp1 are essential in yeast, but only its predicted coiled-coil domains are required for cell viability [Del Priore et al., 1997]. Moreover, biochemical studies revealed that through these C-terminal coiled-coil domains all three subunits of the Nup82 complex interact (Fig. 2.1) [Belgareh et al., 1998, Bailer et al., 2001]. Additionally, Nup82 was proposed to be a platform recruiting the FG-repeat-containing components of the complex (Nsp1 and Nup159) to the NPC [Del Priore et al., 1997, Yoshida et al., 2011]. I focused my interest on Nup159, which may play a role in forming the higher-order structure of the NPC [Stelter et al., 2012]. Nup159 consists of four domains: an amino-terminal  $\beta$ -propeller, the FG domain, the DID motif (dynein light chain interacting domain) and the  $\alpha$ -helical C-domain that includes coiled-coil motifs (Fig. 2.1). The FG domains of both Nup159 and Nsp1 are dispensable for cell viability, while deletions of crystallized  $\beta$ -propellers of either Nup159 or Nup82 lead to temperature-sensitive phenotype [Nehrbass et al., 1990, Grandi et al., 1995a, Weirich et al., 2004, Yoshida et al., 2011].

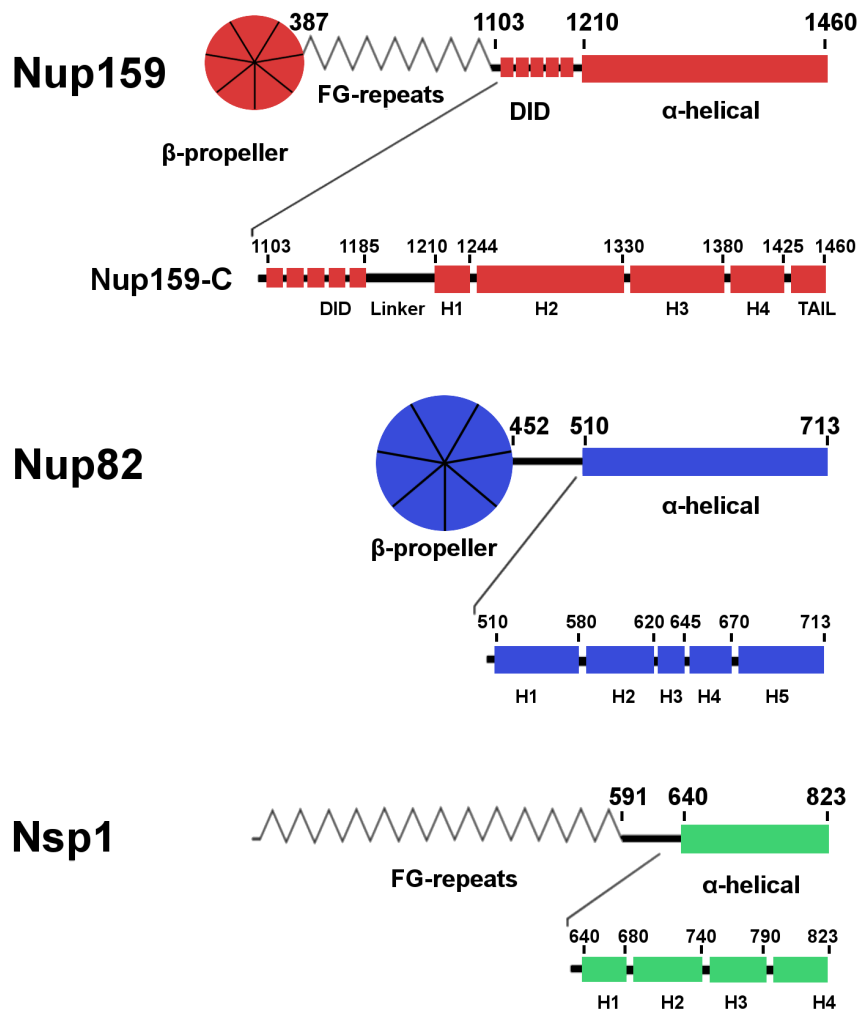


**Figure 2.1:** Architecture of  $\alpha$ -helical domains of Nup159, Nup82 and Nsp1

Domain organization of three components of the Nup82 complex. Amino acid positions are indicated above each scheme and architecture of the C-terminal domains of Nup159, Nup82 and Nsp1 is depicted on the enlarged schemes. The  $\alpha$ -helical sub-domains were defined according to secondary structure predictions (not in scale).

To gain insight into Nup82 complex assembly, I analysed the essential C-terminal domain of Nup159 (Nup159-C), which anchors it to the NPC. To determine which part of the Nup159-C domain is involved in the assembly into the Nup82 complex, I performed a bio-computational analysis, which defined shorter sub-regions of Nup159-C: a Linker sequence after the DID<sub>Nup159</sub> motif,  $\alpha$ -helically predicted regions 1-4 (H1-H4) and previously crystallized tail peptide (tail), bound to the  $\beta$ -propeller of Nup82 (Fig. 2.2).



Within all four  $\alpha$ -helical segments of Nup159-C domain, heptad repeat patterns were observed, which are characteristic for coiled-coil interactions.

## 2.2 An essential $\alpha$ -helical sub-region of Nup159-C is required for the Nup82 complex assembly

To identify, which sub-region of the Nup159-C is required for its targeting to the Nup82 complex, I made deletions within the Nup159-C domain and tested them for complementation of the *nup159* $\Delta$  shuffle strain. Cells were transformed with plasmids carrying *nup159* mutants, under the native *NUP159* promoter. Next, they were spotted in 10-fold serial dilutions on SDC+5-FOA plates, to obtain cells, which have lost the *URA3* shuffle plasmid, expressing the wild-type *NUP159* gene. When grown at different temperatures, some *nup159-C* mutants showed a temperature-sensitive growth defect (Fig. 2.3 A). To exclude that observed defects were caused by reduced amounts of *nup159* mutant proteins, I tested their expression levels and those were comparable to the wild-type (Fig. 2.7 C). Most of *nup159* mutants were viable, except for *nup159* $\Delta$ H1 ( $\Delta$ 1210-1244) mutant which exhibited lethality at all tested temperatures (Fig. 2.3 A). Thus, the essential region of Nup159-C domain, crucial for yeast cell viability, was identified. This 33 amino-acid long sequence, called helix 1, has a typical heptad repeat pattern (*hxxhcxc*, *h* - hydrophobic and *c* - charged amino-acid residues) frequently observed in coiled-coil interacting  $\alpha$ -helices (Fig. 2.2). Interestingly, deletion of the helix 2 (H2) region caused a severe growth inhibition at all tested temperatures. When two shorter sub-regions of H2 were removed (helix 2A or helix 2B), I observed less severe growth defects (Fig. 2.3 A, lanes 4, 5, 6). From these experiments I conclude that yeasts are able to tolerate severe mutations in the essential Nup159-C domain, except for the H1 domain, which is fundamental for Nup159 function.

To check if mutations of the Nup159-C influence the Dyn2-mediated dimerization of

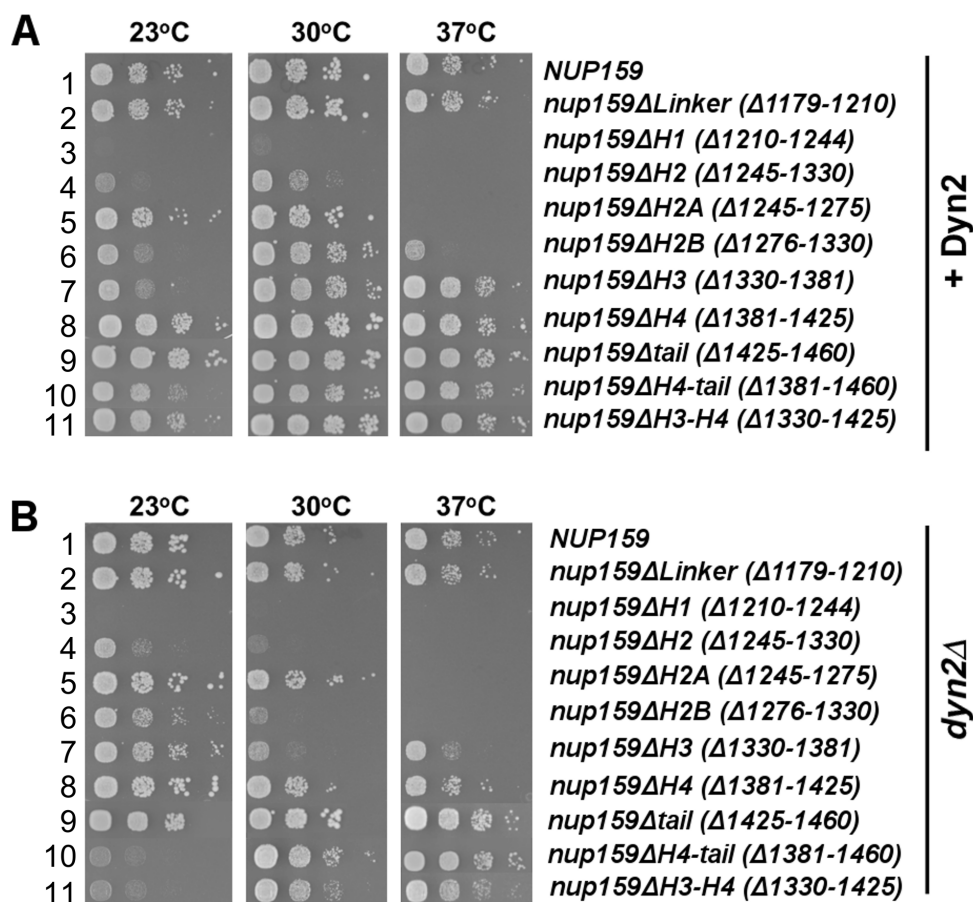


**Figure 2.3:** Dot spot analysis of *nup159* mutants in wild-type or *dyn2Δ* background

(A, B) Yeast growth was tested in a *nup159Δ* shuffle strain, transformed with the indicated *nup159* mutant constructs under the control of the endogenous *NUP159* promoter in either Dyn2 (A) or *dyn2Δ* (B) background. Cells were spotted in 10-fold serial dilutions to SDC+5-FOA plates and incubated at indicated temperatures for 5 days.

the Nup82 complex, I tested for genetic interaction between Dyn2 and *nup159* mutants. Deletion of either Dyn2 (dynein light chain) or Dyn2 Interaction Domain ( $DID_{Nup159}$ ) in yeast is not causing a growth defect [Stelter et al., 2007]. Therefore, plasmids carrying corresponding *nup159* mutations were expressed in *dyn2Δ* strain and analyzed on plates for growth (Fig. 2.3 B). Either none or slight growth inhibition was observed for all tested constructs, except for sub-regions H2, H2B and H3 (Fig. 2.3 B, lanes 4, 6, 7), which exhibited growth defects at 30 °C. Moreover, when combining deletion of two, non-essential regions of Nup159-C (e.g. H3-H4 or H4-tail), the observed growth defect

was enhanced at 23 °C (Fig. 2.3 B, lanes 10 and 11). Strikingly, *nup159* mutant lacking the Linker sub-domain adjacent to DID<sub>Nup159</sub> motif did not exhibit growth defect (Fig. 2.3 B, lane 2). Similarly, deletion of both DID<sub>Nup159</sub> and Linker regions did not affect yeast cell growth either in wild-type or *dyn2* $\Delta$  strains (Supplemental Fig. 7.1).

In summary, deletions of Nup159-C sub-regions in *dyn2* $\Delta$  strain, caused only slight growth defect in yeast, which implies that Dyn2 does not interact genetically with *nup159-C* mutants.

### 2.2.1 Mutant lacking the $\alpha$ -helical (H1) sub-region of Nup159-C loses its association with the NPC

To test, if deletions of particular sub-domains of Nup159-C influence association of Nup159 with the NPC, each mutant protein was tagged with a GFP (green fluorescent protein) and checked for cellular localization in yeast cells. The full-length GFP-Nup159 exhibited a characteristic nuclear rim staining, indicative of NPC localization (Fig. 2.4). Similarly, mutants lacking either Linker, H2, H3 or tail sub-domains also showed nuclear rim staining, with a concomitant mild NPC clustering phenotype (see Fig. 2.4, *nup159* $\Delta$ H2). In contrast the *nup159* $\Delta$ H1 mutant, lacking the essential domain of Nup159, exhibited cytoplasmic staining. This indicates that  $\alpha$ -helical region (H1) of Nup159-C is important for targeting to the NPC.

Next, I sought to characterize the essential function of the  $\alpha$ -helical domain (H1) for Nup159. For this purpose, I performed site-directed mutagenesis of H1 domain to disturb the heptad repeats in the coiled-coil region. I obtained seven mutants with single, double or triple point mutations, in which hydrophobic residues were substituted by charged amino-acids (Fig. 2.5 A). Four out of seven created mutants had no growth defects at any of tested temperatures (Fig. 2.5 B). Two mutants exhibited a lethal phenotype at all temperatures (*nup159 h1-6* and *nup159 h1-7*), suggesting that residues

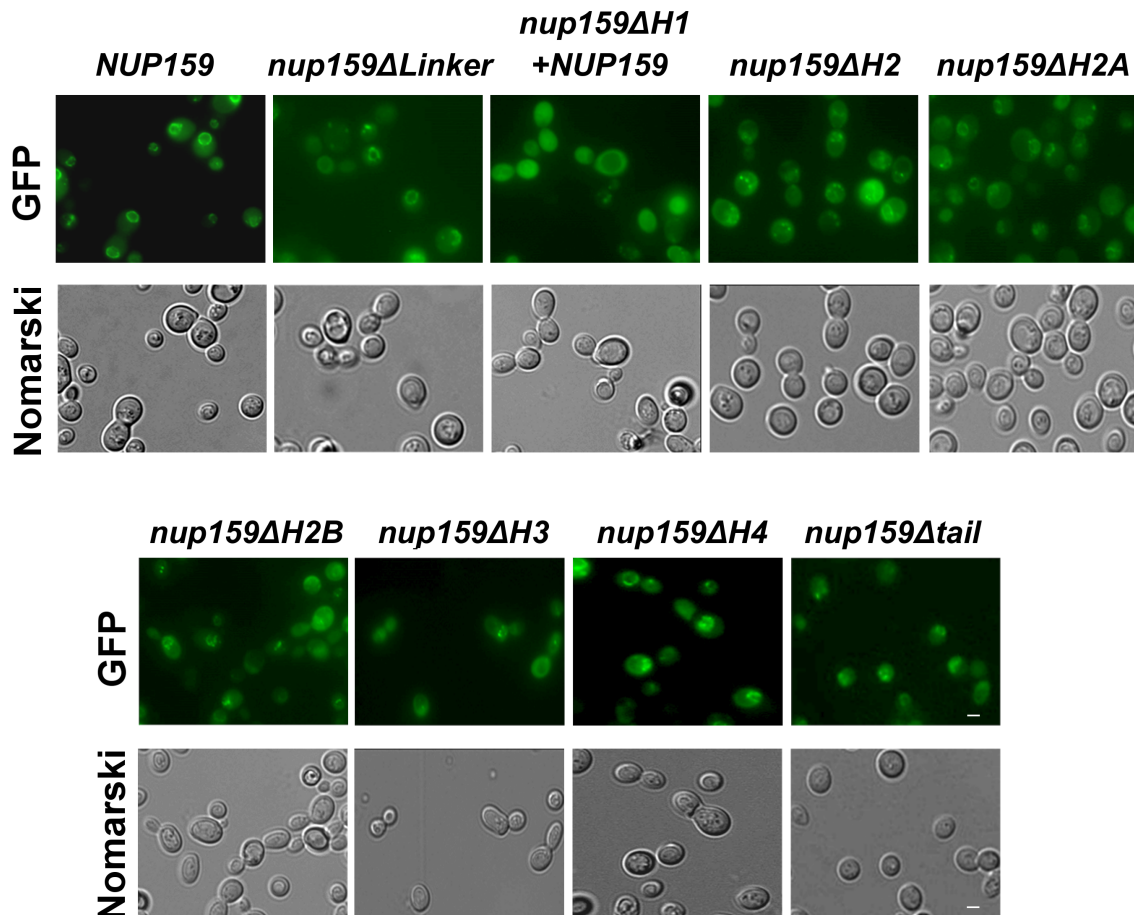


**Figure 2.4:** *In vivo* localization of GFP-*nup159-C* mutants

Cells expressing GFP-labelled wild-type Nup159 and *nup159* mutants, lacking indicated fragments of carboxy-terminal domain, were expressed under the control of an exogenous *NOPI* promoter and grown at 30 °C in YPD. The *nup159ΔH1* mutant was expressed in the presence of wild-type *NUP159* and showed mis-localization into the cytoplasm. The scale bar, 2  $\mu$ m.

Leu-1228 and Met-1235 are crucial for H1 domain function. The *nup159 h1-5* mutant, when grown at elevated temperature, showed strong temperature-sensitive phenotype, thus it was further tested for cellular localization and incorporation into the Nup82 complex.

Cells expressing GFP-tagged *nup159 h1-5* mutant lost the nuclear rim staining, indicating defect in targeting to the NPC (Fig. 2.5 C). To find out if *nup159 h1-5* mutant is assembled into the Nup82 complex, it was affinity-purified and checked for Nup82 and Nsp1 co-enrichment (Fig. 2.5 D). The isolated *nup159 h1-5* mutant co-purified neither

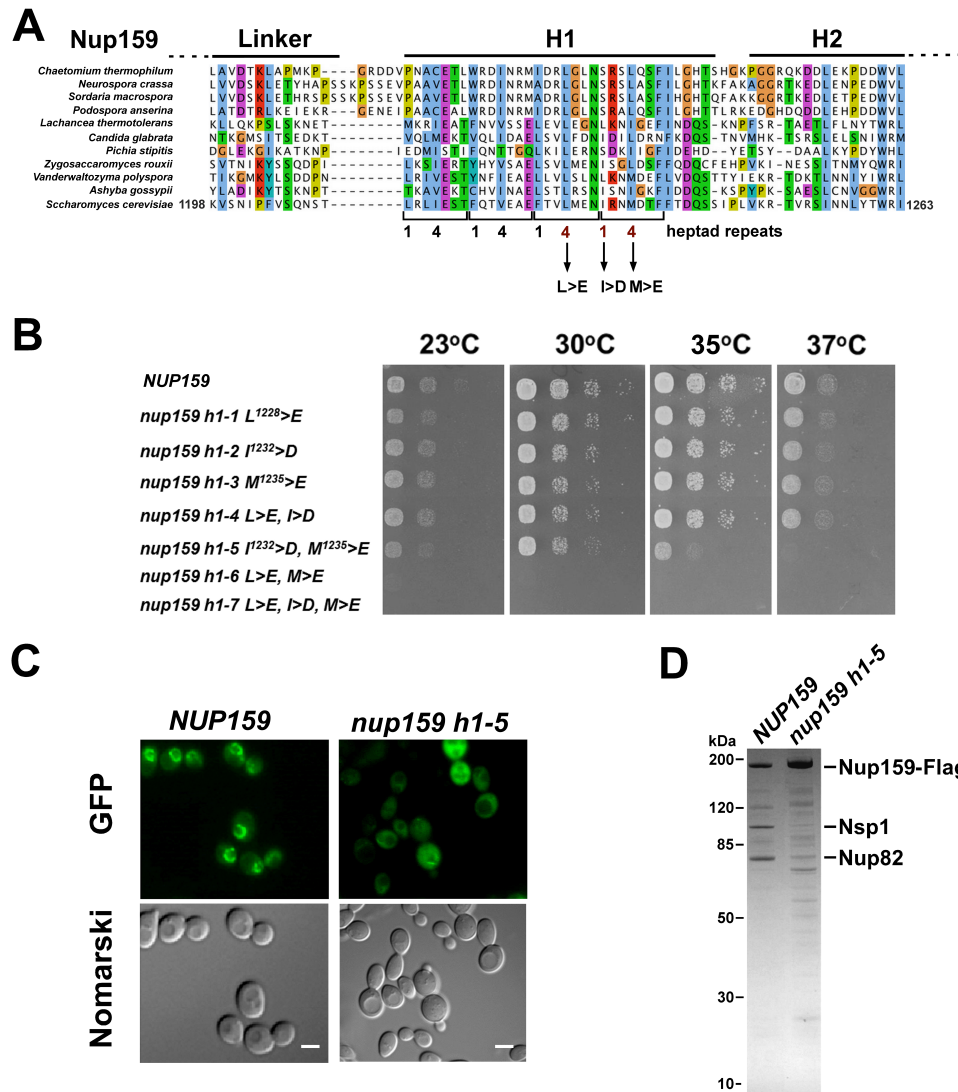


**Figure 2.5:** The essential H1 subdomain of Nup159-C is required for the Nup82 complex assembly

(A) Multi-sequence alignment of Nup159-C fragment from the indicated *fungi* species, shows conserved heptad repeats of Nup159-H1 domain. Red digits 1 and 4 with arrows (below the *S. cerevisiae* sequence) indicate mutated hydrophobic residues in the *nup159-h1* mutants. (B) Growth analysis of *nup159* $\Delta$  shuffle strain, transformed with *nup159-h1* plasmids, bearing single, double or triple point mutations in H1 domain of Nup159, expressed under control of an endogenous *NUP159* promoter. Two mutants (*nup159 h1-6* and *nup159 h1-7*) exhibited lethality and one (*nup159 h1-5*) grew slower at elevated temperatures. (C) GFP-location of wild-type *NUP159* and mutant *nup159 h1-5*, both expressed under control of an exogenous *NOP1* promoter in *nup159* $\Delta$  strain (grown at 30 °C), shows that *nup159 h1-5* mutant has lost the characteristic nuclear rim staining. Scale bar, 2  $\mu$ m. (D) Affinity-purified ProtA-TEV-Flag-Nup159 eluates from cells expressing either wild-type or mutant *nup159 h1-5* bait proteins were analyzed by SDS-PAGE and Coomassie-staining (grown at 30 °C). The Nup159 h1-5-Flag mutant shows defective Nup82 complex assembly.

Nup82 nor Nsp1, hence it was not incorporated into the complex. From these experiments I conclude that double point mutations in Nup159-H1 region disturb assembly of the Nup82 complex.

To determine the physico-chemical properties of Nup159-H1 domain and learn more what could be disturbed in the *nup159 h1-5* mutant, I expressed in *E. coli* a minimal construct containing the last two Dyn2 binding (QT) motifs within DID<sub>Nup159</sub>, followed by the Linker sequence and the H1 domain (see Fig. 2.1). Recombinant proteins (Nup159 QT<sub>4-5</sub>-Linker-H1 and *nup159* QT<sub>4-5</sub>-Linker-h1-5) were subjected to circular dichroism (CD) in the absence of Dyn2 (experiment performed in collaboration with the laboratory of Dr. Elisar Barbar, Oregon, USA). This analysis showed that the construct expressing the wild-type H1 domain forms an  $\alpha$ -helical structure with a melting temperature characteristic for coiled-coils (above 50 °C, Fig. 2.6 A). Consistent with this observation the size exclusion chromatography combined with multiangle light scattering (SEC-MALS) measurement revealed that Nup159-QT<sub>4-5</sub>-Linker-H1 can self-interact, forming most likely a homo-tetramer, while the *h1-5* mutant construct (Nup159 QT<sub>4-5</sub>-Linker-h1-5) was fully disordered and monomeric (Fig. 2.6 B-C).

Taken together this analysis showed that the essential H1 sub-region of Nup159-C is able to self-interact and form a four-stranded coiled-coil *in vitro*. Thus, self-dimerization of Nup159 *in vivo* and its optimal position in respect to DID<sub>Nup159</sub> motif may be important for assembly of the Nup82 complex.

## 2.2.2 Recruitment of dynein light chain (Dyn2) is disturbed in *nup159-C* mutants

Next, I wanted to investigate if assembly of the Nup82 complex is altered *in vivo* in *nup159* mutants. Nup82 complexes were affinity-purified from cells expressing different *nup159-C* mutant proteins in the *nup159* $\Delta$  null strain. In addition, the amount of

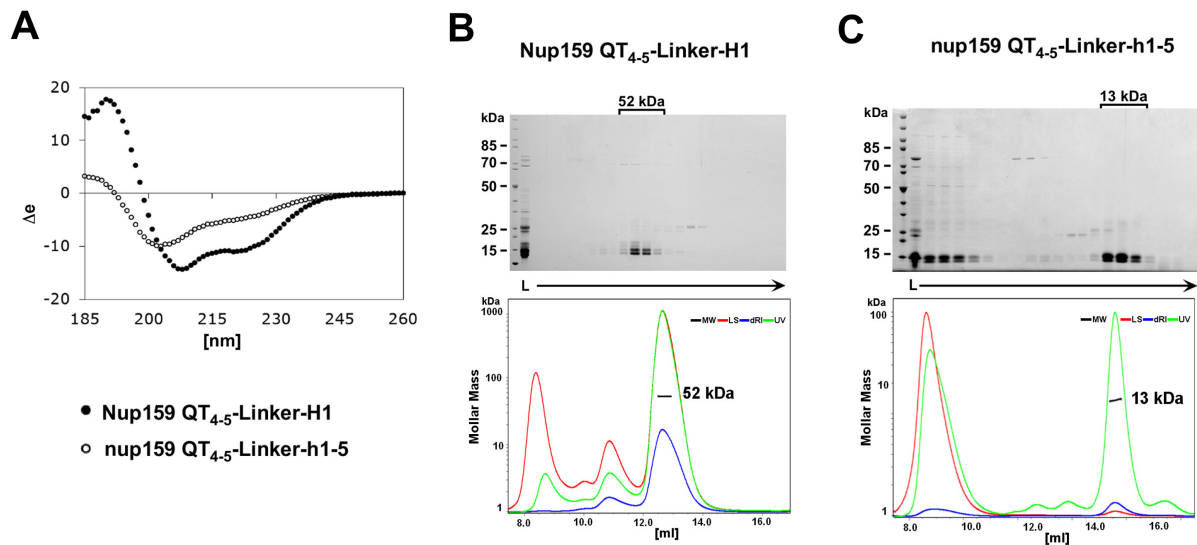


**Figure 2.6:** Heptad repeats within the Nup159-H1 sub-domain are crucial for self-dimerization *in vitro*

(A) Far UV circular dichroism spectra of affinity-purified Nup159-QT<sub>4-5</sub>-Linker-H1 (closed circles) and nup159-QT<sub>4-5</sub>-Linker-h1-5 mutant proteins (open circles), expressed in *E. coli*. Protein harbouring wild-type Nup159-H1 domain has an  $\alpha$ -helical structure as shown by two minima at 208 and 222 nm. In contrast, the nup159-QT<sub>4-5</sub>-Linker-h1-5 mutant was found fully disordered, as observed by a single signal at 203 nm and the absence of signal at 222 nm. (B, C) Size-exclusion chromatography (upper panels) coupled with multiangle light scattering measurements (lower panels) of affinity-purified wild-type Nup159-QT<sub>4-5</sub>-Linker-H1 (B) and h1-5 mutant (C) constructs, indicate a homo-oligomerization of Nup159-H1 sub-domain. Differential refractive index (blue), light scattering (red) and UV (green) are plotted against the elution volumes of Superdex 200 Increase 10/300 GL (GE Healthcare) gel filtration column. Nup159-QT<sub>4-5</sub>-Linker-H1 construct eluted as a homo-tetramer according to the MALS measurement (52 kDa), whereas h1-5 mutant was monomeric (13 kDa) or aggregated.

Dyn2, which co-purifies with Nup159 *in vivo*, was monitored by western blot (Fig. 2.7 A-B). The wild-type Nup159 was assembled into the Nup82 complex and recruited Dyn2 (lane 1); whereas deletion of H2, H2A, H2B or H3 domain caused a severe impairment of the Nup82 complex assembly (Fig. 2.7 A, lanes 3-6). Some of the mutants such as *nup159* $\Delta$ H4-tail (lane 11) or *nup159* $\Delta$ tail (lane 12) were impaired in Nup82 complex assembly, while *nup159* $\Delta$ Linker and *nup159* $\Delta$ H4, still co-purified normal amounts of the Nup82-Nup159-Nsp1 complex (Fig. 2.7 B, lanes 9 and 10). Nup159 devoid of the FG repeats was also affinity-purified as a control to monitor proper Nup82 complex formation and Dyn2 recruitment (Fig. 2.7 A, lane 7). Interestingly, the ability to recruit Dyn2 by the *nup159* $\Delta$ Linker mutant, was completely disturbed (Fig. 2.7 A, lane 2, repeated

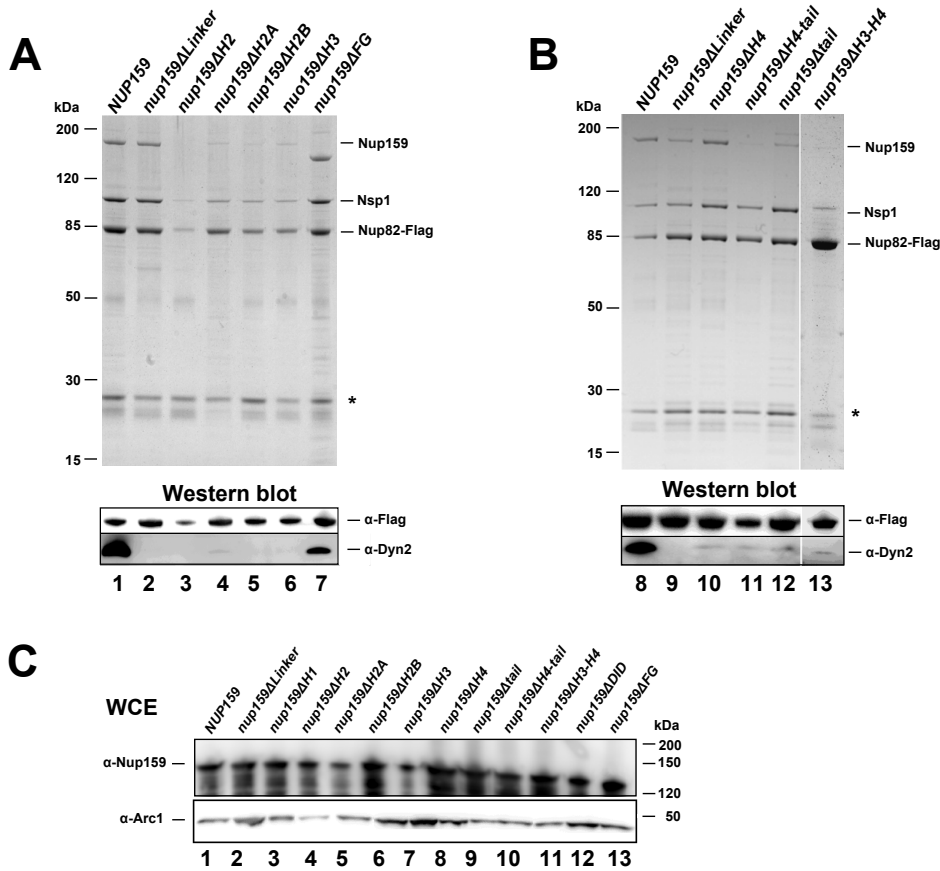


**Figure 2.7:** Mutations in the Nup159-C domain affect the proper Nup82 complex assembly *in vivo*

(A, B) Affinity-purified Nup82-Flag-TEV-ProtA eluates derived from cells expressing either wild-type or indicated *nup159-C* mutants followed by SDS-PAGE and Coomassie-staining (upper panels) or Western blotting using anti-Flag (to detect Nup82) and anti-Dyn2 antibodies (lower panels). Nup159, Nsp1 and Nup82-Flag bands are indicated on the right; \* - TEV protease. (C) Expression levels of Nup159 wild-type and *nup159-C* mutant proteins of the yeast whole cell extracts (WCE) used in this study, analyzed by SDS-PAGE and Western blotting using anti-Nup159 antibody, and anti-Arc1 antibody as loading control. All *nup159* mutants were properly expressed when grown at 30 °C.

in Fig. 2.7 B, lane 9). This unexpected finding suggests that the Linker sequence upstream of H1 sub-domain is critical for DID<sub>Nup159</sub>-Dyn2 interaction, which indicate that DID<sub>Nup159</sub> and H1 require a certain distance for optimal Dyn2 recruitment.

To further investigate impaired binding of Dyn2 to the *Nup159 $\Delta$ Linker* mutant, I checked if Dyn2 recruitment could be restored in the strain overexpressing Dyn2 (Fig. 2.8 A). Cells expressing Nup159, nup159 $\Delta$ DID and nup159 $\Delta$ Linker proteins were affinity-purified via Nup82-Flag-TEV-ProtA (Fig. 2.8 B) from strains in which Dyn2 ex-

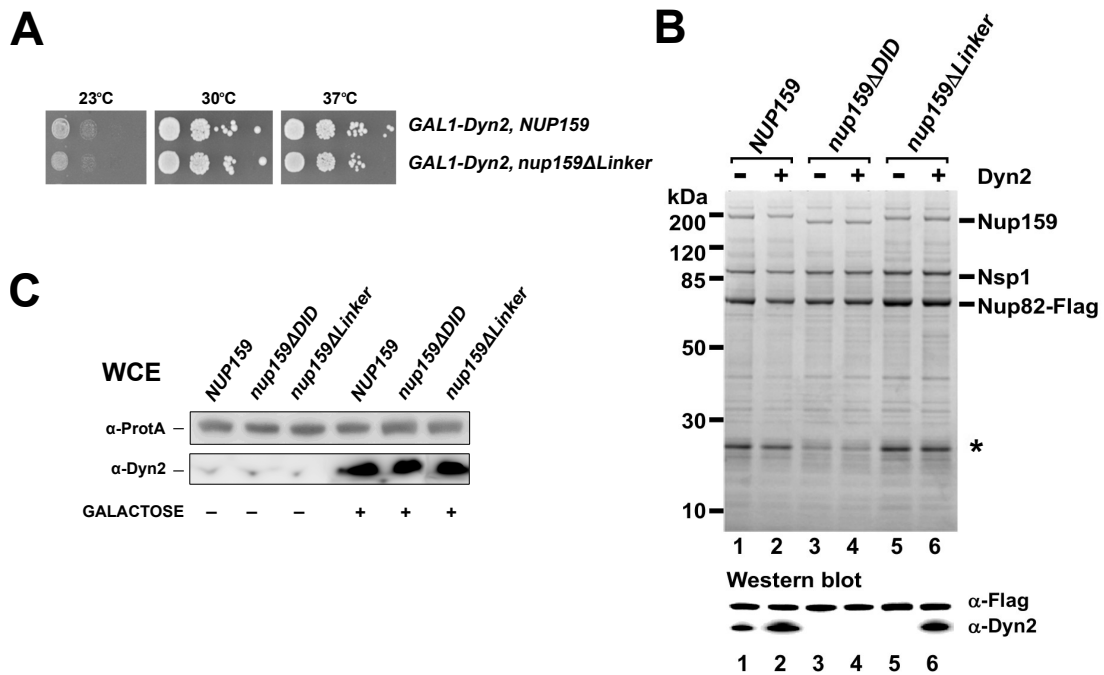


**Figure 2.8:** Overexpression of Dyn2 restores its binding to the *nup159ΔLinker* mutant

(A) Growth analysis of yeast strain expressing the *GAL1-Dyn2* plasmid in 2% galactose for 3.5 days on SGD-Leu plates. (B) Tandem affinity-purified Nup82-Flag-TEV-ProtA eluates derived from cells expressing the *GAL1-Dyn2* plasmid for Dyn2 overexpression and either wild-type or *nup159-C* mutant proteins, were analyzed by SDS-PAGE and Coomassie-staining (upper panel) or Western blotting using anti-Flag (to detect Nup82) and anti-Dyn2 antibodies (lower panel). Co-purified Nup82-Flag, Nup159, Nsp1 bands are marked on the right; \* - TEV protease. Cells were grown with (plus) or without (minus) presence of 2% galactose. (C) Expression levels of Nup82 (anti-protein A antibody) and Dyn2 proteins, detected by Western blot of the whole cell extracts (WCE). Dyn2 expression levels were monitored before (minus) or after (plus) galactose addition.

pression was under control of the inducible *GAL1* promoter. Consistently with earlier results, Dyn2 recruitment by the *nup159ΔLinker* mutant was disturbed (Fig. 2.8 B, lane 5), but it could be reversed by Dyn2 overexpression *in vivo* (Fig. 2.8 B, lane 6).

To sum up, some *nup159* mutants (e.g. *nup159ΔH2*) exhibited severe defects in the whole complex formation, whereas in others (e.g. *nup159ΔLinker*) only Dyn2 recruitment was reversibly disrupted. These data indicate that mutations in Nup159-C domain influence assembly of the Nup82 complex, suggesting multiple interactions of Nup159-C with Nup82 and Nsp1.

## 2.3 Structural analysis of the yeast Nup82 complex

### 2.3.1 Reconstitution of simplified Nup82 complexes from the yeast *Saccharomyces cerevisiae*

In order to gain insight into the structural arrangement of the Nup82 complex, we considered to express simplified Nup82 complexes in budding yeast. Although tandem affinity-purification of the endogenous Nup82 complex from yeast resulted in a biochemically stable assembly, it did not allow us to determine its precise molecular mass and subunit stoichiometry, due to the presence of the natively unstructured and flexible FG repeat sequences of Nsp1 and Nup159 (see Fig. 2.1). To determine the exact molecular mass, I sought to obtain the Nup82 complex devoid of FG repeats. For this purpose, I co-expressed in yeast four genes encoding full-length Nup82 (tagged with Flag-TEV-ProtA), Nup159 $\Delta$ FG, Nsp1-C (lacking the FG repeats) and Dyn2 under the control of inducible *GAL1* promoter (see *Materials and Methods* and Table 4.1). This approach enabled *in vivo* reconstitution of simplified Nup82 complexes. Subsequent affinity purification resulted in biochemically stable Nup82-Nup159 $\Delta$ FG-Nsp1C-Dyn2 complex devoid of FG repeat sequences (Fig. 2.9 B, lane 3). I was also able to reconstitute Nup82 complexes lacking the FG repeats and the  $\beta$ -propeller of Nup159 (Nup159-C) or lacking FG repeats, Nup159's  $\beta$ -propeller and the short tail domain of Nup159 (Nup159-C $\Delta$ tail), which is known to interact with the Nup82  $\beta$ -propeller (Fig. 2.9 B, lanes 1 and 2, respectively). Interestingly, the Nup159-C fragment lacking the tail fragment (Nup159-C $\Delta$ tail) still assembled into the Nup82 complex, which supports previous observation that Nup159-C is involved in multiple interactions with Nup82 and Nsp1.

To find out whether these Nup159 constructs are functional and incorporated into the NPC, I checked a complementation of *nup159* $\Delta$  null strain and intracellular location of GFP-Nup159 wild-type and mutant alleles under galactose-induced growth condi-

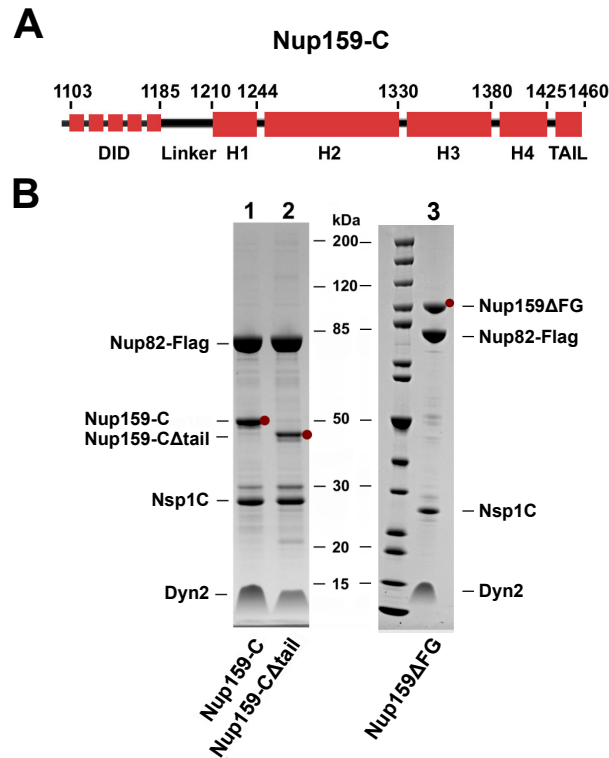


**Figure 2.9:** Reconstitution and purification of simplified Nup82 complexes

(A) Scheme of Nup159-C sub-domains. (B) Nup82 complexes devoid of FG repeat domains of Nsp1 and Nup159 were overexpressed and affinity-purified via Nup82-Flag-TEV-ProtA (lane 3). Lane 1 shows the Nup82-Flag-Nup159C-Nsp1C-Dyn2 complex, missing the  $\beta$ -propeller of Nup159, while lane 2 shows the Nup82-Flag-Nup159-C $\Delta$ tail-Nsp1C-Dyn2 complex, where Nup159-C additionally lacks the tail fragment (expressed Nup159 proteins are marked with red dots).

tions (Fig. 2.10 A-B). All three constructs (*nup159 $\Delta$ FG*, *nup159-C* and *nup159-C $\Delta$ tail*) were complementing the non-viable *nup159 $\Delta$*  null strain (Fig. 2.10 A). The *nup159 $\Delta$ FG* construct complemented noticeably better than *nup159-C* and *nup159-C $\Delta$ tail*. Cells expressing either *nup159-C* or *nup159-C $\Delta$ tail* constructs grew slower, due to lack of the amino-terminal  $\beta$ -propeller domain involved in the mRNA export. The absence of this domain leads to defects in termination of mRNA export, which results in nuclear accumulation of poly(A)<sup>+</sup> RNA and inhibition of cell growth [Del Priore et al., 1997]. GFP-tagged Nup159 $\Delta$ FG and Nup159-C proteins were localized to the nuclear periphery, indicating their assembly into the NPC (Fig. 2.10 B). In contrary, the *nup159-C $\Delta$ tail* construct, which did not rescue the growth of otherwise lethal *nup159 $\Delta$*  null strain at

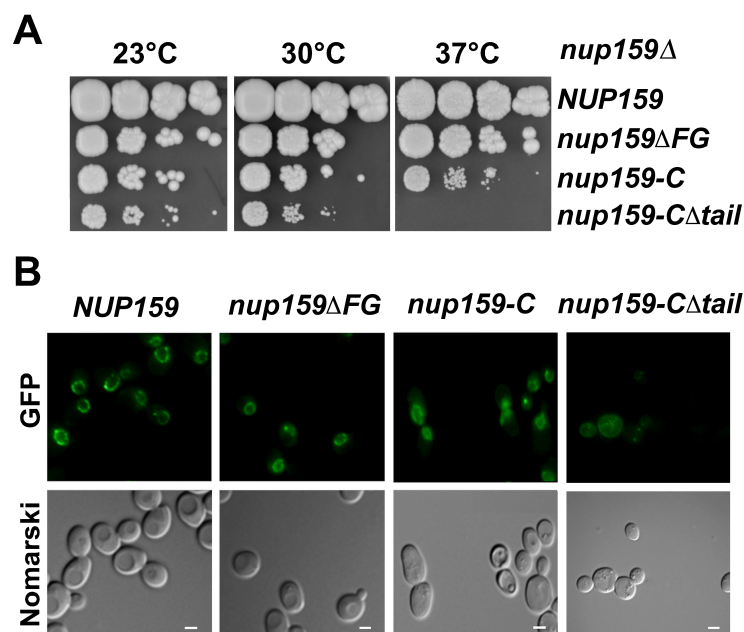


**Figure 2.10:** The *in vivo* reconstituted Nup82-Nup159C-Nsp1C-Dyn2 and Nup82-Nup159ΔFG-Nsp1C-Dyn2 complexes are functional and incorporated into the NPC

(A) Growth analysis of yeast *nup159Δ* shuffle strain, transformed with *LEU2* plasmids harbouring wild-type *NUP159* or mutant constructs under control of the *GAL1* promoter, which were used in biochemical and EM studies. The *URA3-NUP159* shuffle plasmid was shuffled out on galactose-containing SGD+5-FOA plates, yeast colonies were spotted onto YPG plates and grown for 5 days. (B) The cellular localizations of *GAL1*-induced GFP-Nup159 variants, grown at 30 °C under complementing YPG conditions, were visualized in live cells using fluorescence microscopy. Scale bar, 2 μm.

30 °C, was not incorporated into the NPC under tested conditions. From these experiments I conclude that both *nup159ΔFG* and *nup159-C* constructs were functional and assembled into the NPC in contrast to Nup159-CΔtail.

### Simplified Nup82 complexes exhibit unexpectedly large molecular masses

In order to determine the subunit composition of simplified Nup82 complexes, they were affinity-purified and fractionated on the size exclusion column (SEC). First, I analyzed the Nup82-Nup159C-Nsp1C-Dyn2 complex which eluted early from the column, suggesting much higher molecular mass than expected for a dimerized complex (Fig. 2.14 A, Table 2.1). Hence, to determine the exact molecular mass of this complex, inde-

pendently of elongated shape caused by DID<sub>Nup159</sub>-Dyn2 stalk, it was subjected to size exclusion column coupled to multiangle light scattering measurements (SEC-MALS). Precise calculations of molecular weights during MALS measurement are based on the hydrodynamic size of analyzed macromolecules and depend on samples homogeneity. Our reconstitution method of Nup82 complexes in yeasts enabled us to purify  $\mu\text{g}$  quantities of simplified Nup82 complexes, required for meaningful MALS measurements.

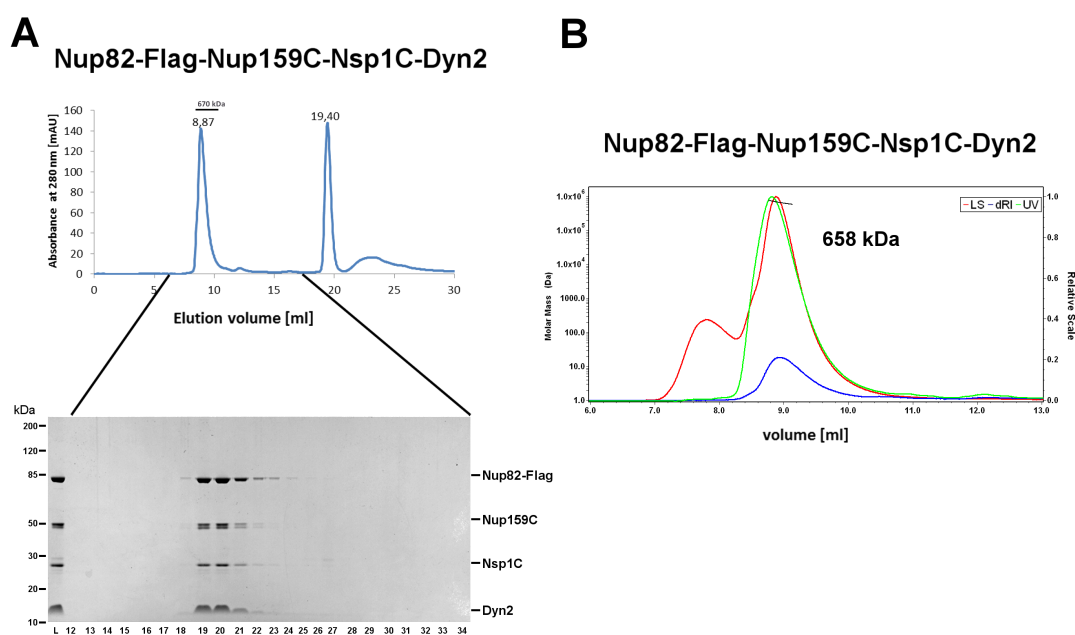


**Figure 2.11:** SEC-MALS analysis of the Nup82-Nup159C-Nsp1C-Dyn2 complex.

(A) The complex was co-expressed in yeast, affinity-purified via Nup82-Flag-TEV-ProtA and subjected to size exclusion column (Superdex 200 Increase 10/300 GL column, GE Healthcare). Gel filtration profile ( $A_{280\text{ nm}}$ ) of the Nup82-Nup159C-Nsp1C-Dyn2 complex with protein standard (670 kDa, upper panel). Indicated fractions were analyzed by SDS-PAGE and Coomassie staining (bottom panel). (B) Multiangle light scattering measurement. Differential refractive index (blue), light scattering (red) and UV (green) graphs are plotted against the elution volumes. Two individual Nup82 complex preparations were analyzed by SEC-MALS, yielding a molecular mass of  $645\pm 3$  and  $672\pm 5$  kDa, respectively, with average molecular weight of  $658\pm 4$  kDa. This value implies a 4:2:4:10 stoichiometry of the Nup82:Nup159-C:Nsp1-C:Dyn2 molecules (calculated molecular weight of Nup82, Nup159-C, Nsp1-C and Dyn2 = 82, 50, 28.5 and 10 kDa, respectively).

The theoretical molecular weight of the Nup82 complex composed of 2 copies of Nup82, 2 copies of Nup159-C, 2 copies of Nsp1-C and 10 copies of Dyn2 equals 421 kDa, while the experimentally determined molecular mass of the Nup82-Nup159C-Nsp1C-Dyn2 complex amounted to  $\sim 660$  kDa (Fig. 2.11 B). Based on this result and

the prediction that two copies of Nup159-C molecules are required for Dyn2-mediated dimerization of the complex, I concluded that more than two copies of Nup82 and Nsp1 may be present in the complex (Table 2.1). The calculated theoretical molecular weight of the complex containing 4 copies of Nup82, 2 copies of Nup159-C, 4 copies of Nsp1-C and 10 copies of Dyn2 molecules (642 kDa) indeed corresponds to the value obtained from two independent MALS measurements ( $645\pm 3$  and  $672\pm 5$  kDa), suggesting a 4:2:4:10 stoichiometry of the isolated Nup82-Nup159C-Nsp1C-Dyn2 complex.

**Table 2.1:** Calculations of theoretical molecular weight of the Nup82-Flag-Nup159C-Nsp1C-Dyn2 complex.

Theoretical molecular weights:  $M_{rNup82}=82$  kDa,  $M_{rNup159C}=50$  kDa,  $M_{rNsp1C}=28.5$  kDa,  $M_{rDyn2}=10$  kDa.

Nup82:Nup159-C:Nsp1C:Dyn2 Ratio	Theoretical Molecular Weight [kDa]
2:2:2:10	421
4:2:4:10	642
4:2:2:10	585
2:2:4:10	478

Next, the Nup82-Nup159 $\Delta$ FG-Nsp1C-Dyn2 complex, which includes the N-terminal  $\beta$ -propeller domain of Nup159, was analyzed by SEC-MALS. As expected the complex was correspondingly larger ( $M_{rNup159\Delta FG}=100$  kDa) with a molecular mass of  $746\pm 7$  kDa (Fig. 2.12 A). This result suggests the 4:2:4:10 stoichiometry of the Nup82 complex, since the calculated theoretical molecular mass of dimer with a predicted 2:2:2:10 stoichiometry only adds up to 521 kDa for the Nup82-Nup159 $\Delta$ FG-Nsp1C-Dyn2 complex.

In addition, a pentameric Nup82 complex, which harbours also the Nup116 autocatalytic C-domain, known to bind to the  $\beta$ -propeller of Nup82 [Yoshida et al., 2011], was reconstituted and isolated from yeast cells. SEC-MALS analysis indicated co-elution of all 5 subunits and a molecular mass of 693 kDa for this complex (Fig. 2.12 B). The difference between molecular masses of the Nup82-Nup159C-Nsp1C-Dyn2 and pentameric

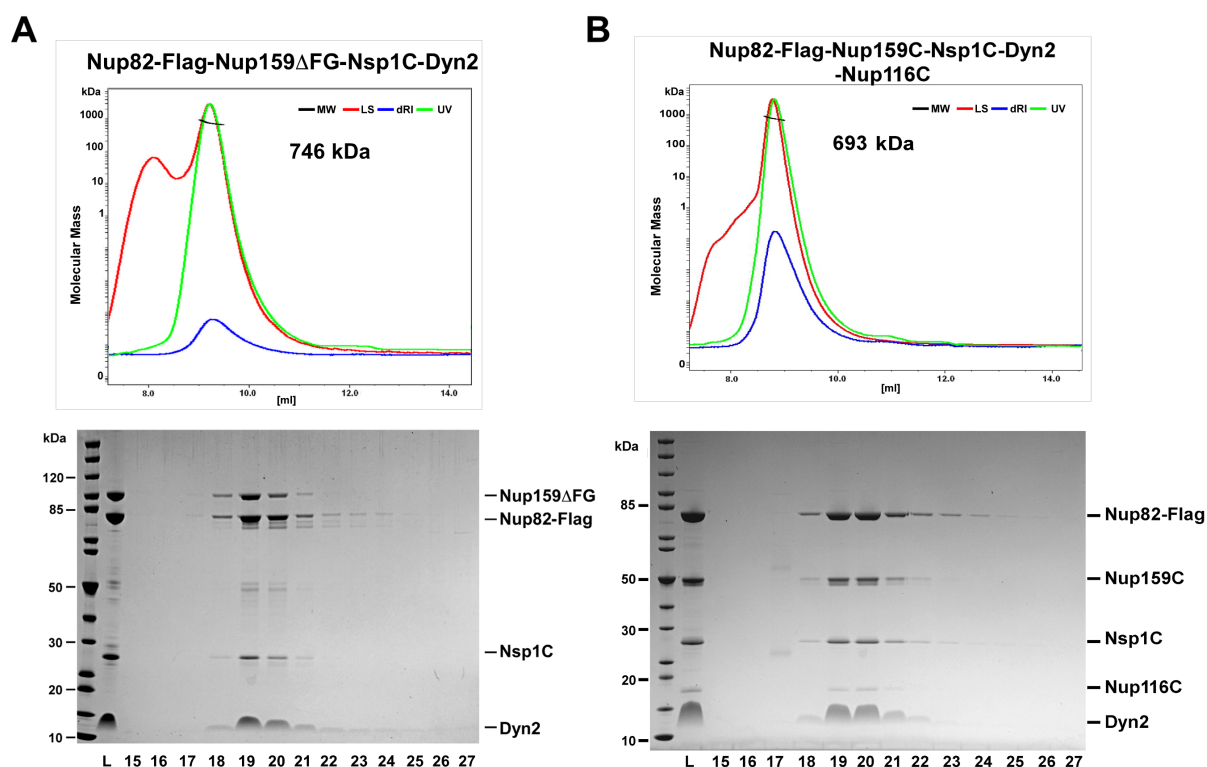


**Figure 2.12:** Molecular mass determination of reconstituted Nup82-Nup159 $\Delta$ FG-Nsp1C-Dyn2 and Nup82-Nup159C-Nsp1C-Dyn2-Nup116C complexes by SEC-MALS

**(A)** The affinity-purified Nup82-Nup159 $\Delta$ FG-Nsp1C-Dyn2 complex, revealed a molecular mass of 746 kDa (calculated molecular weight of Nup159 $\Delta$ FG, Nup82, Nsp1 and Dyn2 equal 100, 82, 28.5 and 10 kDa, respectively) by SEC-MALS analysis. Differential refractive index (blue), light scattering (red) and UV (green) were plotted against the elution volume from the Superdex 200 Increase 10/300 GL (GE Healthcare) column. **(B)** SEC-MALS analysis of the affinity-purified, pentameric Nup82-Nup159C-Nsp1C-Dyn2-Nup116C complex, revealed a molecular weight of  $693 \pm 3$  kDa (calculated molecular weight of Nup116-C equals 18 kDa).

complex with Nup116-C ( $\sim 33$  kDa) suggests two copies of Nup116-C ( $M_{r,Nup116-C}=18$  kDa) bound to only two out of four copies of Nup82  $\beta$ -propellers. In conclusion, the reconstitution of simplified Nup82 complexes in yeast allowed us to determine its molecular weight and estimate subunits composition. Remarkably, all purified Nup82 complexes resulted in large molecular masses ( $> 650$  kDa), indicating a hetero-oligomeric assembly.

### The Nup159-C domain is required to form the hetero-oligomeric Nup82 complex

To gain more detailed insight into the Nup82 complex organization, I tested minimal Nup82 complexes, expressed in yeast. First, I checked whether the stably associated Nup82-Nsp1C sub-complex homo-dimerizes without Nup159 molecules. The Nup82-Flag-Nsp1C sub-complex was affinity-purified and subjected to the SEC-MALS measurement (Fig. 2.13 A). During size exclusion chromatography the aggregated Nup82-Flag protein was found in the void volume, while the soluble Nup82-Flag-Nsp1C sub-complex resulted in molecular weight of 117 kDa, suggesting a hetero-dimeric assembly (Fig. 2.13 A).

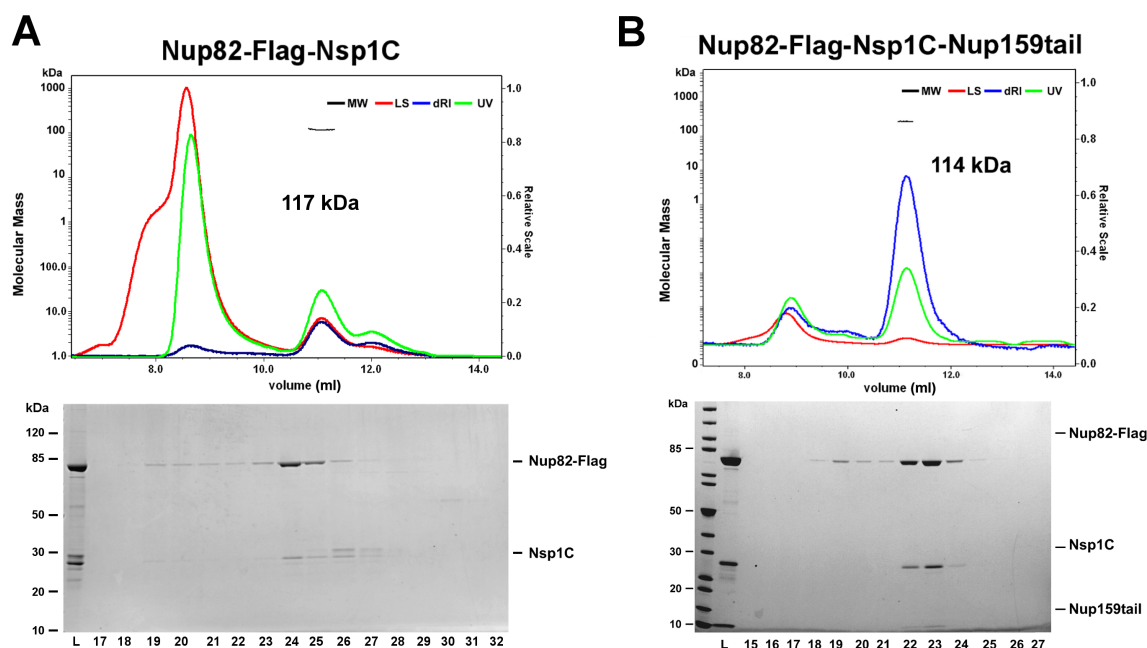


**Figure 2.13:** SEC-MALS analysis of minimal Nup82 sub-complexes

(A) The affinity-purified Nup82-Flag-Nsp1C sub-complex, co-expressed in yeast, was subjected to size exclusion chromatography combined with the multiangle light scattering measurement (SEC-MALS). Determined molecular mass of the Nup82-Flag-Nsp1C sub-complex corresponds to hetero-dimer of 117 kDa ( $M_r=111$  kDa). (B) The Nup82-Nsp1C-Nup159tail-Flag co-purifies as a hetero-trimeric complex with the molecular weight of 114 kDa, determined by SEC-MALS (theoretical  $M_r$  of 123 kDa). Differential refractive index (blue), light scattering (red) and UV (green) are plotted against the elution volume from the Superdex 200 Increase 10/300 GL (GE Healthcare) gel filtration column.

Next, I tested the *in vivo* assembly of the core Nup82-Nsp1C sub-complex co-expressed with the short Nup159-tail-Flag peptide, known to bind Nup82's  $\beta$ -propeller

[Yoshida et al., 2011]. The isolated hetero-trimeric complex behaved as a soluble monomer with MALS-determined molecular weight of 114 kDa (Fig. 2.13 B). This result indicates a 1:1:1 stoichiometry of Nup82-Nsp1C-Nup159tail-Flag sub-complex, due to its theoretical molecular weight of 123 kDa. From these experiments it became evident that the Nup159-C domain not only dimerizes the Nup82 complex but also recruits four Nup82-Nsp1C sub-complexes. Although the tail fragment of Nup159 improved solubility of the Nup82-Nsp1C sub-complex, it did not cause its dimerization. Hereby, assembly of ~660 kDa Nup82 complex requires the remaining part of the Nup159-C domain.

### **2.3.2 The structure of simplified Nup82 complexes revealed by electron microscopy**

To gain insight into the organization of subunits within the Nup82-Nup159C-Nsp1C-Dyn2 complex, it was subjected to negative staining electron microscopy (EM), performed in collaboration with Dr. Dirk Flemming (BZH, EM Facility). EM analysis of endogenous Nup82 complexes (containing FG repeats) did not allow us to obtain clear-cut particles, possibly due to interference of the natively unfolded and flexible FG repeats with the staining procedure (see Fig. 2.1). Therefore, we analyzed the Nup82 complex lacking FG repeats and the N-terminal  $\beta$ -propeller of Nup159 (Nup82-Nup159C-Nsp1C-Dyn2) or the Nup82 complex devoid only of FG repeat sequences (Nup82-Nup159 $\Delta$ FG-Nsp1C-Dyn2) by EM. Affinity-purified complexes were subsequently fractionated either on size exclusion column or on a glycerol-glutaraldehyde gradient, with gentle protein cross-linking (GraFix method, for details see *Materials and Methods*). Afterwards, fractions containing isolated Nup82 complexes were negatively stained and visualized by EM. Obtained micrographs were used to select thousands of single particles, from which two-dimensional (2D) class averages of Nup82 complexes were calculated (Fig. 2.14 A, 2.15 A and 2.16 A).

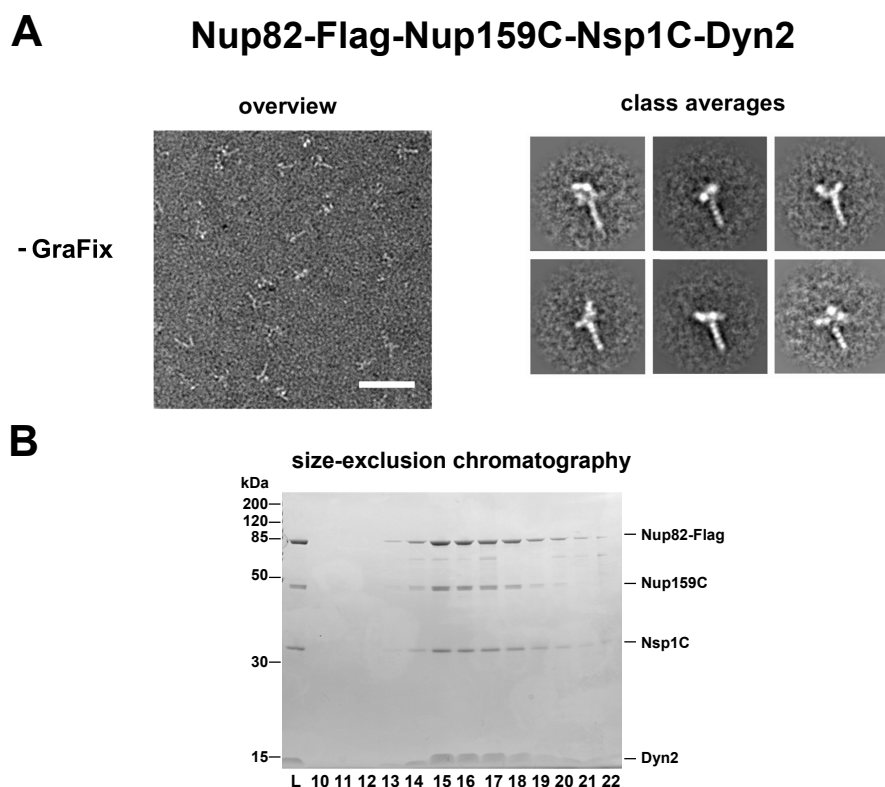


**Figure 2.14:** Negative staining electron microscopy of the affinity-purified Nup82-Nup159C-Nsp1C-Dyn2 complex subjected to size exclusion column

(**A**) Overview and gallery of representative 2D class averages (determined by multivariate statistical analysis performed by Dr. Dirk Flemming) of the affinity-purified Nup82-Flag-Nup159C-Nsp1C-Dyn2 complex followed by size exclusion chromatography and negative staining EM. Scale bar, 50 nm; window size of class averages box, 67.8 nm. (**B**) The affinity-purified complex after size exclusion column was analyzed by SDS-PAGE and Coomassie staining. Fractions 15-16 were analyzed by EM (**A**).

Both EM analyses of either cross-linked (GraFix) or uncross-linked (unfixed) specimens revealed an elongated ( $\sim 30$  nm long) structure of the Nup82 complex. The most prominent feature of the Nup82 complex is a 20 nm long stalk, which is attached to a globular 'head' structure (Fig. 2.14 A and 2.15 A). The stalk is formed by two dynein interaction domains of Nup159 ( $\text{DID}_{\text{Nup159}}$ ), dimerized upon binding of dynein light chain (Dyn2). Five dimers of Dyn2 are aligned like pearls on a string between two extended  $\text{DID}_{\text{Nup159}}$  motifs, forming a rigid  $\text{DID}_{\text{Nup159}}$ -Dyn2 rod, as previously described [Stelter et al., 2007]. After the affinity purification followed by size exclusion chromatography and negative staining we observed high flexibility of the 'head' structure when com-

pared to a cross-linked (GraFix-treated) Nup82 complex (compare Fig. 2.14 and Fig. 2.15).

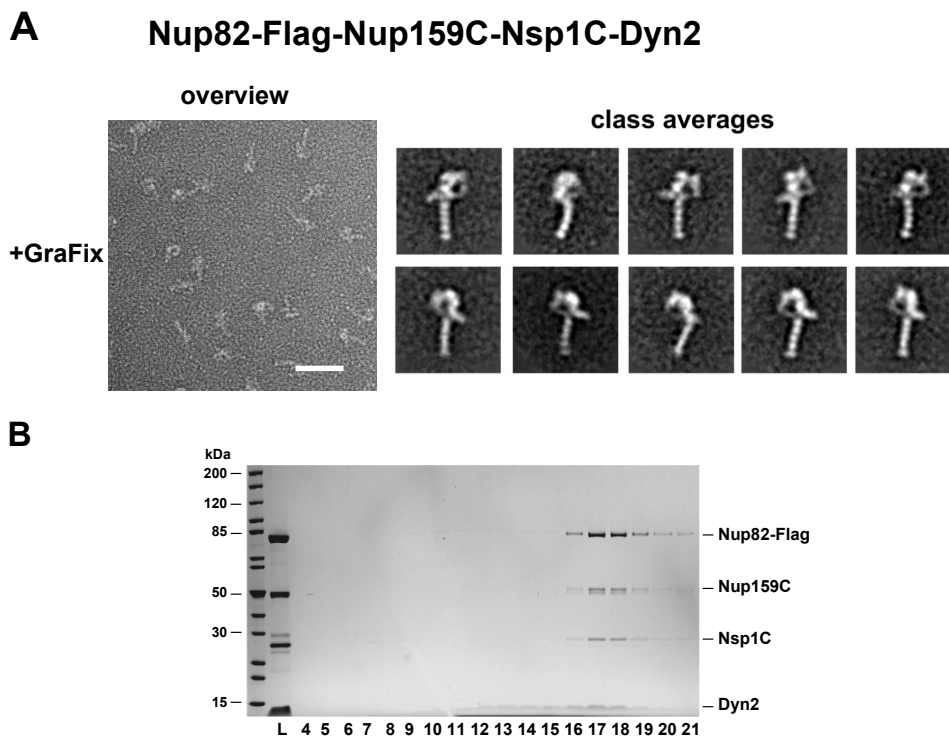


**Figure 2.15:** The EM structure of the Nup82-Nup159C-Nsp1C-Dyn2 complex

(A) Overview of affinity-purified and GraFix-treated Nup82-Flag-Nup159C-Nsp1C-Dyn2 complex (left panel) and representative 2D class averages obtained by EM (right panel, prepared by Dr. Dirk Flemming). Scale bar, 50 nm, window size of the 2D class averages box, 50 nm. (B) Fractions collected after glycerol gradient centrifugation were analyzed by SDS-PAGE and Coomassie staining. Corresponding fractions of parallel glycerol-glutaraldehyde gradient (17-18) were used for EM (A).

2D classes of the GraFix-treated Nup82 complex revealed its unusual structure, which resembles an alphabetic letter 'P'. The observed asymmetric 'head' region of the complex forms a ring structure with the 'spur'-like extension, resembling the head of a rapier. The 'head' is formed by the full length Nup82 (composed of  $\beta$ -propeller and  $\alpha$ -helical domain) and  $\alpha$ -helically predicted parts of both Nup159-C and Nsp1-C (see Fig. 2.1). On some of the 2D classes we could distinguish 3-4 clearly visible globular masses (bright dots, Fig. 2.15 A), which according to their size (5-6 nm in diameter) could correspond to  $\beta$ -propellers of Nup82 [Yoshida et al., 2011].

The EM structure of affinity-purified and GraFix-treated Nup82-Nup159 $\Delta$ FG-Nsp1C-

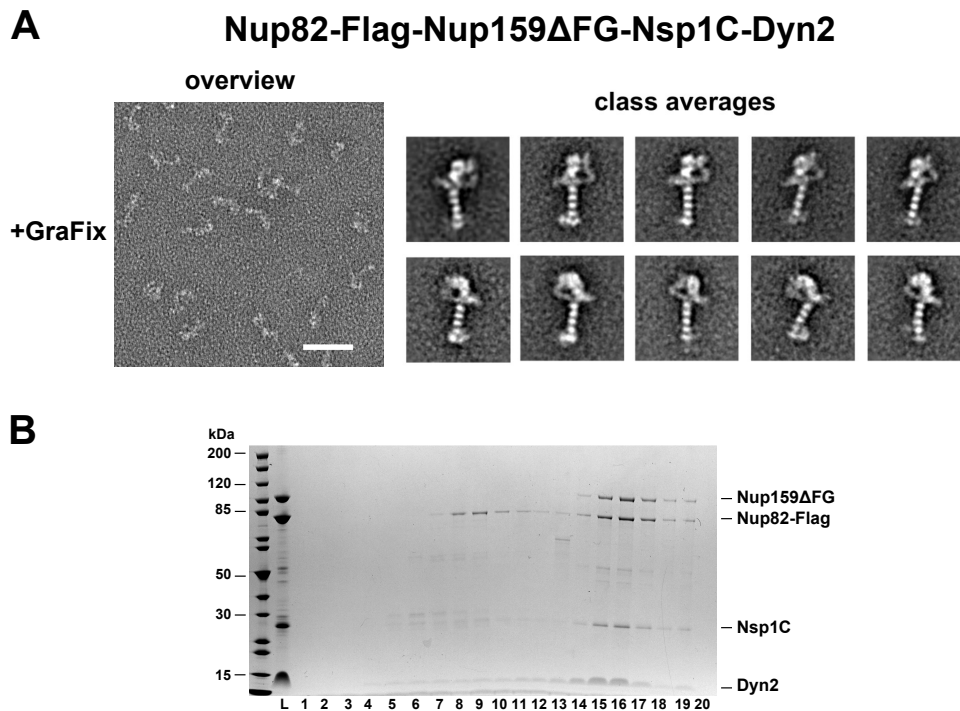


**Figure 2.16:** The EM structure of the Nup82-Nup159 $\Delta$ FG-Nsp1C-Dyn2 complex

(A) Overview of electron micrograph and gallery of representative 2D class averages of the affinity-purified and GraFix-treated Nup82-Flag-Nup159 $\Delta$ FG-Nsp1C-Dyn2 complex. Scale bar, 50 nm, size of the class averages box 50 nm. (Prepared with Dr. Dirk Flemming). (B) SDS-PAGE and Coomassie staining analysis of fractions collected after glycerol gradient centrifugation. Corresponding fractions of glycerol-glutaraldehyde gradient (15-16) were analyzed by EM (A). Note that due to the bigger size of the complex, centrifugation was 2 hours shorter than during the Nup82-Nup159C-Nsp1C-Dyn2 complex preparation.

Dyn2 complex, containing the N-terminal  $\beta$ -propeller domain of Nup159, was also determined (Fig. 2.16). It resembles the EM structure of the Nup82-Nup159C-Nsp1C-Dyn2 complex, although has two additional globular masses preceding the DID<sub>Nup159</sub>-Dyn2 stalk, corresponding to Dbp5-recruiting  $\beta$ -propellers of Nup159 [Weirich et al., 2004].

Taken together, analyses of simplified Nup82 complexes reconstituted in yeast cells, allowed us to visualize the EM structure of the NPC module and confirmed that the complex consists of two Nup159-C and four copies of Nup82, contributing to the molecular mass obtained by MALS measurements.

### The Nup82-Nup159C-Nsp1C-Dyn2 complex contains four copies of Nup82 with distinct properties

To determine if the four observed copies of Nup82 in the complex exhibit different biochemical properties, the Nup82-Nup159 $\Delta$ FG-Nsp1-Flag-Dyn2 complex was affinity-purified under increased ionic strength, which affects the surface charge of proteins, leading to dissociation of less tightly bound subunits of the complex.

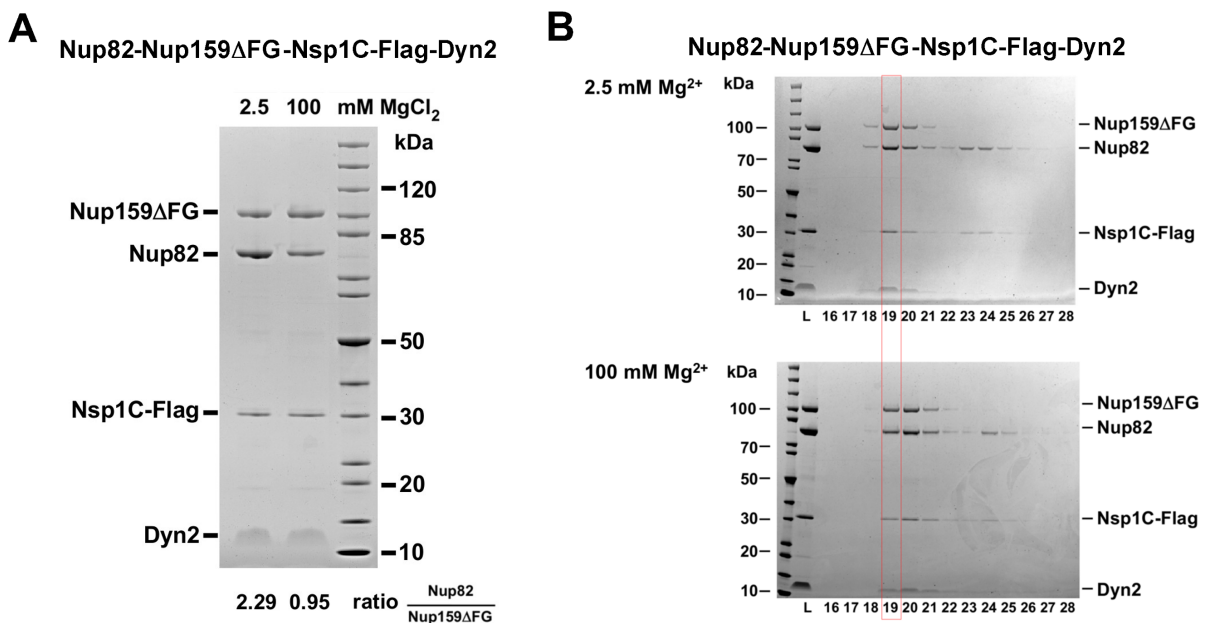


**Figure 2.17:** Purification of the Nup82-Nup159 $\Delta$ FG-Nsp1C-Flag-Dyn2 complex under low and high salt concentrations

(A) The *in vivo* reconstituted and affinity-purified Nup82-Nup159 $\Delta$ FG-Nsp1C-Flag-Dyn2 complex in buffer containing either 2.5 mM Mg<sup>2+</sup> (standard) or 100 mM MgCl<sub>2</sub> was analyzed by SDS-PAGE and Coomassie-staining. For calculating the Nup82:Nup159 $\Delta$ FG ratio, intensities of stained bands were determined by ImageJ software, considering different molecular weights of Nup159 $\Delta$ FG (100 kDa) and Nup82 (82 kDa). (B) The comparison of size exclusion chromatography profiles of Nup82-Nup159 $\Delta$ FG-Nsp1C-Flag-Dyn2 complexes treated with low (upper panel) or high (lower panel) Mg<sup>2+</sup> concentrations. The shift in elution volume is indicated by a red box.

Predicting that only two out of four copies of Nup82 would bind to the two available Nup159 tail domains, the remaining two Nup82 may exhibit other type of interactions. Therefore, I affinity-purified the Nup82-Nup159C-Nsp1 $\Delta$ FG-Dyn2 complex via Nsp1-C-Flag-TEV-ProtA under low and high MgCl<sub>2</sub> concentrations (Fig. 2.17).

To be able to directly compare amounts of co-purified Nup82 in respect of Nup159 $\Delta$ FG,

I used Nsp1-C as a bait protein to avoid the enrichment of either Nup82 or Nup159 $\Delta$ FG. Purification of the complex at low Mg<sup>2+</sup> concentration (2.5 mM in the standard TAP buffer) resulted in 2:1 Nup82:Nup159 $\Delta$ FG ratio. An increase of the Mg<sup>2+</sup> concentration to 100 mM caused a Nup82:Nup159 $\Delta$ FG ratio drop to approximately 1:1 (Fig. 2.17 A). This result indicates that half of the Nup82 molecules present in the complex were dissociated by 100 mM MgCl<sub>2</sub>.

Next, Nup82-Nup159C-Nsp1 $\Delta$ FG-Dyn2 complexes purified in the presence of low and high Mg<sup>2+</sup> concentration, were subjected to size exclusion column (Fig. 2.17 B). The complex isolated at high Mg<sup>2+</sup> concentration shifts one fraction to the right in comparison to the complex purified under low Mg<sup>2+</sup> concentration (Fig. 2.17 B, red box). The observed change in the molecular weight was caused by dissociation of two Nup82 molecules from the complex. Therefore, I conclude that the Nup82 complex is formed by four copies of Nup82, two of them bind to the complex less strongly and can be dissociated upon 100 mM MgCl<sub>2</sub> treatment, while the other two are stably associated with the complex.

To clarify the function of the Nup159-tail fragment in the Nup82 complex organization, I affinity-purified the complex, in which the tail fragment was deleted (Nup159-C $\Delta$ tail, see Fig. 2.9, lane 2). The Nup82-Nup159-C $\Delta$ tail-Nsp1C-Dyn2 complex was assembled *in vivo*, but during gel filtration chromatography it eluted broadly (in a range of 100-670 kDa) from the column (Fig. 2.18 A, left panel). Next, I analyzed how this complex behaves in low and high Mg<sup>2+</sup> concentration. When purified in low Mg<sup>2+</sup> concentration the complex still contained four copies of Nup82, only when purified in the presence of 100 mM MgCl<sub>2</sub> two of them were dissociated as evident from the SEC analysis (Fig. 2.18 A, right panel). Afterwards, I analyzed the GraFix-treated Nup82-Nup159 $\Delta$ tail-Nsp1C-Dyn2 complex by negative staining EM. The obtained 2D class averages revealed the EM structure with typical DID<sub>Nup159</sub>-Dyn2 stalk, however the characteristic ring-like 'head' structure was distorted with a collapse of the 'head' part towards

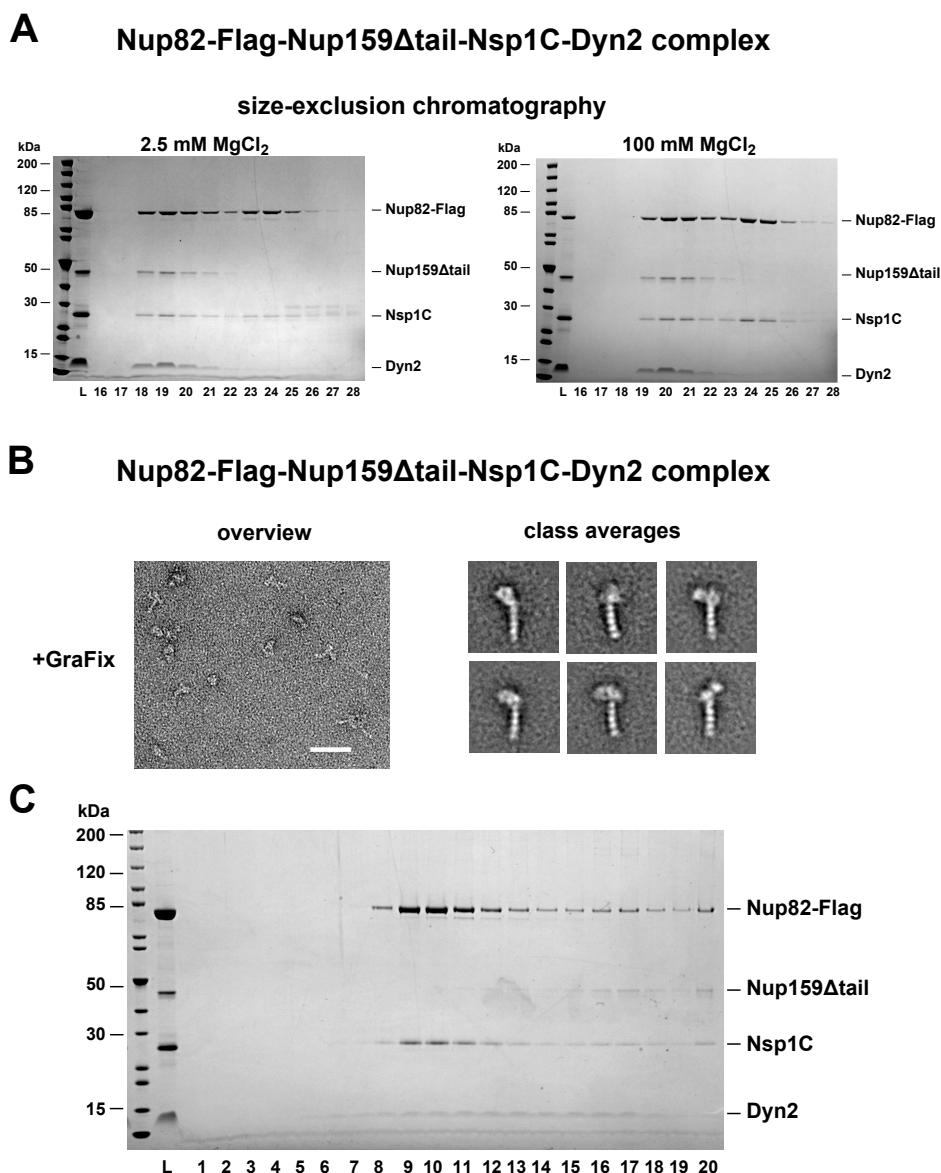


**Figure 2.18:** The structure of the Nup82-Nup159-C $\Delta$ tail-Nsp1C-Dyn2 complex observed by EM

(A) The Nup82-Nup159-C $\Delta$ tail-Nsp1C-Dyn2 complex affinity-purified in either standard or high concentration of  $Mg^{2+}$ , followed by size exclusion chromatography. Note that the complex under standard buffer conditions eluates broadly from the column (left panel). The observed shift in elution fractions from 19 to 20 of the Nup82-Nup159-C $\Delta$ tail-Nsp1C-Dyn2 complex purified in 100 mM  $Mg^{2+}$  in respect to 2.5 mM  $Mg^{2+}$ , corresponds to the loss of two copies of Nup82 (see also Fig. 2.17). (B) Negative staining EM of the GraFix-treated Nup82-Nup159 $\Delta$ tail-Nsp1C-Dyn2 complex, affinity-purified under standard buffer condition. Overview picture (left panel) and a gallery of class averages determined by multivariate statistical analysis (right panel) are shown. Scale bar of the overview, 50 nm. Window size of class averages, 50 nm. Prepared by Dr. Dirk Flemming. (C) Fractions collected after glycerol gradient were analyzed by SDS-PAGE and Coomassie staining. Corresponding fractions of glycerol-glutaraldehyde gradient (18-19) were used for EM analysis (B).

the DID<sub>Nup159</sub>-Dyn2 rod (Fig. 2.18 B and C).

This result confirms that the tail fragment of Nup159 is not essential for Nup82 complex assembly [Yoshida et al., 2011], but contributes to the three-dimensional (3D) organization of the complex, allowing the formation of a ring-like 'head' structure and correct positioning of other binding partners (Nup82 and Nsp1).

### **2.3.3 Cross-linking mass spectrometry of the Nup82-Nup159C-Nsp1C-Dyn2 complex to map interaction surfaces between the subunits**

To identify protein interfaces within the Nup82-Nup159C-Nsp1C-Dyn2 complex, exposed for interactions, a cross-linking mass spectrometry (XL-MS) was performed in collaboration with the laboratory of Dr. Martin Beck (EMBL, Heidelberg, Germany). For this purpose, the affinity-purified complex was incubated with a non-cleavable, two complementary isotope-coded cross-linkers (disuccinimidyl-suberate, DSS or disuccinimidyl-glutarate, DSG), specific for primary amines (lysines and N-termini). The size of cross-linkers enables identification of spatial restraints of two different lengths: up to 35 Å for DSS (long cross-linker) and up to 30 Å for DSG (short cross-linker), measured from the C $\alpha$  to C $\alpha$  of cross-linked lysines [Walzthoeni et al., 2012]. Subsequently, 90 inter and 154 intra protein links, at a false positive discovery rate of 5%, were identified using mass spectrometry [Walzthoeni et al., 2012] (performed by Alexander von Appen, PhD student in the Beck laboratory).

Cross-links occur in the proximity of interaction domains and correspond to regions accessible for soluble cross-linkers. The cross-linking experiment confirmed the interaction surface between the Nup159-tail and the  $\beta$ -propeller of Nup82 [Yoshida et al., 2011]. We have also found cross-links between the  $\beta$ -propeller region of Nup82 and the H3 and H4 carboxy-terminal domains of Nup159-C using long and short cross-linkers

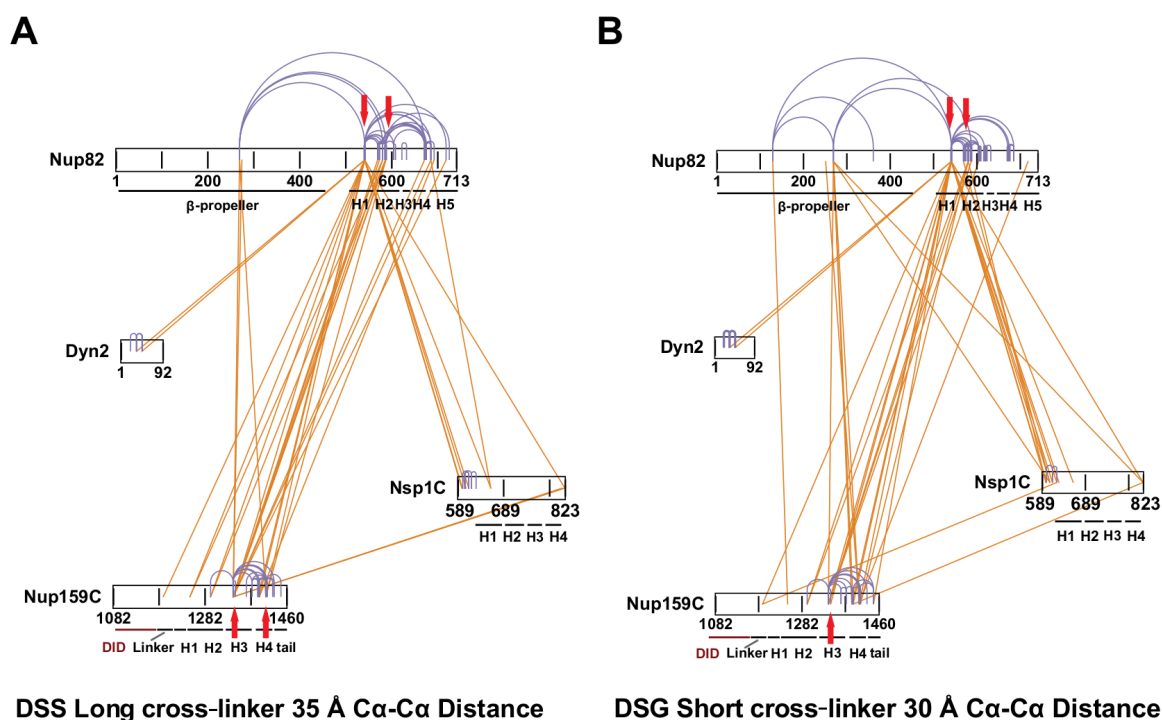


**Figure 2.19:** Cross-linking mass spectrometry analysis of the Nup82-Nup159C-Nsp1C-Dyn2 complex

(A, B) Linear representation of Nup82 complex subunits analyzed by the cross-linking mass spectrometry with either long (disuccinimidyl-suberate, DSS) (A) or short (disuccinimidyl-glutarate, DSG) (B) cross-linker, inter-protein cross-links are represented by orange lines. Blue arches correspond to intra-proteins cross-links, within the same protein. Red arrows indicate homo-dimeric cross-links, connecting two instances of the same lysine residue within self-interacting proteins. Visualization of cross-links was prepared with the xiNET tool from the Rappsilber laboratory (<http://crosslinkviewer.org/index.php>).

(Figure 2.19). Fewer cross-links to Nup82-C and Nup159 H3-H4 were observed for Nsp1-C (known to bind Nup82-C, [Bailer et al., 2001]). Noticeably, Nup159 H1-H2 region exhibited very few cross-links, which is in agreement with previous finding, that H1 domain is forming a self-dimerizing coiled-coil domain (see Fig. 2.5 and Fig. 2.6). Furthermore, the Nup159-H1 sequence has only one lysine available for cross-linkers, which is cross-linked to the Nup82-C domain (Fig. 2.19 A). We have also found distinct restraints formed between Dyn2 and the Nup82-C domain. These cross-links indicate that the  $\alpha$ -helical part of one Nup82 is located in proximity of DID<sub>Nup159</sub>-Dyn2 stalk.

Taking into consideration that four copies of Nup82 and four copies of Nsp1-C are present, it has proven to be difficult to distinguish between cross-links from each copy

of Nup82, since the identified intra-protein cross-links (Fig. 2.19, blue arches) can in principle account for both lysine contact sites within a protein or across two copies of the same protein. Exceptions are cross-links formed across two lysines of the same peptide, which must account for restraints within a homo-dimer (Fig. 2.19, red arrows). We identified four of such restraints, which helped to understand the homo-dimerization interfaces within the Nup82 complex, namely K1343, K1414 (H3-H4) of Nup159 and K541, K580 (H1-H2) of Nup82. Since Nup82 occurs in four, but Nup159 only in two copies within the complex, we speculate that two different interaction interfaces of four Nup82 molecules must exist, which could be confirmed biochemically (see Fig. 2.17). The cross-linking data imply that one homo-dimer interface of Nup82 is formed by helical interactions of the C-terminal region (H1-H2), while the second interface is mediated by the Nup159 C-terminus [Yoshida et al., 2011]. Thus, Nup159 likely homo-dimerizes in the H3-H4 C-terminal region, in addition to the N-terminal region in which dimerization interface is built by the DID<sub>Nup159</sub>-Dyn2 rod and H1 domain.

In summary, we were able to map the protein surfaces accessible for soluble cross-linkers. The XL-MS data thus confirm the biochemical analysis described above and reveal an interaction hub of all three subunits.

To test whether the presence of Nup159-H3-H4 sub-domains would lead to dimerization of the Nup82-Nsp1C-Nup159-H3-H4-tail sub-complex, it was reconstituted *in vivo* and subsequently affinity-purified. Unexpectedly, isolated complex contained the Nup159-H3-H4-tail protein as well as the shorter Nup159-H4-tail fragment, lacking the H3 sub-region (as confirmed by mass spectrometry). After size exclusion chromatography the purified complex was separated into two pools: (1) the complex containing the longer Nup159-H3-H4-tail fragment, which was aggregated and eluted in the void volume and (2) the complex with the shorter Nup159-H4-tail fragment, which formed a soluble hetero-trimeric assembly (Fig. 2.20, left panel). The molecular weight of this soluble Nup82-Nsp1C-Nup159-H4-tail complex, obtained from MALS measurement,

corresponds to 130 kDa, while theoretical value equals 123 kDa (Fig. 2.20, right panel). The  $\alpha$ -helical H3 sub-region of Nup159, which is largely cross-linked to the Nup82-C domain, contributes to the second homo-dimerization interface of the Nup159 (Fig. 2.19 red arrow), which stabilizes the Nup82-Nup159 interaction within the Nup82 complex.

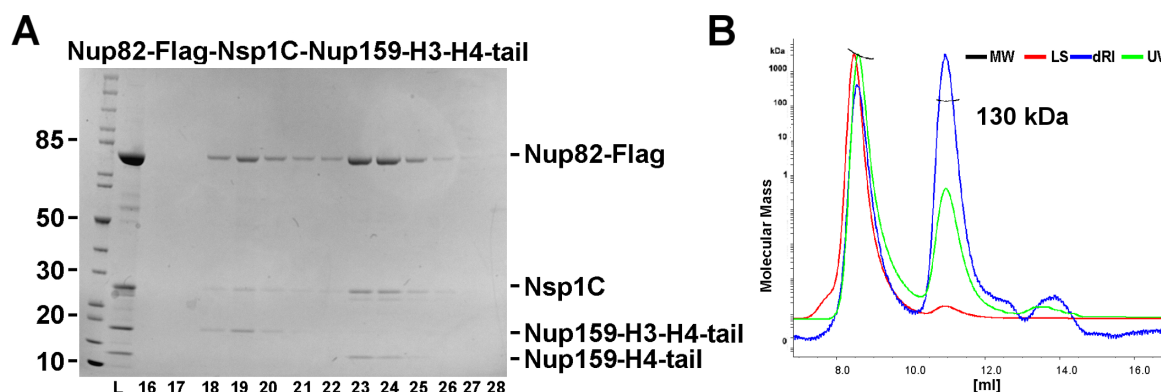


**Figure 2.20:** SEC-MALS of affinity-purified Nup82-Flag-Nsp1C-Nup159-H3-H4-tail complex

(A) Fractions eluted from the gel filtration column were analyzed by SDS-PAGE and Coomassie staining. Next, Nup159 bands were identified by mass spectrometry, to confirm sequences of obtained fragments. The Nup159-H4-tail fragment is protected from proteolysis by interaction with Nup82-Nsp1C hetero-dimer (fractions 23-24), while the Nup159-H3-H4-tail fragment aggregates and elutes with the void volume from the gel filtration column (fractions 18-19). (B) The MALS-determined molecular mass of the Nup82-Flag-Nsp1C-Nup159-H4-tail complex corresponds to 130 kDa. Differential refractive index (blue), light scattering (red) and UV (green) are plotted against the elution volume from the Superdex 200 Increase 10/300 GL column (GE Healthcare).

### 2.3.4 3D electron tomography of the Nup82 complex

Due to complicated asymmetric topology of the Nup82 complex's 'head' structure, we sought to obtain more detailed insight into its architecture using three-dimensional (3D) electron microscopy in collaboration with the Beck laboratory (EMBL, Heidelberg, Germany). To acquire a 3D model of the Nup82 complex, we first collected 91 tomograms of negatively stained complex, then prepared two-dimensional (2D) projections and class averages, used for subsequent calculation of 3D volume. To better resolve the structure of the Nup82 complex we focused the single particle alignment on the 'head' region, while the  $DID_{Nup159}$ -Dyn2 element was averaged out (Fig. 2.21 A). The 3D re-

construction approach revealed a highly asymmetrical structure with the ring-like 'head' region, which consists of three globular domains and a peripheral 'spur' element (Fig. 2.21 B). The dominant feature of the structure is a rod-shaped connector bridging the 'spur' to the most distant globular domain 3. In addition, an elongated 'loop' connects the globular domain 3 to the DID<sub>Nup159</sub>-Dyn2 stalk, forming the characteristic 'P'-shaped structure of the Nup82 module (Fig. 2.21 B, see also Fig. 2.15 A).

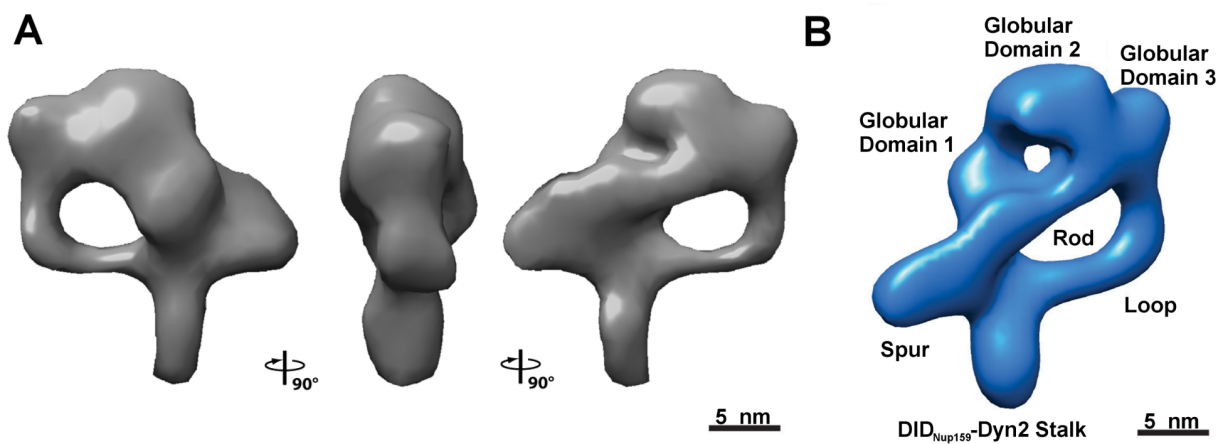


**Figure 2.21:** 3D structure of the Nup82-Nup159C-Nsp1C-Dyn2 complex determined by negative staining electron tomography

(A) 3D volume of the Nup82-Nup159C-Nsp1C-Dyn2 complex, obtained by electron tomography in collaboration with the Beck laboratory. Affinity-purified Nup82-Nup159C-Nsp1C-Dyn2 complex was fixed with GraFix method, negatively stained and subjected to electron microscopy. Three 90° turned views of the volume representation of the Nup82 complex are shown. Part of the DID<sub>Nup159</sub>-Dyn2 rod is averaged out to resolve more details of the 'head' region. (B) Representative class of the Nup82-Nup159C-Nsp1C-Dyn2 complex obtained by 3D electron microscopy. Three distinct globular domains and the 'spur' element orthogonal to the stalk form the backbone structure of the complex. The globular domains 1 and 3 are connected by a 'rod' element.

According to MALS measurements, four Nup82  $\beta$ -propellers should be present in the dimeric Nup82 complex. Based on this prediction, we tried to fit the available crystal structure of the Nup82<sup>NTD</sup>-Nup159-tail hetero-dimer (PDB ID code 3PBP) [Yoshida et al., 2011] into the tomographic 3D volume of the Nup82 complex (see *Discussion*, Fig. 3.4). In this way, it was possible to place two Nup82  $\beta$ -propellers into globular domains 1 and 3 of the 3D volume. In this fit, extra density for the one further Nup82  $\beta$ -propeller in globular domain 2 would be still available. Finally, the last Nup82 could be placed into

the 'spur' or in front of the globular domain 1 (Fig. 2.21 B).

To sum up, electron tomography of the Nup82 complex revealed a 3D topology of the 'head' domain, which enabled us to identify four sites in the 3D volume of the complex, most likely occupied by Nup82  $\beta$ -propellers. Final proving of the proposed model has to await high resolution structural analysis of the Nup82 module.

## 3 Discussion

Structural characterization of the NPC's sub-complexes is crucial to understand how individual proteins contribute to the function and overall architecture of the nuclear pore complex. In my PhD thesis, I structurally and functionally investigated the Nup82 complex from yeast *Saccharomyces cerevisiae*. First, I characterized the carboxy-terminal domain of Nup159 (Nup159-C) and narrowed down its essential part to a 33 amino-acids long sequence, called Nup159-H1. This domain turned out to be required for an efficient Nup82 complex assembly and incorporation into the NPC scaffold. I also analyzed viable *nup159-C* mutants, carrying deletions of subsequent Nup159-C fragments, which exhibit defects in assembly into the Nup82 complex *in vivo*. Finally, the negative staining EM unravelled structural details of the Nup82 complex of which high resolution information was not yet available. A hallmark of the Nup82 complex is its elongated and asymmetric appearance, formed by 4 copies of Nup82, 2 copies of Nup159-C, 4 copies of Nsp1-C and 10 copies of Dyn2. The structure of the complex exhibits certain flexibility which assures movements of FG repeats during the nucleocytoplasmic transport.

The results presented in this PhD thesis revealed, for the first time, the structural organization and stoichiometry of the Nup82 complex from *Saccharomyces cerevisiae* and allowed us to identify interaction surfaces between three components of the complex, which led to the structural model of the Nup82 module.

## 3.1 The Nup159-C domain is an interaction platform organizing the subunits of the Nup82 complex

The essential role of the Nup159-C domain for the Nup82 complex assembly and function has been investigated by biochemical, biophysical and microscopic methods. A major finding was that the Nup159-C domain serves as a scaffold of the Nup82 complex, onto which the other subunits (Nup82, Nsp1 and Dyn2) are assembled. Mutational analysis of  $\alpha$ -helical regions of the Nup159-C domain has shown that only its essential sub-domain (Nup159-H1) is important for targeting to the NPC *in vivo* (see *Results*, Fig. 2.3 and 2.4). We have also found that the essential H1 sub-domain homo-dimerizes *in vitro* via coiled-coil interaction. Thus, we speculate that homo-dimerization of this essential coiled-coil domain is necessary for an optimal organization of the Nup159-C domain, which allows assembly of the Nup82 complex.

Previous studies revealed that dynein light chain (Dyn2) in yeast forms a rigid rod upon dimerization of two Nup159 molecules, which organizes the natively unfolded FG repeats [Stelter et al., 2007]. Our studies suggest that homo-dimerization of Nup159 via H1 domain cooperates with DID<sub>Nup159</sub>-Dyn2 interaction. Analogous to the human dynein light chain (DLC8), which promotes self-association of intermediate chains (IC) in the dynein motor complex, Dyn2 in yeast may stabilize the  $\alpha$ -helical regions of Nup159-C [Barbar, 2008, Morgan et al., 2011, Nyarko and Barbar, 2011]. Specifically, we propose that the homo-dimerization of two Nup159-H1 regions in addition to the binding of five Dyn2 dimers into five QT motifs of DID<sub>Nup159</sub> increases the stability of coiled-coil interactions. Although both Dyn2 and DID<sub>Nup159</sub> are dispensable in yeast, the optimal positioning of the DID<sub>Nup159</sub>-Dyn2 stalk in respect to the Nup159-H1 domain appears key for the function and organization of the Nup82 complex.

In contrast to the yeast complex, vertebrate homologues of Nup82/Nup88 complexes, in which the DID motif is missing, may form stronger and more stable coiled-coil

domains, hence it appears that they do not require a  $\text{DID}_{\text{Nup159}}$ -Dyn2 dimerization device. Indeed, *C. thermophilum* and human have typical heptad repeats pattern within the H1 region of Nup214/Nup159, which could strengthen the coiled-coil interaction (see *Results*, Fig. 2.2).

Sequence analysis of the coiled-coil H1 domain in yeast Nup159 reveals the presence of conserved hydrophobic residues at positions 1 and 4 of the heptad repeat pattern (*hxxhcx*, *h* - hydrophobic and *c* - charged amino-acid residues). However, charged residues at typical positions in classic coiled-coils are less prominent (see *Results*, Fig. 2.2), indicating that the self-interaction of Nup159-H1 domain may be partially compromised and hence may require additional stabilization mechanisms. We propose that homo-dimerization of the Nup159-H1 coiled-coil is supported by the  $\text{DID}_{\text{Nup159}}$ -Dyn2 interaction, as observed in the cytoplasmic dynein-dynactin complex [Morgan et al., 2011].

This studies demonstrated that the Nup159-C is a backbone, which recruits the Nup82-Nsp1 sub-complexes. The Nup82, Nsp1 and Nup159 interaction is mediated by conserved coiled-coil domains of their essential  $\alpha$ -helical carboxy-termini. We observed that mutations within the Nup159-C had a less severe defects on yeast viability and assembly of the Nup82 complex, than the essential H1 sub-domain. Thus, it is conceivable that these sub-regions of Nup159-C domain are less crucial for its function in organizing the Nup82 complex. Moreover, these  $\alpha$ -helical sub-regions are regularly interrupted by helix-breaking residues (e.g. prolines) (see *Results*, Fig. 2.2, Supplemental Fig. 7.2, and 7.3), thus we expect that they fold into a stack of antiparallel helices, instead of forming elongated rod-like structures of typical coiled-coil proteins (e.g. lamins, spectrins or Tpr). As a result, deletions of Nup159-C sub-regions variously influence the Nup82 complex formation, suggesting a redundancy of  $\alpha$ -helical interactions between Nup159, Nup82 and Nsp1. Our cross-linking data indicated that  $\alpha$ -helical domains of all three subunits of the complex form a complicated interaction network, which involves

multiple copies of each subunit (see *Results, Section 2.3.3*).

## 3.2 The conserved Nup82 complex forms a megadalton large and asymmetric assembly

My PhD also brought insight into the structure of the Nup82 complex. It is formed by an elongated DID<sub>Nup159</sub>-Dyn2 stalk and globular 'head' domain with prominent 'spur' and 'loop' elements. In the course of studying the Nup82 complex we determined its stoichiometry consisting of four copies of Nup82, which are associated with only two copies of Nup159-C domains per complex. This is consistent with the EM structure displaying one visible DID<sub>Nup159</sub>-Dyn2 stalk (Fig. 3.1). Although the exact number of Nsp1-C copies per complex is difficult to estimate due to its small molecular weight (28.5 kDa), the observation that Nup82 forms a stable homo-dimer with Nsp1-C (see *Results, Fig. 2.13*) led to the conclusion that four copies of Nsp1-C are present in the Nup82 complex.

Reports characterizing the stoichiometry of the yeast NPC, giving relative amount of each nucleoporins are consistent with our model, although the absolute numbers of Nup82 and Nup159 copies observed in the Nup82 complex are twice as big as presented by Rout and coworkers [Rout et al., 2000, Dreyfus et al., 2012]. They showed that only 1 copy of Nup159 and 2 copies of Nup82 were found per spoke in the yeast NPC [Rout et al., 2000]. The observed discrepancies in obtained results may be caused by different approaches used to determine the stoichiometry of the Nup82 complex. Rout and coworkers analyzed all nucleoporins present in the purified yeast cell fraction, highly enriched for NPC proteins, which could contain reduced amounts of peripherally located nucleoporins. Similarly, the relative amounts of the yeast Y-shaped Nup84 complex components, proposed by Rout [Rout et al., 2000], were shown to be doubled in the mammalian NPC due to dimerization of the Nup84 complex [Hoelz et al., 2011, Bui

et al., 2013, Ori et al., 2013]. Nevertheless, a 1:2 ratio of Nup159:Nup82 in the complex, reported for the yeast NPC is in agreement with our results. If the complex is present once in all 8 spokes of the NPC, we may deduce that the full-length complex containing FG repeats have a molecular weight of 1.24 MDa. Notably, 8 copies of the Nup82 complex sum up to a total mass of  $\sim 10$  MDa, which is one sixth of the entire NPC in yeast [Reichelt et al., 1990, Doye and Hurt, 1997].

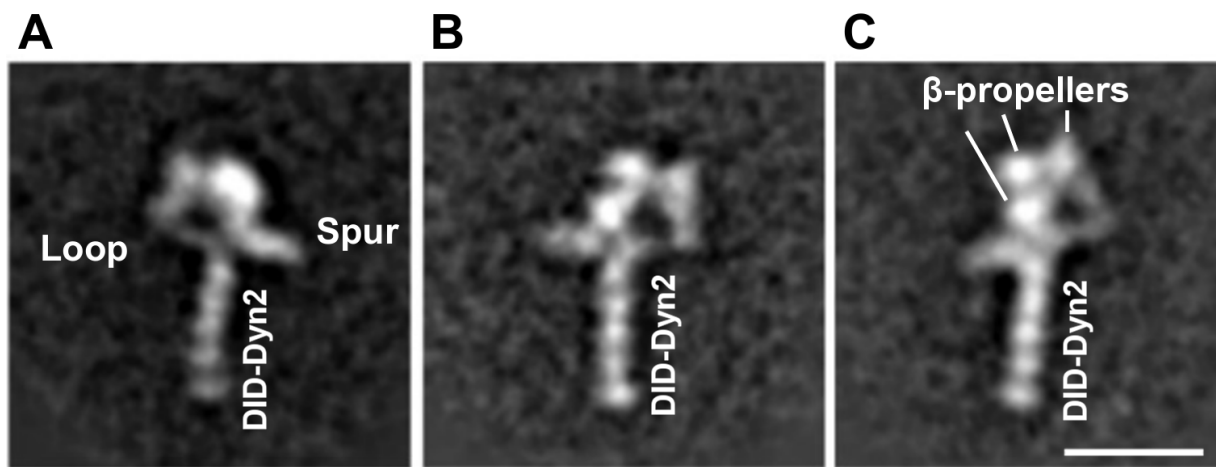


**Figure 3.1:** Class averages of the Nup82-Nup259C-Nsp1C-Dyn2 complex obtained by GraFix-EM

(A-C) Representative class averages of the Nup82 complex with characteristic features: loop, spur,  $\beta$ -propellers and DID<sub>Nup159</sub>-Dyn2 stalk. The scale bar, 20 nm.

Surprisingly, the Nup82 complex exhibits a structural asymmetry, observed quite rarely in homo-dimeric assemblies. The 3D volume of the obtained Nup82-Nup159C-Nsp1C-Dyn2 complex, gives a few possibilities for the overall arrangement of the Nup82 complex. We predict that the Nup82-Nsp1 sub-complex is present in four different copies, organized around the circular backbone of the homo-dimerized Nup159-C core. Our results suggest that from four Nup82 molecules present in the 'P'-complex (Nup82), the two salt-resistant Nup82 have a different interaction site, hence are differently bound to the assembly (see Fig. 3.2; present in globular domain 1 and 3, shown in green). We propose a model wherein two Nup82 molecules bound to the Nup159-tail fragment form one interaction surface, while the remaining two Nup82 molecules may be recruited to

the complex via another interaction. Notably, three  $\beta$ -propellers of Nup82 are clearly distinguishable in some of the 2D class averages (Fig. 3.1 C), while four  $\beta$ -propellers were observed only by EM of the uncross-linked complex (see *Results*, Fig. 2.14 A), thus the fourth Nup82  $\beta$ -propeller presumably overlaps with one of the observed globular masses. We cannot exclude that in the three dimensional arrangement, the fourth  $\beta$ -propeller lays in front of one of the other three  $\beta$ -propellers, hence is not visible in observed EM classes. An alternative possibility is that the prominent 'spur' of the structure corresponds to the fourth  $\beta$ -propeller of Nup82 (Fig. 3.1 and 3.2, shown in grey). Consistent with this model, a stable association of monomeric Nup82-Nsp1C hetero-dimer can be observed *in vivo*, however the Nup159-tail fragment, involved in Nup82 binding [Yoshida et al., 2011], is required for optimal solubility and contributes to the asymmetric organization of the Nup82 complex, by positioning two out of four  $\beta$ -propellers of Nup82 (see *Results*, Fig. 2.18).

A recent study identified only 11 asymmetric complexes out of 223 analyzed homo-oligomeric structures [Swapna et al., 2012]. Six out of eleven complexes bind nucleic acids, where a specific RNA or DNA sequence provides an asymmetric scaffold onto which multiple copies of the same proteins are assembled in structurally distinct conformations. Besides,  $\alpha$ -helical coiled-coils can also induce asymmetry as observed in tropomyosin, where the coiled coil sequence directs its hinge-like bending [Brown, 2010]. In the case of the Nup82 complex, it seems that the C-terminal coiled-coil domains of Nup159 and possibly Nsp1 provide such asymmetric scaffold, which is decorated with at least two structurally distinct subunits of Nup82. Thus, the observed asymmetry driven by hetero-oligomerization of the complex may have an implication for the function of the Nup82 module. In particular, the presence of at least two structurally distinct subunits of Nup82 suggests that they can have different roles in the context of the NPC. We speculate that two salt resistant Nup82-Nsp1 hetero-dimers are involved in the Nup82 complex assembly to the NPC scaffold, while the additional two Nup82-Nsp1

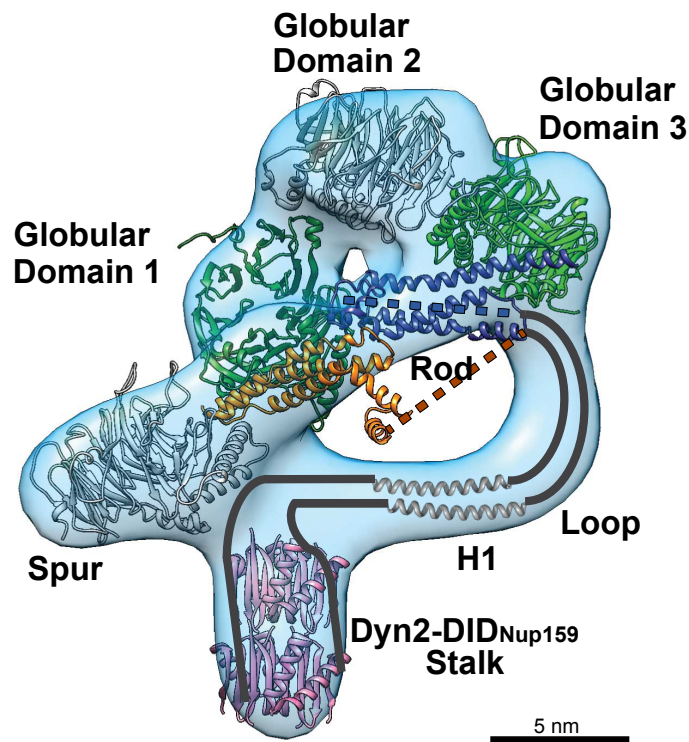


**Figure 3.2:** Structural model of the Nup82-Nup159C-Nsp1C-Dyn2 complex architecture

Structural model of the Nup82-Nup159C-Nsp1C-Dyn2 complex. Four  $\beta$ -propellers of Nup82 are shown in green and gray (globular domains 1-3 and the spur). The predicted  $\alpha$ -helices (H2-H4) of Nup159-C were modelled with I-TASSER [Zhang, 2008] (shown in blue and orange) and combined with the Nup159-H1 domain (grey helices), which may proceed through the 'loop' towards DID<sub>Nup159</sub>-Dyn2 stalk (only two of five Dyn2 dimers are shown). Two Nup159-H1 domains reside closely to the DID<sub>Nup159</sub>-Dyn2 stalk, separated by flexible Linker. The 'spur' and globular domain 2 might be occupied by two additional copies of Nup82. The scale bar, 5 nm.

sub-complexes may fulfil another role (e.g. recruitment of Nup116 and Gle2 involved in the nucleocytoplasmic transport). Alternatively, two additional Nup82-Nsp1 heterodimers may be recruited to the complex after conformational change upon delayed Dyn2 recruitment to the nascent complex in the NPC [Stelter et al., 2012]. We speculate that this event may be crucial to previously reported role of the essential Nup82 complex in the export of ribosomal subunits [Moy and Silver, 1999, Gleizes et al., 2001] or the transport processes.

### 3.3 The Nup82 complex locates in the cytoplasmic ring and protrudes into the central channel of the NPC

Based on the previously reported cytoplasmic location of the human Nup88/Nup214 complex (homologous to the Nup82 complex) [Maimon et al., 2012, Bui et al., 2013], we sought to fit the yeast 'P'-complex to the cytoplasmic protrusions of the human NPC (Fig. 3.3 A). Although it is still unclear whether topologies of the human and yeast NPC are similar, the protrusion specific to the cytoplasmic ring of the human NPC provided sufficient space for docking the 3D structure of the conserved Nup82-Nup159C-Nsp1C-Dyn2 complex (Fig. 3.3 B). The obtained 3D reconstitution of the 'P'-complex (see Fig. *Results*, 2.21 A) allowed a reasonable fit into the cytoplasmic ring of the human NPC map. For this, we arranged the DID<sub>Nup159</sub>-Dyn2 stalk in a way that it protrudes into the transport channel (Fig. 3.3 B, dashed arrow) while the 'spur' protrudes to a side, perpendicularly to the stalk. This arrangement would place the Nup82  $\beta$ -propellers inside the cytoplasmic ring and expose FG repeats into the central channel of the NPC, where they can interact with the shuttling transport receptors. In such an orientation the  $\beta$ -propeller of Nup159 would also be accessible for binding of Dbp5 in order to terminate the mRNA export [Hurwitz et al., 1998, Schmitt et al., 1999, Noble et al., 2011].

The weak protein contacts between modules of the NPC were analysed by Rout's group in detail [Alber et al., 2007a], indicating that the Nup82 complex is located closely to the outer ring of the NPC, where Nup159-H1 sub-domain could contact other modules (inner pore ring module and the Nup84 complex). This concept is in agreement with the tomographic map of the human NPC, where Nup88/Nup214 complex localizes in close proximity to the Nup85 and Nup188 nucleoporins [Maimon et al., 2012, Bui et al., 2013]. In addition, the Nup159-H1 structure may undergo conformational change upon Dyn2 recruitment to the DID<sub>Nup159</sub>, thus playing a governing role in the Nup82 complex assembly and function. Difficulties in obtaining any structural information about the

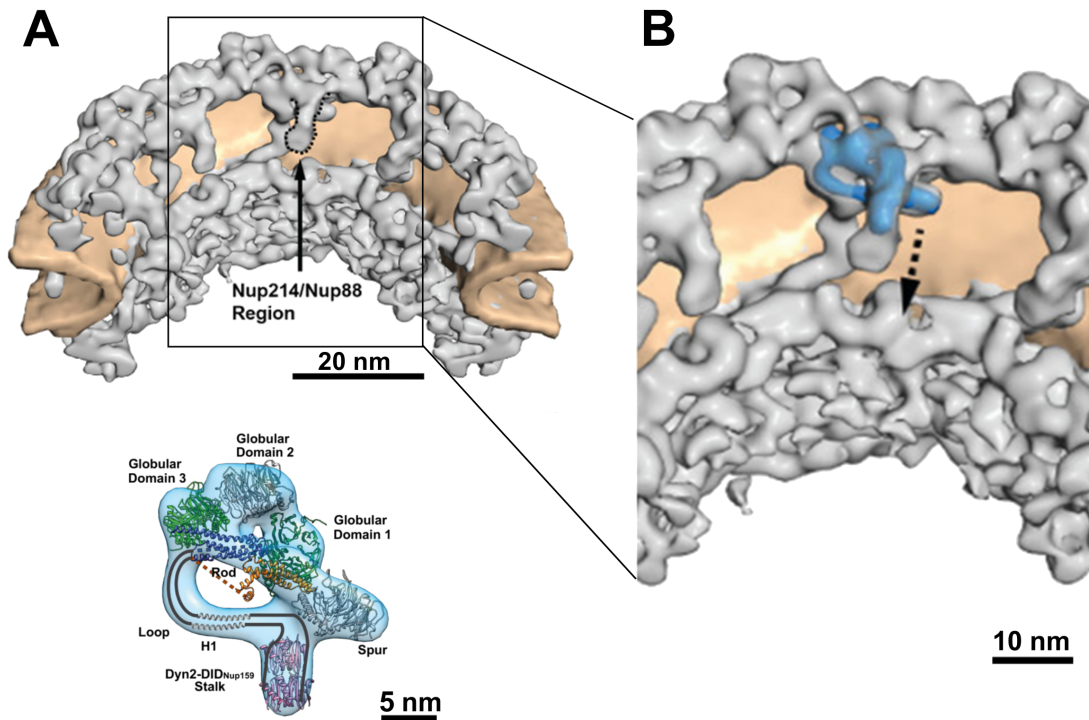


**Figure 3.3:** Docking of the Nup82-Nup159C-Nsp1C-Dyn2 within the tomographic map of the human NPC.

(A) The human Nup214/Nup88 complex occupies a cytoplasmic ring protrusion, facing the central channel of the NPC, black arrow (upper panel) [Bui et al., 2013]. The tomographic 3D map of the yeast Nup82 complex (bottom panel) was docked into the human NPC volume. (B) The potential position of the Nup82-Nup159C-Nsp1C-Dyn2 complex within the human NPC. Direction of the DID<sub>Nup159</sub>-Dyn2 stalk is indicated by dashed arrow, along with the FG repeats of Nup159 protruding into the central channel of the NPC. Figures were prepared together with Alexander von Appen (Beck Group, EMBL, Heidelberg, Germany).

complex suggest its high flexibility, which was also observed by EM of the uncrosslinked Nup82 complex.

In the future, our first insights into the structure of Nup82 complex will help to understand its interaction with the NPC's scaffold. Our reconstitution method of the simplified Nup82 complex could be extended to investigate interaction of the Nup82 complex with neighbouring modules of the NPC (e.g. inner pore ring module).

# 4 Materials and Methods

## 4.1 Molecular biology and genetic methods

### 4.1.1 DNA manipulation and plasmid construction

Recombinant DNA manipulation including polymerase chain reaction (PCR), restriction enzyme digest of PCR products and plasmids, separation of DNA fragments by agarose gel electrophoresis in TAE buffer and ligation reactions were performed as previously described by [Sambrook and Russell, 2001]. All DNA manipulation was done in *Escherichia coli* DH5 $\alpha$  competent cells. PCR products were amplified using Phusion polymerase (Thermo Fisher Scientific) and purified with GeneElute™ PCR Clean-Up or Gel Extraction kits (Sigma Aldrich). Oligonucleotides were synthesized by Sigma Aldrich (Steinheim, Germany). Restriction enzymes were obtained from Thermo Fisher Scientific and New England Biolabs, while subsequent ligation reactions were done using T4 DNA ligase (NEB). Plasmid DNA was isolated from *E. coli* using Miniprep (HP) kit (Sigma Aldrich). Competent *E. coli* cells for plasmid transformation were prepared following the protocol for DH5 $\alpha$  cells [Inoue et al., 1990]. Plasmids were verified by restriction digestion and by DNA sequencing (performed by Eurofins MWG; Ebersberg, Germany). Plasmids used in this study are listed in Table 4.1.

Table 4.1: Plasmids used in this study

Plasmid	Comment(s)	Reference
pRS414- <i>Nup159</i>	endogenous promoter, <i>ADH</i> terminator	[Stelter et al., 2007]
pRS414- <i>nup159</i> Δ <i>DDID</i>	as above, <i>Nup159</i> lacking residues 1086-1185	[Stelter et al., 2007]
pRS414- <i>nup159</i> Δ <i>Linker</i>	as above, <i>Nup159</i> lacking residues 1179-1210	lab collection
pRS414- <i>nup159</i> Δ <i>H1</i>	as above, <i>Nup159</i> lacking residues 1210-1244	lab collection
pRS414- <i>nup159</i> Δ <i>H2</i>	as above, <i>Nup159</i> lacking residues 1245-1330	lab collection
pRS414- <i>nup159</i> Δ <i>H2A</i>	as above, <i>Nup159</i> lacking residues 1245-1275	this study
pRS414- <i>nup159</i> Δ <i>H2B</i>	as above, <i>Nup159</i> lacking residues 1276-1330	this study
pRS414- <i>nup159</i> Δ <i>H3</i>	as above, <i>Nup159</i> lacking residues 1331-1380	lab collection
pRS414- <i>nup159</i> Δ <i>H4</i>	as above, <i>Nup159</i> lacking residues 1381-1425	this study
pRS414- <i>nup159</i> Δ <i>tail</i>	as above, <i>Nup159</i> lacking residues 1425-1460	this study
pRS414- <i>nup159</i> Δ <i>H4-tail</i>	as above, <i>Nup159</i> lacking residues 1381-1460	this study
pRS414- <i>nup159</i> Δ <i>H3-H4</i>	as above, <i>Nup159</i> lacking residues 1331-1425	this study
pRS414- <i>nup159</i> Δ <i>DDID-Linker</i>	as above, <i>Nup159</i> lacking residues 1086-1210	this study
pRS414- <i>nup159</i> Δ <i>DDID-Δtail</i>	as above, <i>Nup159</i> lacking residues 1086-1185 and 1425-1460	this study
pRS414- <i>nup159</i> Δ <i>FG</i>	as above, <i>Nup159</i> lacking residues 459-1083	this study
YEplac351- <i>GAL1-Dyn2</i>	LEU	lab collection
pRS414- <i>nup159</i> H1-1(L1228>E)	<i>nup159</i> point mutation Leu to Glu at residue 1228	this study
pRS414- <i>nup159</i> H1-2(I1232>D)	<i>nup159</i> point mutation Iso to Asp at residue 1232	this study
pRS414- <i>nup159</i> H1-3(M1235>E)	<i>nup159</i> point mutation Met to Gln at residue 1235	this study
pRS414- <i>nup159</i> H1-4(L1228>E, I1232>D)	<i>nup159</i> point mutations Leu to Gln at residue 1228 and Iso to Asp at residue 1232	this study
pRS414- <i>nup159</i> H1-5(I1232>D, M1235>E)	<i>nup159</i> point mutation Iso to Asp at residue 1232 and Met to Gln at residue 1235	this study
pRS414- <i>nup159</i> H1-6(L1228>E, M1235>E)	<i>nup159</i> point mutation Leu to Gln at residue 1228 and Met to Gln at residue 1235	this study
pRS414- <i>GFP-Nup159</i>	<i>pNOP1</i> promoter, <i>ADH</i> terminator	[Stelter et al., 2007]
pRS414- <i>GFP-nup159</i> Δ <i>Linker</i>	as above, <i>Nup159</i> lacking residues 1086-1185	this study
pRS414- <i>GFP-nup159</i> Δ <i>H1</i>	as above, <i>Nup159</i> lacking residues 1210-1244	this study
pRS414- <i>GFP-nup159</i> Δ <i>H2</i>	as above, <i>Nup159</i> lacking residues 1245-1330	this study
pRS414- <i>GFP-nup159</i> Δ <i>H2A</i>	as above, <i>Nup159</i> lacking residues 1245-1275	this study
pRS414- <i>GFP-nup159</i> Δ <i>H2B</i>	as above, <i>Nup159</i> lacking residues 1276-1330	this study
pRS414- <i>GFP-nup159</i> Δ <i>H3</i>	as above, <i>Nup159</i> lacking residues 1331-1380	this study
pRS414- <i>GFP-nup159</i> Δ <i>H4</i>	as above, <i>Nup159</i> lacking residues 1381-1425	this study
pRS414- <i>GFP-nup159</i> Δ <i>tail</i>	as above, <i>Nup159</i> lacking residues 1425-1460	this study
YEplac195-P1 <sub>GAL</sub> - <i>Dyn2-P2-Nup159C</i>	bicistronic yeast expression, galactose induced, 2μ, <i>Nup159-C</i> residues 1082-1460	this study
YEplac181-P1 <sub>GAL</sub> - <i>Nsp1C-P2-Nup82-FTP</i>	as above, <i>Nsp1-C</i> residues 573-823, <i>Nup82-Flag-TEV-ProtA</i>	this study
YEplac195-P1 <sub>GAL</sub> - <i>Dyn2-P2-Nup159</i> Δ <i>tail</i>	as above, <i>Nup159</i> Δ <i>T</i> residues 1082-1426	this study
YEplac195-P1 <sub>GAL</sub> - <i>Dyn2-P2-Nup159</i> Δ <i>FG</i>	as above, <i>Nup159</i> -Δ <i>FG</i> lacking residues 459-1083	this study
YEplac112-P1 <sub>GAL</sub> - <i>Nsp1C-P2-Nup82-FTP</i>	as above	this study
YEplac181-P1 <sub>GAL</sub> - <i>HIS-Nup159tail-Flag</i>	as above, <i>HIS-nup159tail-Flag</i> residues 1425-1460	this study
YEplac181-P1 <sub>GAL</sub> - <i>HIS-Nup116C</i>	as above, <i>Nup116-C</i> residues 967-1113	this study
YEplac181-P1 <sub>GAL</sub> - <i>Nsp1C-FTP-P2-Nup82</i>	as above	this study
pProEX HTb <i>GST-TEV-Dyn2</i>	PCR amplified, cloned <i>NdeI/BamHI</i>	this study
pET-15b- <i>HIS-TEV-nup159-QT<sub>4-5</sub>-Linker-H1</i>	PCR amplified, cloned <i>NdeI/BamHI</i> , 1153-1241 aa	this study
pET-15b- <i>HIS-TEV-nup159-QT<sub>4-5</sub>-Linker-h1-5</i>	PCR amplified, cloned <i>NdeI/BamHI</i> , residues 1153-1241	this study
YEplac195-P1 <sub>GAL</sub> - <i>Dyn2-P2-Nup159</i> Δ <i>tail</i>	<i>HIS-Nup159</i> residues 1082-1419	this study
YEplac195-P1 <sub>GAL</sub> - <i>Dyn2-P2-Nup159H3-T</i>	as above, <i>HIS-Nup159</i> residues 1322-1460	this study
YEplac195-P1 <sub>GAL</sub> - <i>Dyn2-P2-Nup159H4-T</i>	as above, <i>HIS-Nup159</i> residues 1381-1460	this study
YEplac195-P1 <sub>GAL</sub> - <i>Dyn2-P2-Nup159tail</i>	as above, <i>HIS-Nup159</i> residues 1424-1460	this study

## 4.1.2 Reconstitution of *Nup82* complexes in *Saccharomyces cerevisiae*

To perform simultaneous expression of multiple genes of interest in the yeast system, the coding sequences of nucleoporins devoid of FG repeats were inserted into appropriate yeast expression vectors. The multiple cloning site of the YEplac series was exchanged, to contain the opposite oriented, inducible *GAL1* and *GAL10* promoters, to allow over-expression of two genes from one vector (bicistronic). Next, new multiple cloning sites were introduced flanking this promoter for cloning of two open reading frames into one vector, carrying either the *LEU2*, *URA3* or *TRP1* marker cassette. The constructs were co-expressed in yeast by addition of 2% galactose to the medium.

### 4.1.3 Construction of yeast strains and basic yeast methods

Yeast strains used in this study are listed in Table 4.2. Genomic deletion disruption and C-terminal Flag-TEV-ProtA (FTP) tagging of genes were done by homologous recombination method as described before [Longtine et al., 1998, Janke et al., 2004].

**Table 4.2:** Yeast strains used in this study

Strains	Genotype	Reference
Ds1-2b	<i>MAT</i> $\alpha$ , <i>leu2</i> - $\Delta$ 1, <i>trp1</i> - $\Delta$ 63, <i>his3</i> - $\Delta$ 200, <i>ura3</i> -52	[Grandi et al., 1995b]
<i>nup159</i> $\Delta$ shuffle	<i>MAT</i> <b>a</b> , <i>nup159</i> :: <i>NT2</i> , <i>trp1</i> - $\Delta$ 63, <i>his3</i> - $\Delta$ 200, <i>ura3</i> -52, <i>leu2</i> - $\Delta$ 1, <i>pLG4-URA3-NUP159</i>	[Gorsch et al., 1995]
<i>nup159</i> $\Delta$ shuffle/ <i>dyn2</i> $\Delta$	<i>MAT</i> <b>a</b> , <i>nup159</i> :: <i>NT2</i> , <i>trp1</i> - $\Delta$ 63, <i>his3</i> - $\Delta$ 200, <i>ura3</i> -52, <i>leu2</i> - $\Delta$ 1, <i>dyn2</i> :: <i>kanMX</i> , <i>pLG4-URA3-NUP159</i>	[Stelter et al., 2007]
<i>nup159</i> $\Delta$ shuffle, <i>Nup82</i> -FTP	<i>MAT</i> <b>a</b> , <i>nup159</i> :: <i>NT2</i> , <i>trp1</i> - $\Delta$ 63, <i>his3</i> - $\Delta$ 200, <i>ura3</i> -52, <i>leu2</i> - $\Delta$ 1, <i>Nup82</i> -FTP:: <i>HIS3</i> , <i>pLG4-URA3-NUP159</i>	this study

Transformation of *S. cerevisiae* with plasmid DNA was performed as previously described [Ito et al., 1983], using a rapid lithium acetate method. Briefly, exponentially growing cells were harvested, washed with distilled water (dH<sub>2</sub>O) and resuspended in a buffer (10 mM Tris-HCl pH 7.5, 1 mM EDTA, 100 mM LiAc), then added to the mixture of DNA (100-500 ng), 10  $\mu$ l freshly boiled herring sperm carrier DNA 2 mg/ml and 34% PEG-4000 in a buffer (10 mM Tris-HCl pH 7.5, 1 mM EDTA, 100 mM LiAc). The mixture was rotated on a turning wheel for 30 min at room temperature (RT), followed by a 15 minutes heat shock at 42 °C. Transformed cells were centrifuged, resuspended in 50  $\mu$ l of water and plated on appropriate plates for selection of transformants. When transforming with PCR cassettes containing resistance genes (ClonNAT and geneticin) for homologous recombination, cells were grown in YPD for at least 3 hours to allow expression of the resistance genes prior to plating on selective plates.

Genomic DNA was isolated according to the method of Hoffman and Winston, 1987. Cells from a 10 ml overnight culture were collected by centrifugation, resuspended in 500  $\mu$ l of dH<sub>2</sub>O and transferred to a 1.5 ml microcentrifuge tube, centrifuged again and resuspended in the residual liquid. 200  $\mu$ l of Genomic DNA lysis buffer (2% Triton X-100, 1% SDS, 100 mM NaCl, 10 mM Tris-HCl (pH 8), 1 mM EDTA), 200  $\mu$ l of a 1:1

ratio of phenol:chlorophorm and approximately 100 µl of glass beads were added. The cells were lysed by vortexing for 4 min, then 200 µl of TE buffer (10 mM Tris-HCl pH 7.5, 1 mM EDTA) was added and centrifuged at maximum speed. The DNA-containing top phase was transferred to a fresh tube, 1 ml of 100% ethanol was added, mixed by inversion and pelleted for 2 min at maximum speed. The supernatant was removed and the pellet was resuspended in 400 µl of TE buffer and 3 µl of RNase A (10 mg/ml). After incubation at 37 °C for 5 min DNA was precipitated with 10 µl of 4 M NH<sub>4</sub>Ac and 1 ml of 100% ethanol. DNA was collected by centrifugation for 2 min at maximum speed and resuspended in 50 µl dH<sub>2</sub>O after air drying.

## 4.2 Microbiological methods

### 4.2.1 Media for *S. cerevisiae* and *E. coli* growth

Yeast cells were grown at 30 °C in rich YPD medium (1% yeast extract, 2% peptone, 2% glucose) or synthetic defined complete (SDC) medium (2% glucose, 0.67% yeast nitrogen base) complemented with all necessary amino acids excluding those required for selection. The concentration of amino acids was used as described previously [Sherman et al., 1991]. For counter-selection of cells harbouring *URA3* plasmids, SDC supplemented with all amino acids and 2 mg/ml of 5-fluoro-orotic acid (5-FOA), was used. For selection of yeast clones, containing antibiotic resistance, following concentrations were used: 0.2 mg/ml of geneticin and 100 µg/ml neourseothricin (ClonNAT). For galactose induction, yeast cells were grown in synthetic raffinose complete (SRC) medium, lacking selective amino acid and shifted to 2% galactose for 6 hours in YPG medium (1% yeast extract, 2% peptone, 2% galactose). *E. coli* cells were grown at 37 °C in Luria-Bertani (LB) medium (0.5% yeast extract, 1% tryptone, 0.5% sodium chloride) supplemented with antibiotics for plasmids expressing heterologous proteins (100 µg/ml

ampicillin, 30µg/ml kanamycin, 34µg/ml chloramphenicol). Cell density in liquid culture was estimated by optical density measurement at a wavelength of 600 nm (OD<sub>600</sub>).

### 4.2.2 Analysis of yeast cells growth (dot spots)

Exponentially growing yeast cultures were spotted onto agarose plates in 10-fold serial dilution steps (first spot contained cell suspension of OD<sub>600</sub> 1). Plates were incubated at the indicated temperatures for 2-5 days. To analyze functionality of truncated proteins, shuffle strain deletion mutants, carrying wild-type copy protein on the URA plasmid and truncated version on TRP plasmids, were spotted on 5-FOA plates. 5-fluoro-orotic acid (5-FOA) is converted into a toxic 5-fluorouracil in the presence of URA plasmid, thus only viable mutants, which had lost the URA plasmid can grow in the presence of 5-fluoro-orotic acid. Double amount of cells were spotted (first spot of OD<sub>600</sub> 2) onto 5-FOA plates.

## 4.3 Biochemical methods

### 4.3.1 Whole yeast protein extract

To analyse total protein expression, yeast extracts were prepared either by chemical lysis, according to the previously described protocol [Yaffe and Schatz, 1984] or by glass bead lysis. Yeast cells (OD<sub>600</sub> 1-3) were harvested by centrifugation at maximum speed for 1 min, washed once with 1 ml of dH<sub>2</sub>O, resuspended in 400 µl of ice-cold 20% TCA (trichloroacetic acid) and about 100 µl of cold glass beads was added. After vortexing for 3 min at RT, the precipitated protein was centrifuged for 5 min at 13000 rpm, 4 °C. The supernatant was discarded and the pellet was washed with 1 ml of 100% ice-cold ethanol, centrifuged again, dried for at least 10 min and resuspended in 100 µl of 4x sample buffer and 1 µl of 1M Tris-HCl (pH 9.4). After vortexing for 1 min, samples were

boiled at 95 °C for 3 min. From the supernatant 5-15 µl of the sample were loaded on an SDS-PAGE (sodium dodecylsulfate polyacrylamide gel electrophoresis).

### 4.3.2 Reconstitution and affinity purification of Nup82 complexes

The tandem affinity purification (TAP) method was performed according to protocols [Puig et al., 2001, Rigaut et al., 1999]. Yeast cells were grown over night at 30 °C in 2 L YPD or selective medium. Cultures were harvested at OD<sub>600</sub> of 2.0 to 3.0 at 4000 rpm for 5 min at 4 °C and washed once with 30 ml cold buffer (20 mM Tris-HCl or Hepes, pH 7.5, 150 mM NaCl, 50 mM K(OAc), 2 mM Mg(OAc)<sub>2</sub>, 5% glycerol), centrifuged again, frozen in a liquid nitrogen and stored at -20 °C.

Pellets were thawed in a water bath at 37 °C, 20 ml of cold buffer, supplemented with protease inhibitor mix FY (Serva, Heidelberg, Germany), 1 mM phenylmethylsulfonyl fluoride (PMSF), 1 mM dithiothreitol (DTT) and 0.1% NP-40 (lysis buffer) and 25 ml of cold glass beads were added. Cells were lysed with a beater mill at 4 °C, with program: 500 rpm, 4 min, 1 min break, 2 repetitions (Pulverisette, Fritsch, Idar-Oberstein, Germany). The cell lysate was separated from the glass beads and collected by pressing the mixture through a 50 ml syringe (Beckton Dickinson), followed by washing the beads with 10 ml of lysis buffer. Lysates were first centrifuged at 4000 rpm for 10 min at 4 °C and then the supernatant was centrifuged at 17500 rpm for 30 min at 4 °C. After second centrifugation step, the supernatant was incubated with 300 µl of IgG Sepharose beads (IgG Sepharose™ 6D Fast Flow, Amersham Bioscience) for at least 2 hrs, at 4 °C on a turning wheel. Prior to use, beads were washed twice with 10 ml of buffer (without protease inhibitors) and collected by centrifugation at 1300 rpm for 3 min.

After IgG binding step, lysate was removed by centrifugation at 1300 rpm for 5 min at 4 °C and beads were washed with 10 ml of buffer with 0.01% NP40 (wash buffer), collected by centrifugation as previously and transferred to 2.5 ml Mobicol™ minispin column (MoBiTec, Germany). The beads were washed 2 times with 5 ml of wash buffer

by gravity flow. Afterwards, the column was plugged and 350  $\mu$ l of wash buffer, supplemented with 0.5 mM DTT and 10  $\mu$ l (approximately 1 mg/ml) of recombinant tobacco etch virus (TEV) protease were added and incubated for 90 min at 16 °C on a turning wheel. The TEV eluate was collected in a 1.5 ml microcentrifuge tube by centrifugation at 2000 rpm for 1 min and 300  $\mu$ l was transferred to a new 0.8 ml column Micro Bio-Spin™ (Bio-Rad), containing 30  $\mu$ l pre-washed Flag M2 agarose (ANTI-FLAG M2 Affinity Gel, Sigma Aldrich). The rest of TEV eluate was TCA precipitated (10%) for 15 min on ice, freeze-dried and kept for later. The column was sealed and placed on a turning wheel for 1 hr at 4 °C. The flow through was collected by centrifugation at 1000 rpm for 1 min and Flag M2 agarose was washed with 5 ml of wash buffer. Proteins were eluted from the agarose with 1xFlag peptide (Sigma Aldrich) resuspended in 200  $\mu$ l of wash buffer for 45 min at 4 °C on a turning wheel and eluted into a microcentrifuge tube by centrifugation at 2000 rpm for 1 min at 4 °C. The Flag eluate was used for further studies or was precipitated with 10% TCA on ice and centrifuged for 15 min at 13000 rpm, 4 °C. After washing once with 100 % acetone (0.5 ml), pellet was air dried and resuspended in 50  $\mu$ l of 1x sample buffer (250 mM Tris-HCl (pH 6.8), 9.2% SDS, 40% glycerol, 0.2% Bromophenol blue and 100 mM DTT added just before use) and separated on 4-12% gradient or 12% NuPAGE Novex Bis-Tris Gels (Invitrogen, Carlsbad, USA) electrophoresis.

To extract the 2 loosely bound Nup82 molecules from the Nup82 complex,  $MgCl_2$  was added to a final concentration of 100 mM during affinity-purification of Nsp1-Flag-TEV-ProtA as previously described [Schafer and Hurt, 2006] and eluates were analyzed by size exclusion chromatography and multiangle laser light scattering (SEC-MALS). Complexes were separated on a Superdex 200 Increased 10/300 GL column attached to an the Äkta-Basic-System (Amersham Biosciences).

### Protein staining and mass spectrometry

Proteins were stained with Brilliant Blue G colloidal Coomassie (Sigma Aldrich) or with a filtered solution of Coomassie Brilliant Blue R-250 (1.5 g/l) in 30% ethanol and 10% acetic acid, performed as previously described by [Sambrook and Russell, 2001]. After staining procedure, bands were excised from the gel, trypsin digested and identified by mass spectrometry (BZH Facility, Heidelberg, Germany).

#### 4.3.3 Western blot analysis

Proteins were transferred to nitrocellulose membrane by semi-blot system as described before [Sambrook and Russell, 2001]. Transfer of proteins was performed in a transfer buffer (48 mM Tris-HCl, 39 mM glycine, 1.3 mM SDS and 20% methanol) for 60 min at 12 V. After the transfer, proteins were visualized with Ponceau S (Serva, Heidelberg, Germany) to ensure the quality of transfer and the molecular weights of protein standards were marked (Page Ruler™ Unstained Protein Ladder, Thermo Fisher Scientific). The membrane was washed with dH<sub>2</sub>O and blocked in a blocking buffer (1x PBS (phosphate-buffered saline), 5% milk, 0.1% Tween-20) for 2 hrs at RT or over night at 4 °C with gentle shaking. After blocking, the membrane was incubated with a primary antibody in a blocking buffer for 1 hr at RT. Three washing steps of 10 min each at RT with PBS-T (1x PBS, 0.1% Tween-20) were performed, to wash away unspecific antibody binding. Secondary antibody, conjugated with horseradish peroxidase (HRP) was added, if required, and incubated for 1 hr at RT with gentle shaking. Dilutions of used antibodies are listed in Table 4.3. The nitrocellulose membrane was washed 3 times and detection of HRP-conjugated antibodies bound to proteins was performed, using enhanced chemiluminescence (ECL) solution (Amersham Bioscience). The luminescent signals were documented using an ImageQuant Las4000mini (GE Healthcare).

**Table 4.3:** Antibody dilutions

Primary antibody	Secondary antibody
$\alpha$ -protA (1:5000)	-
$\alpha$ -Flag (1:3000)	-
$\alpha$ -Arc1 (1:5000)	$\alpha$ -rabbit (1:2000)
$\alpha$ -GFP (1:3000)	$\alpha$ -mouse (1:3000)
$\alpha$ -Dyn2 (1:2000)	$\alpha$ -rabbit (1:2000)
$\alpha$ -Nsp1 (1:5000)	$\alpha$ -rabbit (1:2000)
$\alpha$ -Nup159 (1:5000)	$\alpha$ -rabbit (1:2000)

#### 4.3.4 Expression and purification of recombinant Nup159

##### constructs from *E. coli* for circular dichroism measurements

Recombinant Nup159 QT<sub>4-5</sub>-Linker-H1 and Nup159 QT<sub>4-5</sub>-Linker-h1-5 were expressed in *E. coli* BL21 Codon Plus. Specifically, cells were transformed with pET15b-HIS-Nup159-QT<sub>4-5</sub>-Linker-H1 or pET15b-HIS-Nup159-QT<sub>4-5</sub>-Linker-h1-5 and grown in LB medium at 37 °C to an OD<sub>600</sub> of 0.5. Expression was induced with 0.1-0.5 mM IPTG for 3 hrs at 23 °C. Cells were lysed in buffer containing 20 mM Hepes pH 7.5, 150 mM NaCl, 5% v/v glycerol, 1 mM  $\beta$ -mercaptoethanol and 10 mM imidazole at pH 8.0 supplemented with protease inhibitor (Serva) and by high-pressure cavitation (Microfluidics Corp., MA, USA) and cleared (17,000 rpm for 15 min at 4 °C). 6HIS-tagged proteins were purified from the supernatant with Ni-NTA affinity column (Qiagen) for 2 hrs at 4 °C. After three washing steps with buffer including 10 mM imidazole, 6HIS-tagged proteins were eluted with buffer including 50-250 mM imidazole gradient.

CD spectra of the protein samples were obtained on a Jasco J-720 spectropolarimeter using a water bath and water-jacketed cells for temperature control. Samples for CD measurements were prepared in 10 mM sodium phosphate, pH 7.0 in the protein concentration range of 3-10  $\mu$ M. Thermal unfolding was measured by monitoring the CD signal at 222 nm in the temperature range of 5 °C - 80 °C. Reversibility was determined by comparing measurements taken at 5 °C before and after thermal unfolding.

## 4.4 Microscopic methods

### 4.4.1 Fluorescence microscopy

Cells expressing GFP-tagged proteins were grown to an early log phase at 30 °C in YPG or selective media and then shifted to 23 °C or 37 °C for 2-4 hrs. Subsequently, exponentially growing cells were pelleted, washed, applied onto glass slides (Roth, Karlsruhe, Germany) and examined by fluorescence microscopy without fixation, using Imager Z1 microscope (Carl Zeiss, Inc.), equipped with a 100x/63x NA 1.4 Plan-Apochromat oil immersion lens. Pictures were acquired with a camera (AxioCam MRm; Carl Zeiss, Inc.) and AxioVision 4.3 software (Carl Zeiss, Inc.).

### 4.4.2 Electron microscopy

For single particle EM analysis of the complex, Flag-TEV-ProtA (FTP) tagged Nup82, together with Nsp1-CTD, Nup159-CTD and Dyn2 were over-expressed in bicistronic expression system under *GAL* promoter, grown in 2-12 L selective media, induced with 2% galactose and purified as described above. Flag eluate was further purified by size exclusion chromatography (Superdex 200 10/300 GL or Superdex 200 Increase 10/300, GE Healthcare) in a buffer (20 mM Tris-HCl or HEPES, pH 7.5, 150 mM NaCl, 50 mM K(OAc), 2 mM Mg(OAc)<sub>2</sub>) with 5% glycerol, no NP-40.

### **Stabilization and purification of Nup82 complexes using the GraFix protocol**

To improve sample quality and resolution for structure determination by single-particle electron microscopy, sample preparation procedure, called GraFix, was applied [Kastner et al., 2008]. Two glycerol gradients with and without cross-linking agent were prepared according to standard protocols. Briefly, filtered solutions of buffers containing glycerol (10-30%) were prepared in a centrifuge tubes with the use of gradient for-

mer (Gradient Master 107, BioComp Instruments, Canada). 0.15% glutaraldehyde (EM grade 25%, Science Services GmbH, Munich, Germany) was added to the 30% glycerol solution. The freshly prepared gradients were kept at 4 °C for one hour before sample loading. 200 µl of Flag eluate was directly applied onto a 200µl cushion of 7.5% (v/v) glycerol in a Hepes-NB buffer (20mM Hepes pH 7.5, 150 mM NaCl, 50 mM K(OAc), 2 mM Mg(OAc)<sub>2</sub>, 5% glycerol), followed by a linear 10-30% (v/v) glycerol and 0-0.15% glutaraldehyde (GA) gradient in a centrifuge tube and centrifuged in a SW 60 Ti Rotor Beckman Coulter) at 50000 rpm, at 4 °C for 16-18 hours (Beckman Coulter). Gradients were run with and without fixation reagent (GA) in parallel as a reference of particle sedimentation. After centrifugation, 200 µl fractions were collected. The non-fixed reference gradient was and analysed on SDS-PAGE. Undiluted fractions containing fixed complexes were negative stained and analyzed by a negative staining EM.

## **2D negative staining electron microscopy and image processing**

Negative staining EM of the Nup82-Nup159C-Nsp1C-Dyn2 complex was performed as described before [Lutzmann et al., 2005]. For negative staining, 5 µl of diluted sample were placed on a freshly glow-discharged, carbon-coated grid, allowed to absorb to the carbon for 10 s, washed three times with water, stained with uranyl acetate (2% w/v) and dried for 5-10 min. Micrographs were recorded with a Tecnai F20 (FEI) electron microscope with a 'Eagle' bottom mounted 4K, HS CCD camera at a nominal magnification of 50.000, operating at 200 kV. 4000 particles for Nup82-Nup159C-Nsp1C-Dyn2 complex, 3416 particles for unfixed Nup82-Nup159C-Nsp1C-Dyn2 complex, 5029 particles for Nup82-Nup159ΔFG-Nsp1C-Dyn2 complex, and 2577 particles for Nup82-Nup159Δtail-Nsp1C-Dyn2 complex were selected manually using 'Boxer' [Ludtke et al., 1999]. Subsequent image processing was carried out in IMAGIC-4D [van Heel et al., 1996], following the program's standard procedures. Particles were band-pass filtered and normalized in their grey value distribution and mass-centred. Alignment, iterative

refinement of class averages, and the calculation of the three-dimensional (3D) maps followed the procedures described in [Lutzmann et al., 2005].

## 4.5 Size exclusion chromatography

Affinity-purified bait proteins were analysed by size exclusion chromatography (SEC) in a buffer without NP-40 (20 mM Tris-HCl or Hepes at pH 7.5, 150 mM NaCl, 50 mM K(OAc), 2 mM Mg(OAc)<sub>2</sub>, 5% glycerol). They were separated on a Superdex 200 10/300 GL or Superdex 200 Increase 10/300 GL column attached to the Åkta-Basic System (Amersham Biosciences). Next, 500 µl fractions were collected and analyzed by SDS-PAGE and standard Coomassie staining protocol.

## 4.6 Multiangle light scattering (MALS)

The chromatography system was connected in series with an eight-angle light scattering detector from DAWN HELEOS (Wyatt Technology Corp., Santa Barbara, CA) with a light scattering SEC-3010 refractometer for dRI (differential refractive index) detection (WGE Dr Bures, Dallgow-Doeritz, Germany) was used to determine the molecular mass of complexes. Data were collected at a flow rate of 0.5 mL/min at 4 °C. Measurement analysis were carried out using the ASTRA 6.1 software and Zimm light scattering model (Wyatt Technology Corp. Santa Barbara, CA), yielding the molar mass and mass distribution (polydispersity) of the sample.

## 4.7 Cross-linking mass spectrometry

100 µg (0.5 µg/ml) of the affinity purified Nup82 truncated complex was cross-linked by addition iso-stoichiometric mixture of H12/D12 isotope-coded di-succinimidyl-

suberate (DSS) or disuccinimidyl-glutarate (DSG, Creative Molecules) to a final concentration of 1.6 mM. After 30 min at 37 °C, the reaction was quenched with 50 mM ammonium bicarbonate for 10 min 37 °C. Cross-linked samples were further processed and analyzed with a LTQ-Orbitrap Velos Pro mass spectrometer (Thermo Scientific) as previously described [Walzthoeni et al., 2012]. The mass spectrometric data was analyzed using xQuest/xProphet software and the false discovery rate was set to 5% [Walzthoeni et al., 2012].

## 4.8 3D EM Data Acquisition

Tomograms of the negatively stained Nup82 complex were collected using a POLARA (300kv FEG, FEI, Eindhoven) operated at 100 kV and equipped with Gatan Camera 2k x2k and GIF 2002 energy filter (Gatan, California) using FEI Batch Tomography Software. In total 90 tomograms were collected over a tilt range of +/- 60 degrees with an angular increment 3 degrees at binning 2 using SerialEM [Mastronarde, 2005], resulting in a nominal pixel size of 6.06 Å. The defocus was 1.5 to 3 mm and the total dose was 300 e-/Å<sup>2</sup>. The 3D structure of Nup82 subcomplex was obtained using a previously described protocol [Bui et al., 2013]. Briefly, the subtomograms of the acquired tomograms from negatively stained Nup82 particles were projected for two-dimensional classification and the resulting classes were subjected to subtomogram averaging. We manually picked 5,941 particles (subtomograms). Subtomograms were projected along the missing wedge axis in order to create an equivalent number of 2D images for subsequent 2D classification using k-means clustering in SPIDER, which resulted in 20 classes. A 3D structure corresponding to each class was then calculated using subtomogram averaging. The resolution of all classes as determined by FSC varied and was 36 Å for the best class.

## 4.9 Miscellaneous

### 4.9.1 Protein alignments and secondary structure prediction

Protein sequences were aligned using T-Coffee (<http://tcoffee.vital-it.ch/apps/tcoffee/do:regular>) and Jalview [Waterhouse et al., 2009], and manually edited to highlight conserved domains. Conserved secondary structures were predicted using Jpred (<http://www.compbio.dundee.ac.uk/www-jpred>) and analyzed with Chimera 1.8.1 (<http://www.cgl.ucsf.edu/chimera>).

### 4.9.2 Structural modelling

Models for the C-terminal,  $\alpha$ -helical part of Nup159 were generated using the I-Tasser webserver [Roy et al., 2010]. Five top-ranking clusters were generated. The two best clusters (according to their c-scores [Zhang, 2008]) shared a common fold for the C-terminal,  $\alpha$ -helical part of Nup159 (including parts of H2, H3, H4 and the tail region; residues 1286-1434) resembling an  $\alpha$ -helical bundle.

## 5 Abbreviations

**Table 5.1:** List of Abbreviations A-F

A-F	
ACE1	Ancestral Coatomeer Element 1
ALPS	ArfGAP1 Lipid Packing Sensor
ArfGAP1	GTPase-Activating Protein (GAP) for Arf1
ATP	Adenosine-5-Triphosphate
CD	Circular Dichroism
Cryo-ET	Cryo Electron Tomography
COPI/II	Coat Protein Complex I/II
CTD	Carboxy-Terminal Domain
3D	Three-Dimensional
DAPI	4', 6-Diamidino-2-phenylindole
DEAD	Aspartic Acid(D)-Glutamic Acid(E)-Alanine(A)-Aspartic Acid(D)
DID	Dynein Light Chain Interacting Domain
DIM	Domain Invasion Motif
DMSO	Dimethyl Sulfoxide
DNA	Deoxyrybonucleic Acid
DSG	Disuccinimidyl-Glutarate
DSS	Disuccinimidyl-Suberate
DTT	Dithiothreitol
Dyn2	Dynein Light Chain (DYL1_YEAST)
EDTA	EthyleneDiamineTetraacetic Acid
EM	Electron Microscopy
ER	Endoplasmic Reticulum
FG	Phenylalanine-Glycine
5-FOA	5-Fluoro-Orotic Acid
FRAP	Fluorescence Recovery After Photobleaching
FTP	Flag-TEV-Protein A
FXFG	Phenylalanine-any Amiono Acid-Phenylalanine-Glycine

**Table 5.2:** List of Abbreviations G-N

G-N	
GA	Glutaraldehyde
GAP	GTPase Activating Protein
GDP	Guanosine-5'-Diphosphate
GEF	Guanine Nucleotide Exchange Factor
GFP	Green Fluorescent Protein
GLFG	Glycine-Leucine-Phenylalanine-Glycine
GraFix	EM Sample Preparation Procedure With Density <u>G</u> radient And Weak Chemical <u>F</u> ixation
GTP	Guanosine-5'-Triphosphate
GTPase	Guanosine-5'-Triphosphate Hydrolase
HCl	Hydrochloric Acid
hr	Hour
HRP	Horseradish Peroxidase
INM	Inner Nuclear Membrane
IPTG	Isopropyl $\beta$ -D-1thiogalactopyranoside
kDa	kilodalton
LB	Luria-Bertani medium
MDa	Megadalton
MES	2-(N-morpholino) ethanesulfonic acid
mg	miligram
min	minute
ml	milliliter
Mlp	Myosin-Like Protein
mM	milimolar
MOPS	2-(N-morpholino) propanesulfonic acid
mRNA	Messenger RNA
mRNP	Messenger Ribonucleoprotein Particle
$\mu$ l	microliter
NE	Nuclear Envelope
NES	Nuclear Export Sequence
NLS	Nuclear Localization Signal
nm	Nanometer
NPC	Nuclear Pore Complex
NTD	Amino(N)-Terminal Domain
NTF2	Nuclear Transport Factor 2
NTR	Nuclear Transport Receptor

**Table 5.3:** List of Abbreviations O-Z

O-Z	
OD	Optical Density
ORF	Open Reading Frame
ONM	Outer Nuclear Membrane
pA	Protein A
PBS	Phosphate Buffered Saline
PCR	Polymerase Chain Reaction
PMSF	Phenylmethanesulfonyl Fluoride
Ran	RAs-related Nuclear Protein
RanBP1	Ran Binding Protein 1
RNA	Rybonucleic Acid
RNP	Ribonucleoprotien
rpm	Revolutions Per Minute
RT	Room Temperature
SDC	Synthetic Defined Complete (Medium)
SDS-PAGE	Sodium-Dodecyl-Sulfate Polyacrylamide Gel Electrophoresis
SV40	Simian Virus 40
TAE	TRIS Acetic Acid EDTA
TAP	Tandem Affinity Purification
TBS	TRIS Buffered Saline
TCA	Trichloroacetic Acid
TEV	Tobacco Etch Virus
Tpr	Translocated Promoter Region (NPC-Associated Protein TPR)
ts	Temperature-sensitive
WCE	Whole Cell Extract
WT	Wild-type
YPD	Yeast Peptone Dextrone

## 6 Own Publications

1. Stelter, P., Kunze, R., **Radwan, M.**, Thomson, E., Thierbach, K., Thoms, M., and Hurt, E. (2012). Monitoring spatiotemporal biogenesis of macromolecular assemblies by pulse-chase epitope labeling. *Molecular Cell*, 47(5):788-796.

2. **Gaik, M.**, Flemming, D., von Appen, A., Kastiris, P., Stelter, P., Bui, H.K., Bassler, J., Fischer J., Barbar, E., Beck, M., and Hurt, E. (2014). Structural basis for assembly and function of megadalton-sized Nup82 complex in the nuclear pore scaffold. *The Journal of Cell Biology*. Under revision.

3. Horwacik, I., **Gaik, M.**, Durbas, M., Boratyn, E., Zając, G., Szychowska, K., Szczodrak, M., Kołoczek, H. and Rokita, H. (2014). Inhibition of autophagy by 3-methyladenine potentiates sulforaphane-induced cell death of human neuroblastoma BE(2)-C cell line. *Molecular Medicine Reports*. In press.

## 7 Supplemental Figures

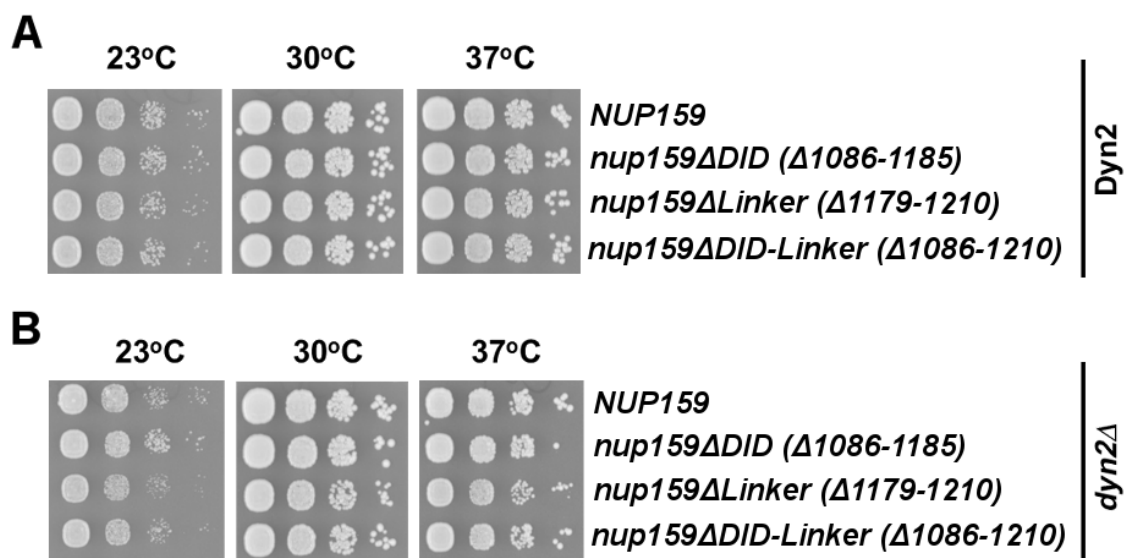


**Figure 7.1:** Growth analysis of *dyn2Δ*, *nup159ΔDID<sub>Nup159</sub>* and *nup159ΔLinker* mutants

(A, B) Dot spot analysis of wild-type and *nup159* deletion strains in Dyn2 or *dyn2Δ* background. The *nup159Δ* shuffle strain was transformed with the indicated *nup159* mutant constructs under the control of the endogenous *NUP159* promoter in Dyn2 (A) or *dyn2Δ* (B) background. Cells were spotted in 10-fold serial dilutions onto SDC+5-FOA plates and incubated at the indicated temperatures for 3 days.

## Nup82-C

```

tjG0ZGT7|G0ZGT7_9PEZI/1-882 627 P A E A L D K P S A V P A W I D N L R T G R R R P L L T O E L R L S M A T L E V F H D G H V V S T E V S D I N D A V A E L F R K C E A L Q G E L R D Q I 703
tjQ7RXL7|Q7RXL7_NEUCR/1-888 632 P S E V L S R P S T L P P W W D A L R T S R K R P L M Q O E V R L S V A T L E I F E S H R L V S S E V F E L N N A V A E L F R K C E A L T Y E L K E Q I 708
tjD1ZMH5|D1ZMH5_SORMK/1-890 634 P A E V L S R P S T L A P W L D S L R T S R K R P L M Q O E V R L S V A T L E I L E G H R L V S S E V F E L N N A V A E L F R K C E A L T Y E L K E Q I 710
tjA1DGF9|A1DGF9_NEOF/1-885 631 V P S I L Y S D S P L E F F V E K H V P H R O R S L K E Q V R L S A T L D L V A A A H R I L S A H T N A L E R A A D L F R R C E R L Q G E M K E Q L 707
tjB6H260|B6H260_PENCW/1-880 629 V P A I F Y A N S P L D S F V E K H V P H R O R H T L K E Q V R L S A T L D L V A T A H R V L S A H T N A L E R A A D L F R R C E R L Q G E M O D L 705
tjC8V2B2|C8V2B2_EMENI/1-870 617 V P S I L Y S D S P L E F F V D K H V P H R O R S L K E Q V L S A T L D L V A A A H R I L S A H T N A L E R A A D L F R R C E R L Q G E L R D L 693
tjQ2TZH9|Q2TZH9_ASPOR/1-886 631 V P A V F Y S D S P L E F F V D K H I P H R O R H T L K E Q V R L S A T L D L V A A A H R I L S A H T N A L E R A A D L F R R C E R L Q G E M O Q L 707
tjR9XF47|R9XF47_ASHAC/1-672 446 L L N T N K E L Q R R K H O P L P - L V P P A L K N I P L N S D L N E O H L A T L T K I S E V M D R I I L S O S V G L L M H N R L S L Q Y F E L H R V 521
tjQ6FPB3|Q6FPB3_CANGA/1-716 491 I Q H Y E Q I Y Y K N L Q N Q N F T K I P L E I R S A P L K N S S N E N Q L E S L K I S E S Y M K M I S M A O T L G Y I Y R K R M I D S I E E F S R O I 567
tjG8C1T5|G8C1T5_TETPH/1-721 497 I N I A V Q R Y K D S C K V P S Y K V I P A N I R Q K P F A N D E N E D Q L A Y I T E I S E I G S K I L O G O T I A L M M H T R L R E Q D D V F A E L 573
tjC5E1G0|C5E1G0_ZYGR/1-692 468 I L S L N A S F Q T E A K K P L S K L V E P S K R O T K L N N E S N E E Q L E I L T T V S K E F L O K I V K A O A L G F N L H N R C L E Q D Y E L T R L O 544
tjQ758C0|Q758C0_ASHGO/1-673 447 I L N T N K E L Q R R K H O P L P - L V P P A L K N I P L N S D L N E O H L A T L T N I S K E V M D R I I L S O S A G L L M H N R L S L Q Y F E L H R V 522
tjQ6CLN4|Q6CLN4_KLULA/1-687 469 L D M L L T K Y K T E A N - G F I S G I P D S L A P L P L K N N S N E R O L E V V S E L Y K E T M K R V K L G O M I L F R M F N K S N E E V A E L H R L O 544
tjC5E363|C5E363_LACTC/1-691 461 V O T L N Q K V Q S L L K S P L S T V I P A A L R O K T L N N T D N E D Q L S L L D I S K E V L S R V T L A O T L G L S L H L R L L G Q O D L A O L H 537
tjA7TKI9|A7TKI9_VANPO/1-717 487 L K A A N Y K F Q E A V S V P Y S K V I P A A N I K Q V P F G S N A M E Q L K I L N D I S R D V G S K I V O G G S L G L M L Y D R L L E Q Q D K L S L O 563
sp|P40368|NUP82_YEAST/1-713 488 I L I L N D N F Q K A C I S P C E R I P S A D R Q I P L K N E A S E N Q L E I F T D I S K E F L O R I V K A O T L G V S I H N R I H E Q C F E L T R L 564
    
```

## H1

```

tjG0ZGT7|G0ZGT7_9PEZI/1-882 704 K K V N E V K N R I H T I T G D D L S - - - D P P V S E D Q L I K O I R V A R E P O E E L A N R M E R L R K K F G R T T R E L S D K E K A W I E E V 777
tjQ7RXL7|Q7RXL7_NEUCR/1-888 709 T K Y Y V N Q R I E T I S G E S R S T K E O N I S E E M L V R N I D V M K V R O E N L A R R V D N L R K R L G O V S T R E L S D K E K A W A E E V 785
tjD1ZMH5|D1ZMH5_SORMK/1-890 711 T K Y Y V N Q R I E T I S G E S R S D K E O N I S E E M L V R N I D V M K V R O E N L A R R V D N L R K R L G O V S T R E L S D K E K A W I E E V 787
tjA1DGF9|A1DGF9_NEOF/1-885 708 K Q L S D V A E R I K G V S S D I G E D G O R R K E G S R S D E A L D K R L K A A K E R Q A O L A E R Y E S L R N K V L K S G G R P L S E R E K A W I T E V 784
tjB6H260|B6H260_PENCW/1-880 706 K Q L A D V A E R V K G V T S E I G E D G H R K E G V R N G E A L D K R L Q A A Q D K Q S E L N R R Y E A L R T K V L N S G G R P L S E R E K A W I T E V 782
tjC8V2B2|C8V2B2_EMENI/1-870 694 G O I A D V A D R I K G V S S E I G E D G O R R K E G S R S T A A L N A R L K A A K D R Q S E L V W R Y E A I R N K V L K S G G R P L S E K E S S W I A E V 770
tjQ2TZH9|Q2TZH9_ASPOR/1-886 708 K Q L T D V S E R I K G V S S E I G E D G E R K E N S R S G E A L D K R L Q A A K D K Q E O L V O R Y E A I R N K V L K S G G R P L S E K E K A W S V E 784
tjR9XF47|R9XF47_ASHAC/1-672 522 E T V A D L S S R H S V L R E S A D A M S S R L A S V L K - - - - - D R R L K O R M G M L Q S T L N R I N - S S H K F S D L P L S K K E A D W F R E L 591
tjQ6FPB3|Q6FPB3_CANGA/1-716 568 E T T Y Q I N K F W D N F E Q I R E V Q N T K I D K V K E - - - - - K Q Q L M E R L S S L Y D K V E G O K - E M G S M N N S N I A A E S E W F A E I 637
tjG8C1T5|G8C1T5_TETPH/1-721 574 M H I N K E L L H N K T I K Q T Y D I Q S T K I K H I T E - - - - - R N T K L N E R T S K L I E M M E K I K - O S Q Y K N M P I N D S E S K L F K E I 643
tjC5E1G0|C5E1G0_ZYGR/1-692 545 Q Y S E I L S K Q D K L R S K A O S Q S S E C E S K I Q - - - - - R Q D K L O R F N S L S E K L G R I N - E S P K F R E M N I T O K E M A W F R E I 614
tjQ758C0|Q758C0_ASHGO/1-673 523 E T V A D I C S R H S V L R D S S E A M S S R L S V L K - - - - - D R R L K O R L C M L Q S T L N R I N - S S H K F S D L P L S K K E A D W F R E L 592
tjQ6CLN4|Q6CLN4_KLULA/1-687 545 R K N E I E M L R N K L N G N L G D L O E R Y S R Y E E - - - - - K S K T L E K R L D L K E T F S S I E - N N E K L R T S S I S E A E L W W F K S I 614
tjC5E363|C5E363_LACTC/1-691 538 R D V S E L R T K K E R V S A H L A S Q K P R W E A I Q E - - - - - K N K S I A L R F E L H R N M T I S - K S S L Q S S O P I A K A E M O L F K E L 607
tjA7TKI9|A7TKI9_VANPO/1-717 564 I I I N K I L I R A K K V O G D Y P A Q L S K L D E K L K - - - - - K Q E H L E K I L L K M E S N L N T I Q - E S Q K L K S L P L S E K E I Q L F K E L 633
sp|P40368|NUP82_YEAST/1-713 565 Q S C K I I S K D D D L R R K F E A Q N K K W D A Q L S - - - - - R Q S E L M E F S K L S K L S O J A - E S N K F K E K K I S H G E M K W F K E I 634
    
```

## H2

## H3

```

tjG0ZGT7|G0ZGT7_9PEZI/1-882 778 G N M A T S I L G - P E A G O G A L A T T P N L A K O P W K R L E E I K T L R N A L M A E A E Q L Q V G D D T E E S T F - - A S O M P S L K I P S E I R 851
tjQ7RXL7|Q7RXL7_NEUCR/1-888 786 R T L A G S I L G D E E E E D T T S A S I S T A G K L K R F E E V O T L R D A L F E Q A Q Q L O S T - - D S V D G T - - - A S P M P V M K I P S E I R 857
tjD1ZMH5|D1ZMH5_SORMK/1-890 788 R T L A S S I L G D E E E E D T T T A S I N T A G H L K R F E E V O T L R D A L F E Q A Q Q L O S T - - D S I D G T - - - P S P M P V M K I P S D I R 859
tjA1DGF9|A1DGF9_NEOF/1-885 785 E A L S A S L E R E K K E - - - - - E E K D Q S L S Q R L E T V K E L A A D L L V E A K S I A A K A P G A R E P G S P A S P T A A G R V P Q R L Q 853
tjB6H260|B6H260_PENCW/1-880 783 K T L S A S L Q Q M E E Q - - - - - E E E Q P L V S R L E T V K R L A R D L M A O T K S V A G K M P S P - E L G T P S S P G G - Q P K V P Q R L Q 848
tjC8V2B2|C8V2B2_EMENI/1-870 771 E A L S O S F D K E R K E - - - - - E S A Q H I A K R L D A V K D I A S E L I T E A K S V A A R I F T T T P S T P T S A Q P R V P Q R L Q 838
tjQ2TZH9|Q2TZH9_ASPOR/1-886 785 E T L S E S F G D R Q E G - - - - - R D N G Q O O L S E R L E T V K E I A A D L L A E A K S I A V K A P S P T E P G S P A S P G G S Q P R V P Q R L Q 854
tjR9XF47|R9XF47_ASHAC/1-672 592 K N O A I F N D Y V L G S - - - - - A Q L R D E L A F L K N E L E S L P E H R O H D R Q E E E P F - - - - - D F O R L 641
tjQ6FPB3|Q6FPB3_CANGA/1-716 638 K R S V I E F N S Y V R K A - - - - - S T N H Q E L F L K E Q Q A Q I A N O K P D I I S S E N G K E - - - - - W N N D L 686
tjG8C1T5|G8C1T5_TETPH/1-721 644 K K Q V L I F N D A V N R Q - - - - - Q E Q Q E A I K F L Q T E L N N I I E O P - A Q S H D A I D S D E D - - - - - E W N E L 662
tjC5E1G0|C5E1G0_ZYGR/1-692 615 R N Q V L V F N Q V V H H O - - - - - K N Q Q D O L R Y L Q K E L E N I S L E D K D V - G E K S K S - - - - - E W T E L 663
tjQ758C0|Q758C0_ASHGO/1-673 593 K N O A I F N D Y V L G S - - - - - A Q L R D E L A F L K N E L E S L P E H R O H D R Q E E E P F - - - - - D F R R L 642
tjQ6CLN4|Q6CLN4_KLULA/1-687 615 K N Q V L F N N Y V H L T - - - - - N K R E E L E F D T O L R S T I K G D D F S E L E - - - - - F S S L 660
tjC5E363|C5E363_LACTC/1-691 608 R N Q V V R F N R L V H E Q - - - - - Q D L A E A N I G F L K S L E Y V R V D S A E A A S R S K K S A S A G G V P - - - - - W D E L 664
tjA7TKI9|A7TKI9_VANPO/1-717 634 R S O I L L F N F V H K Q - - - - - K D O K Q L I G F L K E L O K I I D I S R S E S S K M L N I - - - - - E W E E L 683
sp|P40368|NUP82_YEAST/1-713 635 R N Q I L Q F N S F V H S Q - - - - - K S L Q D L S Y L K S E L T R I E A E T I K V - D K S Q N - - - - - E W D E L 683
    
```

## H3

## H4

```

tjG0ZGT7|G0ZGT7_9PEZI/1-882 852 K A K M A Q V M S L L E R E F A L V D A V K A R I E R L S I G - - - 882
tjQ7RXL7|Q7RXL7_NEUCR/1-888 858 K Q K V A Q V M S L L D R E T A L V E A V K S R L E R L S I E - - - 888
tjD1ZMH5|D1ZMH5_SORMK/1-890 860 K Q K V A Q V M S L L D R E T A L V E A V K S R L E K L S I D - - - 890
tjA1DGF9|A1DGF9_NEOF/1-885 854 R A K I S D A M R M V E R E S A V I E A I T S R L N R L N S S I - - - 885
tjB6H260|B6H260_PENCW/1-880 849 R A K V A D A M R M V E R E S A V I E A I T S R L E R L N T S L - - - 880
tjC8V2B2|C8V2B2_EMENI/1-870 839 R A K I A D A M K M V E R E S A V I E S I T A R L A R L N T L V - - - 870
tjQ2TZH9|Q2TZH9_ASPOR/1-886 855 R A K I A D A M K M V E R E S A V I E A I S R R L E R L N A S I - - - 886
tjR9XF47|R9XF47_ASHAC/1-672 642 Q E L L K L D S K I I T E C T D N L S A A A R E L E R L C I - - - 672
tjQ6FPB3|Q6FPB3_CANGA/1-716 687 Q Q L L R T D L K I I S E F E K K O D T A V N G I N Q L K I - - - 716
tjG8C1T5|G8C1T5_TETPH/1-721 697 C D L L N R D A K I I E D C N A E L S S A S G L I - - - - - 721
tjC5E1G0|C5E1G0_ZYGR/1-692 664 L S I L E S D T K I I K E C N N O L A H A S S E V G F S T - - - - 692
tjQ758C0|Q758C0_ASHGO/1-673 643 Q E L L K L D S K I I T E C T D N L S A A A R E L E R L C I - - - 673
tjQ6CLN4|Q6CLN4_KLULA/1-687 661 Q O M L L N D K K V I N S C M N E L S A S I E D L A V - - - - 687
tjC5E363|C5E363_LACTC/1-691 665 Q A M L A K D S R I I K E C O A E L Q C T T O E L D S - - - - 691
tjA7TKI9|A7TKI9_VANPO/1-717 684 R Q I L A D D A K I I K E C N E O L T Q I S K E L D T K N T V T N S - - - 717
sp|P40368|NUP82_YEAST/1-713 684 R K M L E I D S K I I K E C N E E L L O V S Q E T T K T Q - - - - 713
    
```

## H5

Figure 7.2: Multi-sequence alignment of the  $\alpha$ -helically predicted C-domain of Nup82

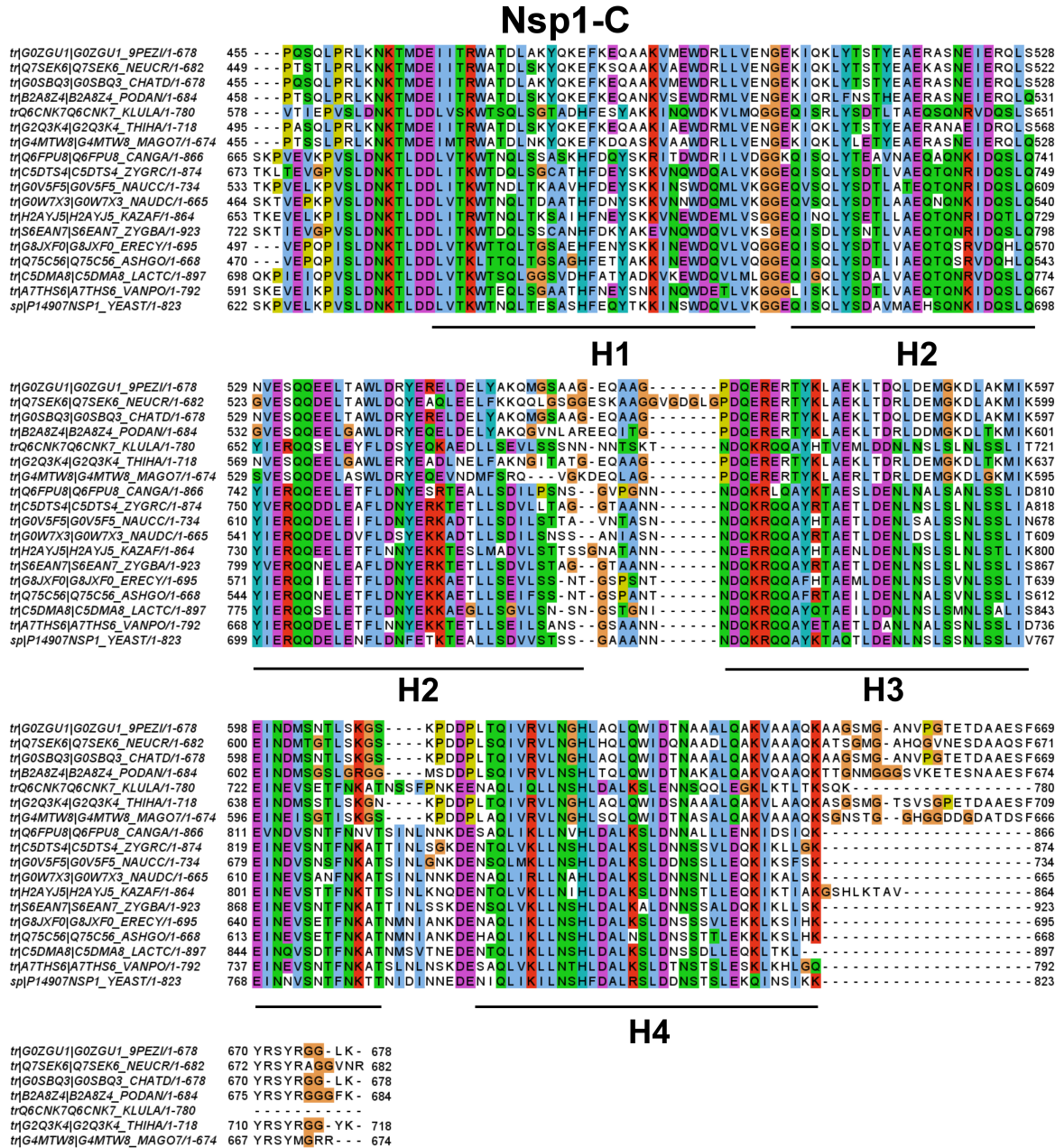


Figure 7.3: Multi-sequence alignment of the  $\alpha$ -helically predicted C-domain of Nsp1

# Bibliography

- [Adams and Wente, 2013] Adams, R. L. and Wente, S. R. 2013. Uncovering nuclear pore complexity with innovation. *Cell*, 152(6):1218–1221.
- [Aitchison and Rout, 2012] Aitchison, J. D. and Rout, M. P. 2012. The yeast nuclear pore complex and transport through it. *Genetics*, 190(3):855–883.
- [Akey and Radermacher, 1993] Akey, C. W. and Radermacher, M. 1993. Architecture of the xenopus nuclear pore complex revealed by three-dimensional cryo-electron microscopy. *J Cell Biol*, 122(1):1–19.
- [Alber et al., 2007a] Alber, F., Dokudovskaya, S., Veenhoff, L. M., Zhang, W., Kipper, J., Devos, D., Suprpto, A., Karni-Schmidt, O., Williams, R., Chait, B. T., Rout, M. P., and Sali, A. 2007a. Determining the architectures of macromolecular assemblies. *Nature*, 450(7170):683–694.
- [Alber et al., 2007b] Alber, F., Dokudovskaya, S., Veenhoff, L. M., Zhang, W., Kipper, J., Devos, D., Suprpto, A., Karni-Schmidt, O., Williams, R., Chait, B. T., Sali, A., and Rout, M. P. 2007b. The molecular architecture of the nuclear pore complex. *Nature*, 450(7170):695–701.
- [Amlacher et al., 2011] Amlacher, S., Sarges, P., Flemming, D., van Noort, V., Kunze, R., Devos, D. P., Arumugam, M., Bork, P., and Hurt, E. 2011. Insight into structure and assembly of the nuclear pore complex by utilizing the genome of a eukaryotic thermophile. *Cell*, 146(2):277–289.
- [Bailer et al., 2001] Bailer, S. M., Balduf, C., Hurt, E. D., Heidelberg, B.-z., and Heidelberg, D. 2001. The Nsp1p carboxy-terminal domain is organized into functionally distinct coiled-coil regions required for assembly of nucleoporin subcomplexes and nucleocytoplasmic transport. *Mol Cell Biol*, 21(23):7944–7955.
- [Bailer et al., 2000] Bailer, S. M., Balduf, C., Katahira, J., Podtelejnikov, A., Rollenhagen, C., Mann, M., Pante, N., and Hurt, E. 2000. Nup116p associates with the Nup82p-Nsp1p-Nup159p nucleoporin complex. *J Biol Chem*, 275(31):23540–23548.
- [Barbar, 2008] Barbar, E. 2008. New Concepts Dynein Light Chain LC8 Is a Dimerization Hub Essential in Diverse. *Biochemistry*, 47(2):1–6.
- [Bayliss et al., 2000] Bayliss, R., Littlewood, T., and Stewart, M. 2000. Structural basis for the interaction between FxFG nucleoporin repeats and importin-beta in nuclear trafficking. *Cell*, 102(1):99–108.
- [Bayliss et al., 1999] Bayliss, R., Ribbeck, K., Akin, D., Kent, H. M., Feldherr, C. M., Görlich, D., and Stewart, M. 1999. Interaction between NTF2 and xFxFG-containing nucleoporins is required to mediate nuclear import of RanGDP. *J Moll Biol*, 293(3):579–93.
- [Beck et al., 2004] Beck, M., Förster, F., Ecke, M., Plitzko, J. M., Melchior, F., Gerisch, G., Baumeister, W., and Medalia, O. 2004. Nuclear pore complex structure and dynamics revealed by cryoelectron tomography. *Science*, 306(5700):1387–1390.
- [Beck et al., 2007] Beck, M., Lucić, V., Förster, F., Baumeister, W., and Medalia, O. 2007. Snapshots of nuclear pore complexes in action captured by cryo-electron tomography. *Nature*, 449(7162):611–5.
- [Belgareh et al., 1998] Belgareh, N., Snay-Hodge, C., Pasteau, F., Dagher, S., Cole, C. N., and Doye, V. 1998. Functional characterization of a Nup159p-containing nuclear pore subcomplex. *Mol Biol Cell*, 9(12):3475–3492.

- [Bernad et al., 2004] Bernad, R., Velde, H. V. D., Fornerod, M., and Pickersgill, H. 2004. Nup358/RanBP2 attaches to the nuclear pore complex via association with Nup88 and Nup214/CAN and plays a supporting role in CRM1-mediated nuclear protein export. *Mol Cell Biol*, 24(6):2373–2384.
- [Bradatsch et al., 2007] Bradatsch, B., Katahira, J., Kowalinski, E., Bange, G., Yao, W., Sekimoto, T., Baumgärtel, V., Boese, G., Bassler, J., Wild, K., Peters, R., Yoneda, Y., Sinning, I., and Hurt, E. 2007. Arx1 functions as an unorthodox nuclear export receptor for the 60S preribosomal subunit. *Mol Cell*, 27(5):767–79.
- [Brickner and Walter, 2004] Brickner, J. H. and Walter, P. 2004. Gene recruitment of the activated INO1 locus to the nuclear membrane. *PLoS Biol*, 2(11):e342.
- [Brohawn et al., 2008] Brohawn, S. G., Leksa, N. C., Spear, E. D., Rajashankar, K. R., and Schwartz, T. U. 2008. Structural evidence for common ancestry of the nuclear pore complex and vesicle coats. *Science*, 322(11):1369–1373.
- [Brohawn et al., 2009] Brohawn, S. G., Partridge, J. R., Whittle, J. R., and Schwartz, T. U. 2009. The nuclear pore complex has entered the atomic age. *Structure*, 17:1156–1168.
- [Brown, 2010] Brown, J. H. 2010. How sequence directs bending in tropomyosin and other two-stranded alpha-helical coiled coils. *Prot Scien*, 19:1366–1375.
- [Bui et al., 2013] Bui, K. H., von Appen, A., Diguilio, A. L., Ori, A., Sparks, L., Mackmull, M.-T., Bock, T., Hagen, W., Andrés-Pons, A., Glavy, J. S., and Beck, M. 2013. Integrated structural analysis of the human nuclear pore complex scaffold. *Cell*, 155(6):1233–43.
- [Cabal et al., 2006] Cabal, G. G., Genovesio, A., Rodriguez-Navarro, S., Zimmer, C., Gadai, O., Lesne, A., Buc, H., Feuerbach-Fournier, F., Olivo-Marin, J.-C., Hurt, E. C., and Nehrbass, U. 2006. SAGA interacting factors confine sub-diffusion of transcribed genes to the nuclear envelope. *Nature*, 441(7094):770–3.
- [Casolari et al., 2004] Casolari, J. M., Brown, C. R., Komili, S., West, J., Hieronymus, H., and Silver, P. a. 2004. Genome-wide localization of the nuclear transport machinery couples transcriptional status and nuclear organization. *Cell*, 117(4):427–39.
- [Chook and Blobel, 1999] Chook, Y. M. and Blobel, G. 1999. Structure of the nuclear transport complex. *Nature*, 399(May):230–237.
- [Cronshaw et al., 2002] Cronshaw, J. M., Krutchinsky, A. N., Zhang, W., Chait, B. T., and Matunis, M. J. 2002. Proteomic analysis of the mammalian nuclear pore complex. *J Cell Biol*, 158(5):915–927.
- [Davis and Fink, 1990] Davis, L. I. and Fink, G. R. 1990. The NW7 Gene Encodes an Essential of the Yeast Nuclear Pore Complex. *Cell*, 61:965–976.
- [Debler et al., 2008] Debler, E. W., Ma, Y., Seo, H.-S., Hsia, K.-C., Noriega, T. R., Blobel, G., and Hoelz, A. 2008. A fence-like coat for the nuclear pore membrane. *Mol Cell*, 32(6):815–26.
- [Del Priore et al., 1997] Del Priore, V., Heath, C. V., Snay, C. A., Macmillan, A., Gorsch, L. C., Dagher, S., Cole, C. N., and Priore, V. D. 1997. A structure/function analysis of Rat7p/Nup159p, an essential nucleoporin of *Saccharomyces cerevisiae*. *J Cell Biol*, 110 ( Pt 2):2987–99.
- [Delphin et al., 1997] Delphin, C., Guan, T., Melchior, F., and Gerace, L. 1997. RanGTP Targets p97 to RanBP2, a Filamentous Protein Localized at the Cytoplasmic Periphery of the Nuclear Pore Complex. *Mol Biol Cell*, 8(12):2379–2390.
- [Denning et al., 2003] Denning, D. P., Patel, S. S., Uversky, V., Fink, A. L., and Rexach, M. 2003. Disorder in the nuclear pore complex: the FG repeat regions of nucleoporins are natively unfolded. *PNAS*, 100(5):2450–5.
- [Devos et al., 2004] Devos, D., Dokudovskaya, S., Alber, F., Williams, R., Chait, B. T., Sali, A., and Rout, M. P. 2004. Components of coated vesicles and nuclear pore complexes share a common molecular architecture. *PLoS Biol*, 2(12):e380.

- [Devos et al., 2006] Devos, D., Dokudovskaya, S., Williams, R., Alber, F., Eswar, N., Chait, B. T., Rout, M. P., and Sali, A. 2006. Simple fold composition and modular architecture of the nuclear pore complex. *PNAS*, 103(7):2172–7.
- [Doucet and Hetzer, 2010] Doucet, C. M. and Hetzer, M. W. 2010. Nuclear pore biogenesis into an intact nuclear envelope. *Chromosoma*, 119(5):469–477.
- [Doucet et al., 2010] Doucet, C. M., Talamas, J. a., and Hetzer, M. W. 2010. Cell cycle-dependent differences in nuclear pore complex assembly in metazoa. *Cell*, 141(6):1030–1041.
- [Doye and Hurt, 1997] Doye, V. and Hurt, E. 1997. From nucleoporins to nuclear pore complexes. *Curr Opin Cell Biol*, 9(3):401–11.
- [Doye and Hurt, 1995] Doye, V. and Hurt, E. C. 1995. Genetic approaches to nuclear pore structure and function. *Trends Genet*, 11(6):235–241.
- [Dreyfus et al., 2012] Dreyfus, T., Doye, V., and Cazals, F. 2012. Assessing the reconstruction of macromolecular assemblies with toleranced models. *Proteins*, 80(9):2125–36.
- [Drin et al., 2007] Drin, G., Casella, J.-F. F., Gautier, R., Boehmer, T., Schwartz, T. U., and Antony, B. 2007. A general amphipathic alpha-helical motif for sensing membrane curvature. *Nat Struct Mol Biol*, 14(2):138–146.
- [Eisele et al., 2013] Eisele, N. B., Labokha, A. a., Frey, S., Görlich, D., and Richter, R. P. 2013. Cohesiveness tunes assembly and morphology of FG nucleoporin domain meshworks - Implications for nuclear pore permeability. *Biophys J*, 105(8):1860–70.
- [Elad et al., 2009] Elad, N., Maimon, T., Frenkiel-Krispin, D., Lim, R. Y. H., and Medalia, O. 2009. Structural analysis of the nuclear pore complex by integrated approaches. *Curr Opin Struc Biol*, 19(2):226–32.
- [Fabre and Hurt, 1997] Fabre, E. and Hurt, E. 1997. Yeast genetics to dissect the nuclear pore complex and nucleocytoplasmic trafficking. *Annu Rev Genet*, 31:277–313.
- [Fahrenkrog and Aebi, 2003] Fahrenkrog, B. and Aebi, U. 2003. The nuclear pore complex: nucleocytoplasmic transport and beyond. *Nat Rev Mol Cell Biol*, 4(10):757–66.
- [Fahrenkrog et al., 1998] Fahrenkrog, B., Hurt, E. C., Aebi, U., and Panté, N. 1998. Molecular architecture of the yeast nuclear pore complex: localization of Nsp1p subcomplexes. *J Cell Biol*, 143(3):577–88.
- [Fasken and Corbett, 2009] Fasken, M. B. and Corbett, A. H. 2009. Mechanisms of nuclear mRNA quality control. *RNA Biol*, 6(3):237–41.
- [Flemming et al., 2009] Flemming, D., Sarges, P., Stelter, P., Hellwig, A., Böttcher, B., and Hurt, E. 2009. Two structurally distinct domains of the nucleoporin Nup170 cooperate to tether a subset of nucleoporins to nuclear pores. *J Cell Biol*, 185(3):387–395.
- [Fornerod et al., 1997] Fornerod, M., van Deursen, J., van Baal, S., Reynolds, A., Davis, D., Murti, K. G., Fransen, J., and Grosveld, G. 1997. The human homologue of yeast CRM1 is in a dynamic subcomplex with CAN/Nup214 and a novel nuclear pore component Nup88. *EMBO J*, 16(4):807–16.
- [Frenkiel-Krispin et al., 2010] Frenkiel-Krispin, D., Maco, B., Aebi, U., and Medalia, O. 2010. Structural analysis of a metazoan nuclear pore complex reveals a fused concentric ring architecture. *J Mol Biol*, 395(3):578–586.
- [Frey et al., 2006] Frey, S., Richter, R. P., and Görlich, D. 2006. FG-rich repeats of nuclear pore proteins form a three-dimensional meshwork with hydrogel-like properties. *Science*, 314(5800):815–7.
- [Fried and Kutay, 2003] Fried, H. and Kutay, U. 2003. Nucleocytoplasmic transport: taking an inventory. *Cell Mol Life Sci*, 60(8):1659–1688.
- [Gall, 1967] Gall, J. G. 1967. Octagonal nuclear pores. *J Cell Biol*, 32(2):391–9.

- [Galy et al., 2004] Galy, V., Gadai, O., Fromont-racine, M., Romano, A., Jacquier, A., and Nehrbass, U. 2004. Nuclear retention of unspliced mRNAs in yeast is mediated by perinuclear Mlp1. *Cell*, 116:63–73.
- [Gleizes et al., 2001] Gleizes, P. E., Noaillac-Depeyre, J., Léger-Silvestre, I., Teulières, F., Dauxois, J. Y., Pommet, D., Azum-Gelade, M. C., and Gas, N. 2001. Ultrastructural localization of rRNA shows defective nuclear export of preribosomes in mutants of the Nup82p complex. *J Cell Biol*, 155(6):923–936.
- [Goldberg and Allen, 1993] Goldberg, M. W. and Allen, T. D. 1993. The nuclear pore complex: three-dimensional surface structure revealed by field emission, in-lens scanning electron microscopy, with underlying structure uncovered by proteolysis. *J Cell Sci*, 106 ( Pt 1:261–74.
- [Görlich and Kutay, 1999] Görlich, D. and Kutay, U. 1999. Transport Between the Cell Nucleus and the Cytoplasm. *Annu Rev Cell Dev Biol*, 15:607–660.
- [Gorsch et al., 1995] Gorsch, L., Dockendorff, T., Cole, C., Gorsch, L., and Cole, C. N. 1995. A conditional allele of the novel repeat-containing yeast nucleoporin RAT7/NUP159 causes both rapid cessation of mRNA export and reversible clustering of nuclear pore complexes. *Cell*, 129(4):939–955.
- [Grandi et al., 1997] Grandi, P., Dang, T., Pane, N., Shevchenko, A., Mann, M., Forbes, D., and Hurt, E. 1997. Nup93, a vertebrate homologue of yeast Nic96p, forms a complex with a novel 205-kDa protein and is required for correct nuclear pore assembly. *Mol Biol Cell*, 8:2017–2038.
- [Grandi et al., 1993] Grandi, P., Doye, V., and Hurt, E. C. 1993. Purification of NSP1 reveals complex formation with ' GLFG ' nucleoporins and a novel nuclear pore protein. *EMBO J*, 12(8):3061–3071.
- [Grandi et al., 1995a] Grandi, P., Emig, S., Weise, C., Hucho, F., Pohl, T., and Hurt, E. C. 1995a. A novel nuclear pore protein Nup82p which specifically binds to a fraction of Nsp1p. *J Cell Biol*, 130(6):1263–73.
- [Grandi et al., 1995b] Grandi, P., Schlaich, N., Tekotte, H., and Hurt, E. C. 1995b. Functional interaction of Nic96p with a core nucleoporin complex consisting of Nsp1p, Nup49p and a novel protein Nup57p. *EMBO J*, 14(1):76–87.
- [Güttler and Görlich, 2011] Güttler, T. and Görlich, D. 2011. Ran-dependent nuclear export mediators: a structural perspective. *EMBO J*, 30(17):3457–74.
- [Harbury et al., 1993] Harbury, P. B., Zhang, T., Kim, P. S., and Alber, T. 1993. A switch between two-, three-, and four-stranded coiled coils in GCN4 leucine zipper mutants. *Science*, 262:1401–1407.
- [Hinshaw et al., 1992] Hinshaw, J. E., Carragher, B. O., and Milligan, R. a. 1992. Architecture and design of the nuclear pore complex. *Cell*, 69(7):1133–1141.
- [Ho et al., 2000] Ho, A. K., Shen, T. X., Ryan, K. J., Levy, M. A., Allen, T. D., Susan, R., Kiseleva, E., and Wenthe, S. R. 2000. Assembly and preferential localization of Nup116p on the cytoplasmic face of the nuclear pore complex by interaction with Nup82p. *Mol Cell Biol*, 20(15):5736–5748.
- [Hodge et al., 1999] Hodge, C. A., Colot, H. V., Stafford, P., and Cole, C. N. 1999. Rat8p / Dbp5p is a shuttling transport factor that interacts with Rat7p / Nup159p and Gle1p and suppresses the mRNA export defect of xpo1-1 cells. *EMBO J*, 18(20):5778–5788.
- [Hoelz et al., 2011] Hoelz, A., Debler, E. W., and Blobel, G. 2011. The structure of the nuclear pore complex. *Annu Rev Biochem*, 80:613–43.
- [Hsia et al., 2007] Hsia, K.-C., Stavropoulos, P., Blobel, G., and Hoelz, A. 2007. Architecture of a coat for the nuclear pore membrane. *Cell*, 131(7):1313–1326.
- [Hurt, 1988] Hurt, E. C. 1988. A novel nucleoskeletal-like protein located at the nuclear periphery is required for the life cycle of *Saccharomyces cerevisiae*. *EMBO J*, 7(13):4323–4334.
- [Hurwitz and Blobel, 1995] Hurwitz, M. E. and Blobel, G. 1995. NUP82 is an essential yeast nucleoporin required for poly(A)<sup>+</sup> RNA export. *J Cell Biol*, 130(6):1275–1281.

- [Hurwitz et al., 1998] Hurwitz, M. E., Strambio-de Castillia, C., and Blobel, G. 1998. Two yeast nuclear pore complex proteins involved in mRNA export form a cytoplasmically oriented subcomplex. *PNAS*, 95(September):11241–11245.
- [Inoue et al., 1990] Inoue, H., Nojima, H., Okoyama, H., Plant, T. E., Co, T., and City, T. 1990. High efficiency transformation of *Escherichia coli* with plasmids. *Gene*, 96:23–28.
- [Ito et al., 1983] Ito, H., Fukuda, Y., Murata, K., and Kimura, A. 1983. Transformation of intact yeast cells treated with alkali cations. *J Bacteriology*, 153(1):163–8.
- [Izaurralde et al., 1997] Izaurralde, E., Kutay, U., von Kobbe, C., Mattaj, I. W., and Görlich, D. 1997. The asymmetric distribution of the constituents of the Ran system is essential for transport into and out of the nucleus. *EMBO J*, 16(21):6535–47.
- [Janke et al., 2004] Janke, C., Magiera, M. M., Rathfelder, N., Taxis, C., Reber, S., Maekawa, H., Moreno-Borchart, A., Doenges, G., Schwob, E., Schiebel, E., and Knop, M. 2004. A versatile toolbox for PCR-based tagging of yeast genes: new fluorescent proteins, more markers and promoter substitution cassettes. *Yeast*, 21(11):947–962.
- [Kampmann and Blobel, 2009] Kampmann, M. and Blobel, G. 2009. Three-dimensional structure and flexibility of a membrane-coating module of the nuclear pore complex. *Nat Struct Mol Biol*, 16(7):782–788.
- [Kastner et al., 2008] Kastner, B., Fischer, N., Golas, M. M., Sander, B., Dube, P., Boehringer, D., Hartmuth, K., Deckert, J., Hauer, F., Wolf, E., Uchtenhagen, H., Urlaub, H., Herzog, F., Peters, J. M., Poerschke, D., and Lu, R. 2008. GraFix : sample preparation for single- particle electron cryomicroscopy. *Nat Methods*, 5(1):53–55.
- [Katahira et al., 1999] Katahira, J., Strässer, K., Podtelejnikov, A., Mann, M., Jung, J. U., and Hurt, E. 1999. The Mex67p-mediated nuclear mRNA export pathway is conserved from yeast to human. *EMBO J*, 18(9):2593–609.
- [Kiseleva et al., 2004] Kiseleva, E., Allen, T. D., Rutherford, S., Bucci, M., Wentz, S. R., and Goldberg, M. W. 2004. Yeast nuclear pore complexes have a cytoplasmic ring and internal filaments. *J Struct Biol*, 145(3):272–88.
- [Kiseleva et al., 1998] Kiseleva, E., Goldberg, M. W., Allen, T. D., and Akey, C. W. 1998. Active nuclear pore complexes in *Chironomus*: visualization of transporter configurations related to mRNP export. *J Cell Science*, 111 ( Pt 2):223–36.
- [Köhler and Hurt, 2010] Köhler, A. and Hurt, E. 2010. Gene regulation by nucleoporins and links to cancer. *Mol Cell*, 38(1):6–15.
- [Kosova et al., 2000] Kosova, B., Panté, N., Podtelejnikov, A., Mann, M., Aeby, U., Hurt, E., Panté, N., and Rollenhagen, C. 2000. Mlp2p, a component of nuclear pore attached intranuclear filaments, associates with Nic96p. *J Biol Chem*.
- [Kraemer et al., 1994] Kraemer, D., Wozniak, R. W., Blobel, G., and Radu, A. 1994. The human CAN protein, a putative oncogene product associated with myeloid leukemogenesis, is a nuclear pore complex protein that faces the cytoplasm. *PNAS*, 91(4):1519–23.
- [Kraemer et al., 1995] Kraemer, D. M., Strambio-de Castillia, C., Blobel, G., and Rout, M. P. 1995. The essential yeast nucleoporin NUP159 is located on the cytoplasmic side of the nuclear pore complex and serves in karyopherin-mediated binding of transport substrate. *J Biol Chem*, 270(1):19017–19021.
- [Lange et al., 2007] Lange, A., Mills, R. E., Christopher, J., Stewart, M., Devine, S. E., Corbett, A. H., and Lange, C. J. 2007. Classical Nuclear Localization Signals : definition, function and interaction with Importin alpha. *J Biol Chem*, 282:5101–5105.
- [Lee et al., 2000] Lee, S. J., Imamoto, N., Sakai, H., Nakagawa, A., Kose, S., Koike, M., Yamamoto, M., Kumasaka, T., Yoneda, Y., and Tsukihara, T. 2000. The adoption of a twisted structure of importin-beta is essential for the protein-protein interaction required for nuclear transport. *J Mol Biol*, 302(1):251–264.

- [Lim et al., 2007] Lim, R. Y. H., Fahrenkrog, B., Köser, J., Schwarz-Herion, K., Deng, J., and Aebi, U. 2007. Nanomechanical basis of selective gating by the nuclear pore complex. *Science*, 318(5850):640–3.
- [Lin et al., 2013] Lin, D. H., Zimmermann, S., Stuwe, T., Stuwe, E., and Hoelz, A. 2013. Structural and functional analysis of the C-terminal domain of Nup358/RanBP2. *J Mol Biol*, 425(8):1318–29.
- [Lindern et al., 1992] Lindern, M. V. O. N., Baal, S. V., Wiegant, J., and Raap, A. 1992. Can, a putative oncogene associated with myeloid leukemogenesis, may be activated by fusion of its 3' half to different genes : characterization of the set gene. *Mol Cell Biol*, 12(8):3346–3355.
- [Longtine et al., 1998] Longtine, M. S., McKenzie, A., Demarini, D. J., Shah, N. G., Wach, A., Brachat, A., Philippsen, P., and Pringle, J. R. 1998. Additional modules for versatile and economical PCR-based gene deletion and modification in *Saccharomyces cerevisiae*. *Yeast*, 14(10):953–961.
- [Ludtke et al., 1999] Ludtke, S. J., Baldwin, P. R., and Chiu, W. 1999. EMAN: semiautomated software for high-resolution single-particle reconstructions. *J Struc Biol*, 128(1):82–97.
- [Lutzmann et al., 2002] Lutzmann, M., Kunze, R., Buerer, A., Aebi, U., and Hurt, E. 2002. Modular self-assembly of a Y-shaped multiprotein complex from seven nucleoporins. *EMBO J*, 21(3):387–397.
- [Lutzmann et al., 2005] Lutzmann, M., Kunze, R., Stangl, K., Stelter, P., Tóth, K. F., Böttcher, B., and Hurt, E. 2005. Reconstitution of Nup157 and Nup145N into the Nup84 complex. *J Biol Chem*, 280(18):18442–18451.
- [Maillet et al., 1996] Maillet, L., Boscheron, C., Gotta, M., Marcand, S., Gilson, E., and Gasser, S. M. 1996. Evidence for silencing compartments within the yeast nucleus: a role for telomere proximity and Sir protein concentration in silencer-mediated repression. *Genes Dev*, 10(14):1796–1811.
- [Maimon et al., 2012] Maimon, T., Elad, N., Dahan, I., and Medalia, O. 2012. The human nuclear pore complex as revealed by cryo-electron tomography. *Structure*, 20(6):998–1006.
- [Makio et al., 2013] Makio, T., Lapetina, D. L., and Wozniak, R. W. 2013. Inheritance of yeast nuclear pore complexes requires the Nsp1p subcomplex. *J Cell Biol*, 203(2):187–96.
- [Martínez et al., 1999] Martínez, N., Alons, A., Moragues, M. D., Alonso, A., and Moragues, D. 1999. The nuclear pore complex protein Nup88 is overexpressed in tumor cells. *Cancer Res*, 59:5408–5411.
- [Mason et al., 2005] Mason, D. A., Shulga, N., Undavai, S., Ferrando-May, E., Rexach, M. F., and Goldfarb, D. S. 2005. Increased nuclear envelope permeability and Pep4p-dependent degradation of nucleoporins during hydrogen peroxide-induced cell death. *FEMS Yeast Res*, 5(12):1237–51.
- [Mason and Arndt, 2004] Mason, J. M. and Arndt, K. M. 2004. Coiled coil domains: stability, specificity, and biological implications. *Chembiochem*, 5(2):170–6.
- [Mastronarde, 2005] Mastronarde, D. N. 2005. Automated electron microscope tomography using robust prediction of specimen movements. *J Struc Biol*, 152(1):36–51.
- [Melcák et al., 2007] Melcák, I., Hoelz, A., and Blobel, G. 2007. Structure of Nup58/45 suggests flexible nuclear pore diameter by intermolecular sliding. *Science*, 315(5819):1729–32.
- [Montpetit et al., 2011] Montpetit, B., Thomsen, N. D., Helmke, K. J., Seeliger, M. a., Berger, J. M., and Weis, K. 2011. A conserved mechanism of DEAD-box ATPase activation by nucleoporins and InsP6 in mRNA export. *Nature*, 472(7342):238–42.
- [Morgan et al., 2011] Morgan, J. L., Song, Y., and Barbar, E. 2011. Structural dynamics and multiregion interactions in dynein-dynactin recognition. *J Biol Chem*, 286(45):39349–39359.
- [Moy and Silver, 1999] Moy, T. I. and Silver, P. a. 1999. Nuclear export of the small ribosomal subunit requires the ran-GTPase cycle and certain nucleoporins. *Genes Dev*, 13(16):2118–33.
- [Nachury and Weis, 1999] Nachury, M. V. and Weis, K. 1999. The direction of transport through the nuclear pore can be inverted. *PNAS*, 96(17):9622–7.

- [Nagy et al., 2009] Nagy, V., Hsia, K.-C., Debler, E. W., Kampmann, M., Davenport, A. M., Blobel, G., and Hoelz, A. 2009. Structure of a trimeric nucleoporin complex reveals alternate oligomerization states. *PNAS*, 106(42):17693–17698.
- [Napetschnig et al., 2007] Napetschnig, J., Blobel, G., and Hoelz, A. 2007. Crystal structure of the N-terminal domain of the human protooncogene Nup214/CAN. *PNAS*, 104(6):1783–1788.
- [Nehrbass et al., 1990] Nehrbass, U., Kern, H., Mutvei, a., Horstmann, H., Marshallsay, B., and Hurt, E. C. 1990. NSP1: a yeast nuclear envelope protein localized at the nuclear pores exerts its essential function by its carboxy-terminal domain. *Cell*, 61(6):979–89.
- [Noble et al., 2011] Noble, K. N., Tran, E. J., Alcázar-Román, A. R., Hodge, C. a., Cole, C. N., Wentz, S. R., and Content, R. 2011. The Dbp5 cycle at the nuclear pore complex during mRNA export II: nucleotide cycling and mRNP remodeling by Dbp5 are controlled by Nup159 and Gle1. *Genes Dev*, 25(10):1065–77.
- [Nyarko and Barbar, 2011] Nyarko, A. and Barbar, E. 2011. Light chain-dependent self-association of dynein intermediate chain. *J Biol Chem*, 286(2):1556–66.
- [Nyarko et al., 2013] Nyarko, A., Song, Y., Nováček, J., Židek, L., and Barbar, E. 2013. Multiple recognition motifs in nucleoporin Nup159 provide a stable and rigid Nup159-Dyn2 assembly. *J Biol Chem*, 288(4):2614–22.
- [Onischenko and Weis, 2011] Onischenko, E. and Weis, K. 2011. Nuclear pore complex-a coat specifically tailored for the nuclear envelope. *Curr Opin Cell Biol*, 23(3):293–301.
- [Ori et al., 2013] Ori, A., Banterle, N., Iskar, M., Andrés-Pons, A., Escher, C., Khanh Bui, H., Sparks, L., Solis-Mezarino, V., Rinner, O., Bork, P., Lemke, E. a., and Beck, M. 2013. Cell type-specific nuclear pores: a case in point for context-dependent stoichiometry of molecular machines. *Mol Syst Biol*, 9(648):648.
- [Panté and Aebi, 1996] Panté, N. and Aebi, U. 1996. Molecular dissection of the nuclear pore complex. *Crit Revi Biochem Mol Biol*, 31(2):153–99.
- [Peters, 2009a] Peters, R. 2009a. Functionalization of a nanopore: the nuclear pore complex paradigm. *Biochim Biophys Acta*, 1793(10):1533–1539.
- [Peters, 2009b] Peters, R. 2009b. Translocation through the nuclear pore: Kaps pave the way. *Bioessays*, 31(4):466–77.
- [Puig et al., 2001] Puig, O., Caspary, F., Rigaut, G., Rutz, B., Bouveret, E., Bragado-Nilsson, E., Wilm, M., and Séraphin, B. 2001. The tandem affinity purification (TAP) method: a general procedure of protein complex purification. *Methods*, 24(3):218–229.
- [Rapali et al., 2011] Rapali, P., Szenes, A., Radnai, L., Bakos, A., Pál, G., and Nyitray, L. 2011. DYNLL/LC8: a light chain subunit of the dynein motor complex and beyond. *FEBS J*, 278(17):2980–96.
- [Rasala et al., 2006] Rasala, B. a., Orjalo, A. V., Shen, Z., Briggs, S., and Forbes, D. J. 2006. ELYS is a dual nucleoporin/kinetochore protein required for nuclear pore assembly and proper cell division. *PNAS*, 103(47):17801–6.
- [Reichelt et al., 1990] Reichelt, R., Holzenburg, A., Buhle, E. L., Jarnik, M., Engel, A., and Aebi, U. 1990. Correlation between structure and mass distribution of the nuclear pore complex and of distinct pore complex components. *J Cell Biol*, 110(4):883–894.
- [Ren et al., 2010] Ren, Y., Seo, H.-S., Blobel, G., and Hoelz, A. 2010. Structural and functional analysis of the interaction between the nucleoporin Nup98 and the mRNA export factor Rae1. *PNAS*, 107(23):10406–10411.
- [Ribbeck and Görlich, 2001] Ribbeck, K. and Görlich, D. 2001. Kinetic analysis of translocation through nuclear pore complexes. *EMBO J*, 20(6):1320–1330.

- [Ribbeck et al., 1998] Ribbeck, K., Lipowsky, G., Kent, H. M., Stewart, M., and Görlich, D. 1998. NTF2 mediates nuclear import of Ran. *EMBO J*, 17(22):6587–98.
- [Rigaut et al., 1999] Rigaut, G., Shevchenko, A., Rutz, B., Wilm, M., Mann, M., and Séraphin, B. 1999. A generic protein purification method for protein complex characterization and proteome exploration. *Nat Biotech*, 17(October):7–9.
- [Rout et al., 2003] Rout, M., Aitchison, J. D., Magnasco, M. O., and Chait, B. T. 2003. Virtual gating and nuclear transport: the hole picture. *Trends Cell Biol*, 13(12):622–628.
- [Rout et al., 2000] Rout, M. P., Aitchison, J. D., Suprpto, A., Hjertaas, K., Zhao, Y., and Chait, B. T. 2000. The yeast nuclear pore complex: composition, architecture, and transport mechanism. *J Cell Biol*, 148(4):635–51.
- [Rout and Blobel, 1993] Rout, M. P. and Blobel, G. 1993. Isolation of the yeast nuclear pore complex. *J Cell Biol*, 123(4):771–83.
- [Roy et al., 2010] Roy, A., Kucukural, A., and Zhang, Y. 2010. I-TASSER: a unified platform for automated protein structure and function prediction. *Nat Protoc*, 5(4):725–738.
- [Schafer and Hurt, 2006] Schafer, T. and Hurt, E. 2006. Hrr25-dependent phosphorylation state regulates organization of the pre-40S subunit. *Nature*, 441(June):651–655.
- [Schlaich et al., 1997] Schlaich, N. L., Haner, M., Lustig, A., Aebi, U., and Hurtoll, E. C. 1997. In Vitro Reconstitution of a Heterotrimeric Nucleoporin Complex Consisting of Recombinant. *Mol Cell Biol*, 8(January):33–46.
- [Schmitt et al., 1999] Schmitt, C., von Kobbe, C., Bachi, A., Pante, N., Rodrigues, P., Rigaut, G., Wilm, M., Carmo-fonseca, M., and Izaurralde, E. 1999. Dbp5, a DEAD-box protein required for mRNA export, is recruited to the cytoplasmic fibrils of nuclear pore complex via a conserved interaction with CAN / Nup159p. *EMBO J*, 18(15):4332–4347.
- [Schrader et al., 2008] Schrader, N., Stelter, P., Flemming, D., Kunze, R., Hurt, E., and Vetter, I. R. 2008. Structural basis of the Nic96 subcomplex organization in the nuclear pore channel. *Mol Cell*, 29(1):46–55.
- [Schwartz, 2005] Schwartz, T. U. 2005. Modularity within the architecture of the nuclear pore complex. *Curr Opin Struct Biol*, 15(2):221–6.
- [Segref et al., 1997] Segref, A., Sharma, K., Doye, V., Hellwig, A., Huber, J., Lührmann, R., and Hurt, E. 1997. Mex67p, a novel factor for nuclear mRNA export, binds to both poly(A)<sup>+</sup> RNA and nuclear pores. *EMBO J*, 16(11):3256–3271.
- [Seo et al., 2009] Seo, H.-S., Ma, Y., Debler, E. W., Wacker, D., Kutik, S., Blobel, G., and Hoelz, A. 2009. Structural and functional analysis of Nup120 suggests ring formation of the Nup84 complex. *PNAS*, 106(34):14281–14286.
- [Sherman et al., 1991] Sherman, M. a., Dean, S. a., Mathiowetz, a. M., and Mas, M. T. 1991. Site-directed mutations of arginine 65 at the periphery of the active site cleft of yeast 3-phosphoglycerate kinase enhance the catalytic activity and eliminate anion-dependent activation. *Protein Eng*, 4(8):935–940.
- [Siniossoglou et al., 2000] Siniossoglou, S., Lutzmann, M., Santos-rosa, H., Leonard, K., Mueller, S., Aebi, U., and Hurt, E. 2000. Structure and assembly of the Nup84p complex. *J Cell Biol*, 149(1):41–53.
- [Siniossoglou et al., 1996] Siniossoglou, S., Wimmer, C., Rieger, M., Doye, V., Tekotte, H., Weise, C., Emig, S., Segref, A., and Hurt, E. C. 1996. A novel complex of nucleoporins, which includes Sec13p and a Sec13p homolog, is essential for normal nuclear pores. *Cell*, 84(2):265–275.
- [Solmaz et al., 2013] Solmaz, S. R., Blobel, G., and Melcák, I. 2013. Ring cycle for dilating and constricting the nuclear pore. *PNAS*, 110(15):5858–63.

- [Solmaz et al., 2011] Solmaz, S. R., Chauhan, R., Blobel, G., and Melčák, I. 2011. Molecular architecture of the transport channel of the nuclear pore complex. *Cell*, 147(3):590–602.
- [Stelter et al., 2007] Stelter, P., Kunze, R., Flemming, D., Höpfner, D., Diepholz, M., Philippsen, P., Böttcher, B., and Hurt, E. 2007. Molecular basis for the functional interaction of dynein light chain with the nuclear-pore complex. *Nat Cell Biol*, (December 2006).
- [Stelter et al., 2012] Stelter, P., Kunze, R., Radwan, M., Thomson, E., Thierbach, K., Thoms, M., and Hurt, E. 2012. Monitoring spatiotemporal biogenesis of macromolecular assemblies by pulse-chase epitope labeling. *Mol Cell*, 47(5):788–796.
- [Stoffler et al., 2003] Stoffler, D., Feja, B., Fahrenkrog, B., Walz, J., Typke, D., and Aebi, U. 2003. Cryo-electron tomography provides novel insights into nuclear pore architecture: implications for nucleocytoplasmic transport. *J Mol Biol*, 328(1):119–130.
- [Strambio-de Castillia et al., 1999] Strambio-de Castillia, C., Blobel, G., and Rout, M. P. 1999. Proteins connecting the nuclear pore complex with the nuclear interior. *J Cell Biol*, 144(5):839–855.
- [Strässer et al., 2000] Strässer, K., Bassler, J., and Hurt, E. 2000. Binding of the Mex67p/Mtr2p heterodimer to FXFG, GLFG, and FG repeat nucleoporins is essential for nuclear mRNA export. *J Cell Biol*, 150(4):695–706.
- [Strawn et al., 2004] Strawn, L. A., Shen, T., Shulga, N., Goldfarb, D. S., and Wentz, S. R. 2004. Minimal nuclear pore complexes define FG repeat domains essential for transport. *Nat Cell Biol*, 6(3):197–206.
- [Swapna et al., 2012] Swapna, L. S., Srikeerthana, K., and Srinivasan, N. 2012. Extent of structural asymmetry in homodimeric proteins: prevalence and relevance. *PloS One*, 7(5):e36688.
- [Teixeira et al., 1999] Teixeira, M. T., Fabre, E., and Dujon, B. 1999. Self-catalyzed cleavage of the yeast nucleoporin Nup145p precursor. *J Biol Chem*, 274:32439–32444.
- [Terry and Wentz, 2009] Terry, L. J. and Wentz, S. R. 2009. Flexible gates: dynamic topologies and functions for FG nucleoporins in nucleocytoplasmic transport. *Eukaryot cell*, 8(12):1814–27.
- [Tetenbaum-Novatt and Rout, 2010] Tetenbaum-Novatt, J. and Rout, M. P. 2010. The mechanism of nucleocytoplasmic transport through the nuclear pore complex. *Cold Spring Harb Symp Quant Biol*, 75:567–84.
- [Tran et al., 2007] Tran, E. J., Zhou, Y., Corbett, A. H., and Wentz, S. R. 2007. The DEAD-box protein Dbp5 controls mRNA export by triggering specific RNA:protein remodeling events. *Mol Cell*, 28(5):850–9.
- [Vallee et al., 2004] Vallee, R. B., Williams, J. C., Varma, D., and Barnhart, L. E. 2004. Dynein: An ancient motor protein involved in multiple modes of transport. *J Neurobiol*, 58(2):189–200.
- [van Heel et al., 1996] van Heel, M., Harauz, G., Orlova, E. V., Schmidt, R., and Schatz, M. 1996. A new generation of the IMAGIC image processing system. *J Struct Biol*, 116(1):17–24.
- [Walther et al., 2002] Walther, T. C., Pickersgill, H. S., Cordes, V. C., Goldberg, M. W., Allen, T. D., Mattaj, I. W., and Fornerod, M. 2002. The cytoplasmic filaments of the nuclear pore complex are dispensable for selective nuclear protein import. *J Cell Biol*, 158(1):63–77.
- [Walzthoeni et al., 2012] Walzthoeni, T., Claassen, M., Leitner, A., Herzog, F., Bohn, S., Förster, F., Beck, M., and Aebersold, R. 2012. False discovery rate estimation for cross-linked peptides identified by mass spectrometry. *Nat Met*, 9(9):901–3.
- [Wang et al., 2004] Wang, L., Hare, M., Hays, T. S., and Barbar, E. 2004. Dynein Light Chain LC8 promotes assembly of the coiled-coil domain of swallow protein. *Biochemistry*, 43(1):4611–4620.
- [Waterhouse et al., 2009] Waterhouse, A. M., Procter, J. B., Martin, D. M. a., Clamp, M., and Barton, G. J. 2009. Jalview Version 2—a multiple sequence alignment editor and analysis workbench. *Bioinformatics*, 25(9):1189–91.

- [Weirich et al., 2004] Weirich, C. S., Erzberger, J. P., Berger, J. M., and Weis, K. 2004. The N-terminal domain of Nup159 forms a beta-propeller that functions in mRNA export by tethering the helicase Dbp5 to the nuclear pore. *Mol Cell*, 16(5):749–60.
- [Whittle and Schwartz, 2009] Whittle, J. R. R. and Schwartz, T. U. 2009. Architectural nucleoporins Nup157/170 and Nup133 are structurally related and descend from a second ancestral element. *J Biol Chem*, 284(41):28442–52.
- [Wu et al., 1995] Wu, J., Matunis, M., Kraemer, D., Blobel, G., and Coutavas, E. 1995. Nup358, a cytoplasmically exposed nucleoporin with peptide repeats, Ran-GTP binding sites, zinc fingers, a cyclophilin A homologous domain, and a leucine-rich region. *J Biol Chem*, 270(23):14209–14213.
- [Yaffe and Schatz, 1984] Yaffe, M. P. and Schatz, G. 1984. Two nuclear mutations that block mitochondrial protein import in yeast. *PNAS*, 81(15):4819–4823.
- [Yamada et al., 2010] Yamada, J., Phillips, J. L., Patel, S., Goldfien, G., Calestagne-Morelli, A., Huang, H., Reza, R., Acheson, J., Krishnan, V. V., Newsam, S., Gopinathan, A., Lau, E. Y., Colvin, M. E., Uversky, V. N., and Rexach, M. F. 2010. A bimodal distribution of two distinct categories of intrinsically disordered structures with separate functions in FG nucleoporins. *Mol Cell Proteomics*, 9(10):2205–24.
- [Yang et al., 1998] Yang, Q., Rout, M. P., and Akey, C. W. 1998. Three-Dimensional Architecture of the Isolated Yeast Nuclear Pore Complex : Functional and Evolutionary Implications. *Mol Cell*, 1:223–234.
- [Yao et al., 2007] Yao, W., Roser, D., Köhler, A., Bradatsch, B., Bassler, J., and Hurt, E. 2007. Nuclear export of ribosomal 60S subunits by the general mRNA export receptor Mex67-Mtr2. *Mol Cell*, 26(1):51–62.
- [Yoshida et al., 2011] Yoshida, K., Seo, H. S., Debler, E. W., Blobel, G., and Hoelz, A. 2011. Structural and functional analysis of an essential nucleoporin heterotrimer on the cytoplasmic face of the nuclear pore complex. *PNAS*, 108(40):16571–16576.
- [Zeitler and Weis, 2004] Zeitler, B. and Weis, K. 2004. The FG-repeat asymmetry of the nuclear pore complex is dispensable for bulk nucleocytoplasmic transport in vivo. *J Cell Biol*, 167(4):583–90.
- [Zhang, 2008] Zhang, Y. 2008. I-TASSER server for protein 3D structure prediction. *BMC Bioinformatics*, 9:40.
- [Zhao and Blobel, 2005] Zhao, X. and Blobel, G. 2005. A SUMO ligase is part of a nuclear multiprotein complex that affects DNA repair and chromosomal organization. *PNAS*, 102(13):4777–82.

# List of Figures

1.1	Model of the nuclear pore complex (NPC)	2
1.2	Scheme of the nuclear pore complex obtained from <i>Dictyostelium discoideum</i>	4
1.3	Domain architecture and location of nucleoporins	7
1.4	The arrangement of nucleoporins into NPC modules in yeast and vertebrates	11
1.5	The overview of NPC's substructures and their nucleoporin composition	12
1.6	Topology of the Nup84 complex	13
1.7	The architecture of yeast Nup82 complex and human Nup214/CAN	17
1.8	Simplified model of RanGTP/RanGDP-mediated transport across the NPC	20
1.9	Models of cargo translocation across the NPC	22
2.1	Architecture of $\alpha$ -helical domains of Nup159, Nup82 and Nsp1	25
2.2	$\alpha$ -helically predicted carboxy-terminal domain of Nup159 is conserved among <i>fungi</i>	26
2.3	Dot spot analysis of <i>nup159</i> mutants in wild-type or <i>dyn2</i> $\Delta$ background	28
2.4	<i>In vivo</i> localization of GFP- <i>nup159-C</i> mutants	30
2.5	The essential H1 subdomain of Nup159-C is required for the Nup82 complex assembly	31
2.6	Heptad repeats within the Nup159-H1 sub-domain are crucial for self-dimerization <i>in vitro</i>	33
2.7	Mutations in the Nup159-C domain affect the proper Nup82 complex assembly <i>in vivo</i>	34
2.8	Overexpression of Dyn2 restores its binding to the <i>nup159</i> $\Delta$ <i>Linker</i> mutant	35
2.9	Reconstitution and purification of simplified Nup82 complexes	37
2.10	The <i>in vivo</i> reconstituted Nup82-Nup159C-Nsp1C-Dyn2 and Nup82-Nup159 $\Delta$ FG-Nsp1C-Dyn2 complexes are functional and incorporated into the NPC	38
2.11	SEC-MALS analysis of the Nup82-Nup159C-Nsp1C-Dyn2 complex	39
2.12	Molecular mass determination of reconstituted Nup82-Nup159 $\Delta$ FG-Nsp1C-Dyn2 and Nup82-Nup159C-Nsp1C-Dyn2-Nup116C complexes by SEC-MALS	41
2.13	SEC-MALS analysis of minimal Nup82 sub-complexes	42
2.14	Negative staining electron microscopy of the affinity-purified Nup82-Nup159C-Nsp1C-Dyn2 complex subjected to size exclusion column	44
2.15	The EM structure of the Nup82-Nup159C-Nsp1C-Dyn2 complex	45
2.16	The EM structure of the Nup82-Nup159 $\Delta$ FG-Nsp1C-Dyn2 complex	46
2.17	Purification of the Nup82-Nup159 $\Delta$ FG-Nsp1C-Flag-Dyn2 complex under low and high salt concentrations	47
2.18	The structure of the Nup82-Nup159-C $\Delta$ tail-Nsp1C-Dyn2 complex observed by EM	49
2.19	Cross-linking mass spectrometry analysis of the Nup82-Nup159C-Nsp1C-Dyn2 complex	51
2.20	SEC-MALS of affinity-purified Nup82-Flag-Nsp1C-Nup159-H3-H4-tail complex	53
2.21	3D structure of the Nup82-Nup159C-Nsp1C-Dyn2 complex determined by negative staining electron tomography	54
3.1	Class averages of the Nup82-Nup259C-Nsp1C-Dyn2 complex obtained by GraFix-EM	59
3.2	Structural model of the Nup82-Nup159C-Nsp1C-Dyn2 complex architecture	60
3.3	Docking of the Nup82-Nup159C-Nsp1C-Dyn2 within the tomographic map of the human NPC	63
7.1	Growth analysis of <i>dyn2</i> $\Delta$ , <i>nup159</i> $\Delta$ <i>DID</i> <sub>Nup159</sub> and <i>nup159</i> $\Delta$ <i>Linker</i> mutants	82
7.2	Multi-sequence alignment of the $\alpha$ -helically predicted C-domain of Nup82	83
7.3	Multi-sequence alignment of the $\alpha$ -helically predicted C-domain of Nsp1	84

# List of Tables

- 2.1 Calculations of theoretical molecular weight of the Nup82-Flag-Nup159C-Nsp1C-Dyn2 complex. . . . . 40
- 4.1 Plasmids used in this study . . . . . 65
- 4.2 Yeast strains used in this study . . . . . 66
- 4.3 Antibody dilutions . . . . . 72
  
- 5.1 List of Abbreviations A-F . . . . . 78
- 5.2 List of Abbreviations G-N . . . . . 79
- 5.3 List of Abbreviations O-Z . . . . . 80